

Filtration at the mega-scale: Exploring the filter morphology and filtration mechanisms in the
cartilaginous fishes

Erin Winters-Mist Paig-Tran

A dissertation submitted in partial fulfillment of the

requirements for the degree of

Doctor of Philosophy

University of Washington

2012

Reading Committee:

Adam Summers, Chair

Jennifer Ruesink

Megan Dethier

Lara Ferry

Program Authorized to Offer Degree:

Biology

©Copyright [2012]

Erin Winters-Mist Paig-Tran

Dedication

I would like to dedicate this dissertation to my family, friends,
and especially my husband David.

Thank you for supporting my marine biology dreams and helping me to
continue swimming with giants.

Acknowledgements

There are many people and organizations that have contributed to this dissertation. I am greatly indebted to each and every one of you.

I would like to first thank all of my funding sources, for without you this dissertation could not have moved forward. Thank you to the UC-Mexus program for fostering a fruitful collaboration between Dr. Felipe Galván-Magana and Silvia Hinojosa in Mexico and Dr. Adam Summers and myself in the United States of America. We look forward to continuing our manta ray work in the Yucatán for many years to come. Thank you to the National Geographic Waitt Funding for generously providing funds for attaching PSAT tags to manta rays in the Yucatán. Sigma Xi provided support for modeling equipment costs. Thank you to the Dr. Richard and Megumi Strathmann Fellowship for providing funding for housing at Friday Harbor Laboratories. Thank you to the University of Washington Biology Department, the WRF-Hall Fellowship, and the Sargent Award for providing funding for conferences, one quarter of tuition, and travel funding to museums. Thank you also to the Society of Integrative and Comparative Biologists and the American Elasmobranch Society for providing travel support to many meetings.

I could not have completed this dissertation without the advisement, mentorship, and patience of my adviser, Dr. Adam Summers. Thank you for taking a chance on someone interested in filter-feeding, even though it wasn't your focus. I have learned a great deal from you and I hope that our collaborative efforts will continue far into the future. Our morning coffee meetings always ended up with me having more work than I may have liked at the time, but ultimately led to several manuscripts. You really are a fantastic mentor and I tell everyone that you spew academic gold. You taught me how to tell an exciting story and how to hold my

audience captive (mentally of course). Your faith in my academic abilities has never wavered even though I have, on occasion, been known to completely freeze up with intimidation when trying to impress you on the white board. My greatest academic achievement may be the day you told me I was ready to have my own lab, complete with my own graduate students. Your endorsement means the world to me.

Thank you to my past and present advisory committees at the University of Washington and the University of California. My committee at the University of Washington: Dr. Jennifer Ruesink, Dr. Lara Ferry, Dr. Megan Dethier, Dr. Emily Carrington, and Dr. Angela Ginorio. My committee at the University of California, Irvine: Dr. Mathew McHenry and Dr. James Hicks. Thank you for providing me with helpful feedback on my dissertation and for your support and guidance throughout this process. Lara, thank you so much for being a fantastic mentor and a great friend. I have enjoyed hearing your perspective on academia, experiments, and life in general. Megan, thank you for stepping in with little notice and then rocking my world with your speedy reviews of my manuscripts. I think very highly of you and your work at FHL. Thank you Matt for providing me with a home at UCI and continuing to give me support even when I was no longer a UCI graduate student.

Thank you to the amazing administrative staff at the University of Washington in Seattle and at the Friday Harbor Laboratories. Judy Farrow, you made navigating administrative hurdles easy. I am greatly appreciative of Aimee Urata, Vikky Dauciunas, Kathy Cowell, and Stacy Markman. You ladies run a tight ship at the labs and are the reason my dissertation work went so smoothly. You have become friends and confidants. You have always fought for me, pulled for me, and in some cases nurtured and mothered me. Thank you to Scott Schwinge for help with funding and post-doctoral paperwork. I couldn't have gotten that NIH grant in without you.

Thank you to Craig Staude for spending many hours with me setting up microscopes and working through computer programs. You have made my transition to UW so much easier. Thank you to Kristy Kull for helpful boat training. To Jeannie Merridith, thank you for your patience as I attempted to navigate the stockroom at all hours of the day. Thank you to Tim Dwyer for reading and providing helpful comments on many drafts of manuscripts and grant proposals. I'm so proud to have such a competent editor and scientist critiquing my work. You are perhaps the person at FHL that has inspired me the most to continue to strive for excellence in work and in life. To Moose O'Donnell, thank you for all your helpful tidbits and entertaining quips while I powered through my experiments. And of course, thank you for always being there to share sweets with me because glucose is brain food. Many thanks to the FHL maintenance staff, without whom none of this (really none of it) would have been possible. You guys are the true movers and shakers at the labs.

I would like to give a special thank you to my past and present lab colleagues: Joseph Bizzarro, Stephanie Crofts, Marianne Porter, Mason Dean, Andrew Clark, Jaquan Horton, Jennie Beltran, Rey Jacinto, Justin Schaefer, Thomas Kleinteich, and Anja Kleinteich. Joe, you have been my rock throughout this process and I have nothing but the utmost respect for you. I can't tell you how much your friendship and mentorship has meant to me. You are good peeps for sure. You are my eating buddy, my confidant, and my friend. Stephanie, I could never have made it through grad school without you and our many, many, many coffee sessions. I love you a ton. Marianne, you are an incredible mentor and I wish you all the best. Big things are in store for you. Mason, thank you for being the "best of the best" and for letting me tag along to learn from a true master in our field. You've always been my "go to" guy for ray questions and I appreciate your patience with me. You taught me how to give a presentation, how to make a

figure, and how to get CT scanning for a reduced rate. Andrew (and Mary), you are a great inspiration and I have enjoyed our academic (and non-academic) talks. Thanks for being a terrific boss at FHL. You both are amazing. I can't express enough thanks to Thomas and Anja Kleinteich. Thomas, I have greatly enjoyed your input on my work and I would not have made it through the winter at FHL without you and Anja. I love you both (Lea and Ada too).

I could not have finished this dissertation without the generous support and assistance of many museum personnel. Thank you to the museum specialists who made specimen collection possible. HJ Walker, I can't even begin to tell you how instrumental you were to this research. I have enjoyed my trips down to Scripps for specimen collections coupled with berry and nut consumption a plenty. Thank you to Jeff Seigel at the LANHM for digging through so many specimen vats to find me a *Mobula thurstoni* and allowing me to open up the megamouth enclosure mid-day. I'm sure the visiting school children will never forget the smell of ethanol wafting throughout the exhibit halls. Thank you to Lynn Parenti, Jeff Clayton, and Jerry Finan at the Smithsonian Natural History Museum. Jerry, you have perhaps the coolest job I can think of and I can't believe you opened some of those huge coffins just for me. It was well worth the effort, those *Mobula hypostoma* went to good use. I may never get to be that close to a *Mola mola* again. You were a fantastic host, especially since you were only notified of my arrival a day in advance.

Thank you to all the lab personnel at FHL and UCI, especially Tomasz Owerkowics. Tomasz, you were a huge factor in this Ph.D. and I would not have been able to successfully work remotely without you providing lab space, equipment, and guidance on my histology chapter. You are a second adviser and I cannot express enough thanks for all you have done. I'm so appreciative that you always made time for coffee chats, even when you were quite literally

up to your arms in gators. Thank you to my UCI support system. James Strother, you have been an instrumental academic mentor on fluid dynamics and on the woes of isopropanol. Thanks to William Van Trump, Karla Feitl, Victoria Ngo, Alex Jackson, Cassondra Williams, Heidi Contreras, Gilberto Cardenas, Johnny Yang, and Mathew Wong for all your help and support throughout this process. Gilberto, you were such a trooper in Mexico. Thank you to Tim Dwyer, Alex Lowe, Kristy Kull, Jackie O'Mara, Ryan Knowles, Ryan McLaughlin, Laura Newcomb, Matt George, Hilary Hayford, Connie Sullivan, Robin Elahi, Kevin Turner, Autumn Turner, and Orissa Moulton for entertaining me at FHL and providing me a wonderful support system to lean on when I needed it. May Herbs be ever open. Thank you to Dylan Wainwright and Ashley Peterson for your general awesomeness as undergraduate/post baccalaureate researchers. You two are phenomenal and I look forward to this collaboration. Dylan, the feet would only have been green for a week.

This work would not have been possible without my many friends and collaborators. Thank you to Dr. Yannis Papastamatiou, you are an amazing scientist and I enjoyed hosting you for manta work in the Yucatán. I'm sorry for dragging you out in monsoonal conditions, but at least you got to swim with whale sharks and manta rays. Dr. Nick Wegner, thank you for your hard work and dedication to the manta project. It may have taken many days at sea with no mantas before we finally tagged them, but you stuck with it and we finally tagged them. Thank you to Silvia Hinojosa for simply being the best collaborator I could ever ask for. I look forward to many more years working on the Caribbean Manta Project. Thank you to all of the boat captains in the Yucatán. I know that I asked you to go out when there were 15 foot waves and yet you always came through for us. Thank you to Dr. Phil Motta and Dr. Andrea Marshall for all

your input into manta ray morphology and movement patterns. I can't express how much you have improved this dissertation.

Thank you to Dr. Katie Staab, Claire Waggoner, and Eva Young for your guidance and support throughout this process. Katie, I value your opinion on all things (academic and life) more than just about anyone else's. Thank you for reading every manuscript along the way and lifting me up when I thought I would fall. You have been my support system since the day I walked into our dorm room at Friday Harbor. You are my conference buddy, my better academic half, and partner in crime. You are the most incredible bestie and I love you more than I can ever express. Claire, thank you so much for talking science with me for hours on end and for helping me stay excited about this career path. I know good things are in store for you. You are such an amazing scientist and friend. Thank you for the many pep talks in the spa and sushi/Lebanese/Crepe runs throughout these five years. Eva, you have always believed in me as I have always believed in you. You've "geeked out" with me on science since we were marine biology undergraduates at CSULB. I can't thank you all enough for your support and the love you've shown me throughout this process. I love that we got to hug it out with grey whales in Mexico together. So many memories.

Finally, but perhaps most importantly, thank you to my family for everything you have done. Thank you to my parents, David and Linda Paig, for encouraging me to follow my heart and strive for the Ph.D. Dad, your dedication to your own studies inspired me to climb all the way up the academic ladder one rung at a time. Mom, you have always been my biggest champion and the one person I knew I could always go to no matter what. Thank you to my sisters Skye, Sunshine, and Tara. Ladies, I've finally done it. I've become Dr. Awesome and you must now all bow to me. Sisters are the greatest support system anyone can have and I appreciate

you dealing with me throughout this process. Thank you to Thomas Rider who spent many a night talking science and arguing the biological definition of a zombie. Thank you to Lily, Roland, Gwen, Atticus, Dashiell, Kenneth, Ashlynn, Jacob, Bella, Jill, and Everett for keeping me so entertained for the past five years. Thank you to Jack Soren for keeping my heart beating during this process. Thank you to Syairah for inspiring me to take breaks and enjoy some BigBang now and then. Thank you to Jason for being a great father to my little Jack. I'd also like to express my thanks to the entire Tran family: Viet, Lan, Grandma, Tuan, Mathew, Dai, Khanh, Mai, Katelynn, Sydney, Diane, Greg, Rachel, Nicky, Sarah, Justin, Ryan, Denise, Megan, Melissa, Ethan, Nicole, Sean, Chris, Caressa, Kevin, and Kaely.

David, the love of my life, I could not have possibly made it through this entire experience without your support, encouragement, and love. I know that it has been a long, long, long journey and you have never wavered in your support. You have always encouraged me to follow my dreams, even when you knew it was going to be a rough road. I could not have possibly completed this dissertation without you. You've supported me financially, mentally, and spiritually. You lifted me up when I was down. You gracefully put up with my many hours of obsessive K pop/youtube surfing. You accept me as I am, even during bad moods and good moods and everything in between. I love you so much. These 15 years have been a blessing with you. I couldn't ask for a more wonderful husband, friend, and partner. Here's to a lifetime together, hand in hand, beating all the odds and turning our dreams into reality.

University of Washington

Abstract

Filtration at the mega-scale: Exploring the filter morphology and filtration mechanisms in the
cartilaginous fishes

Erin Winters-Mist Paig-Tran

Chair of the Supervisory Committee:

Adam Summers

Associate Director of the University of Washington's Friday Harbor Laboratories

and Professor

Biology

Suspension feeding in the cartilaginous fishes evolved approximately 66-22 million years ago and is manifest in four independently evolved lineages of fishes (Cetorhinidae, Megachasmidae, Rhincodontidae, and Mobulidae). The mechanisms of filtration used by fishes are reflective of the morphology and composition of the filtering tissues. I found the filter morphology and the mechanisms of filtration in the 11 species of devil rays are different from all other filtering fishes. I used a combination of gross anatomical descriptions, scanning electron microscopy (SEM), histology, modeling, and live performance data to describe the anatomy and filtration mechanisms in the devil rays. The filter pads are offset, chevron-shaped, rigid, cartilaginous structures composed of repeating filter lobes located on the anterior (toward the incoming flow) and posterior (toward the esophagus) surfaces of the epibranchial and ceratobranchial arches. SEM and histology show that the ultrastructure of the leaf-like, ascending filter lobes varies between species; however, most are keratinous and can be either smooth or covered in cilia and some include the presence of denticles. The shape and surface of the terminal filtering lobes are distinct in each species and may be used as a tool for species identification. In some species, the stratified squamous epithelium contains a high density of mucus cells, likely serving as a mechanism for sticky sieve filtration while in others the mucus producing cells are absent. Fluid flow in the devil rays is unusual; it does not follow a continuous, parallel trajectory through the buccopharyngeal cavity as in other suspension feeding fishes. Instead there is an abrupt 90° turn from the initial inflowing path to move through the laterally directed branchial filter pores, over the gill tissue, and out the ventrally located gill slits. The deviation from the incoming flow results in tangential shearing stress (cross-flow) across the filter surface. This implies that devil rays can use cross-flow filtration to clear the filter after particles are caught by inertial impaction, direct interception, and/or sieving mechanisms.

Table of Contents

Dedication.....	3
Acknowledgements.....	4
Abstract of Dissertation.....	11
List of Figures.....	14
List of Tables.....	16
List of Symbols.....	17
Chapter 1: Introduction.....	20
Chapter 2: Bottles as models: Predicting the effects of swimming speed and morphology on size selectivity and filtering efficiency in fishes.....	28
Chapter 3: The filter pads and filtration mechanisms of the devil rays: variation at macro and microscopic scales.....	72
Chapter 4: The structure of suspension feeding elasmobranch filters.....	118
Chapter 5: Conclusion.....	162
References.....	164

List of Figures

Figure 1.1.....	26
Figure 2.1.....	54
Figure 2.2.....	56
Figure 2.3.....	58
Figure 2.4.....	60
Figure 2.5.....	62
Figure 2.6.....	64
Figure 2.7.....	66
Figure 2.8.....	68
Figure 2.9.....	70
Figure 3.1.....	97
Figure 3.2.....	99
Figure 3.3.....	101
Figure 3.4.....	103
Figure 3.5.....	105
Figure 3.6.....	107
Figure 3.7.....	109

Figure 3.8.....	111
Figure 3.9.....	113
Figure 3.10.....	115
Figure 4.1.....	134
Figure 4.2.....	136
Figure 4.3.....	138
Figure 4.4.....	140
Figure 4.5.....	142
Figure 4.6.....	144
Figure 4.7.....	146
Figure 4.8.....	148
Figure 4.9.....	150
Figure 4.10.....	152
Figure 4.11.....	154
Figure 4.12.....	156
Figure 4.13.....	158
Figure 4.14.....	160

List of Tables

Table 2.1.....	51
Table 2.2.....	52
Table 2.3.....	53
Table 3.1.....	93
Table 3.2.....	95
Table 3.3.....	96

List of Symbols

A = Area

AFP = Anterior filter pad

AL = Ascending lobe

ANODEV = Analysis of deviance

ANOVA = Analysis of variance

β = Average open pore area

BF = Branchial filters

(BL) s^{-1} = Body length per second

BW = Bow wave

CB = Ceratobranchial

Cil = Cilia see also MC

CT = Computed tomography or connective tissue

D or Dent = Denticles

DCT = Dense connective tissue

D_h = Hydraulic diameter

DL = Disc length

DW = Disc width

E = Filtration efficiency

EB = Epibranchial

FL = Fork Length

FP = Filter plates or filter pore

g = Gravity

GLM = Generalized linear model

GT = Gill tissue

h = height

L = permeability of mesh rakers

LCT = Loose connective tissue

LS = Lateral stay

MC = Microcilia or mucus cells

P = Pressure

P = finger-like projections

P2 = Anterior projection, rostrum to rear tip of pelvic fin

PC = Pulp cavity

Pé = Péclet number

PFP = Posterior filter pad

Pr = Prandtl number

PV = Primary vanes

ρ = Density of seawater

Q = Flow rate

R = Resistance

Re = Reynolds number

SE = Surface epithelium

SEM = Scanning electron microscopy

SmE = Smooth epithelium

SQET = Squamous epithelium

SS = Secondary structure

SV = Secondary vanes

TL = Total Length or Terminal lobe

μ = Fluid viscosity

μm = micron

ν = Kinematic viscosity of seawater

Ves = Vessel

Introduction

The four independent evolutions of filter feeding in cartilaginous (chondrichthyan) fishes presents an opportunity to explore the links between filtration performance and filter morphology both in a theoretical and an *in vivo* context. This group of megaplanktivores includes: 11 species of Myliobatiforms within the family Mobulidae which are: the mantas (*Manta birostris* and *Manta alfredi*) and the devil rays all within the genus *Mobula*; (*M. hypostoma*, *M. munkiana*, *M. rochebrunei*, *M. eregoodootenekee*, *M. kuhlii*, *M. thurstoni*, *M. japonica*, *M. mobular*, and *M. tarapacana*), one species of Orectolobiform (the whale shark, *Rhincodon typus*, in the family Rhincodontidae), and two species of Lamniform sharks from separate families (basking shark, *Cetorhinus maximus* in the family Cetorhinidae and megamouth shark, *Megachasma pelagios*, in the family Megachasmidae). Determining the morphological, mechanical, and performance differences between these fishes is key to understanding how biological filtration occurs in high flow environments. This dissertation addresses several important issues: 1) the use of physical models to test predictions about how filtration mechanisms are related to live performance data and morphology, 2) gross morphological descriptions of gill rakers/filter pads from each species and gill filter micro structure examinations using scanning electron microscopy (SEM), and 3) histological preparations of the gill filter to determine whether the filtration modality is dependent upon elevated levels of mucus secretions often associated with sticky sieve filtration.

The devil rays are the largest of all the rays, the largest of which is the manta ray (*Manta birostris*) which reaches a disc width of 6.7 m and a weight of up to 1360 kg (Bigelow and Schroeder 1953). Like all filter feeding fishes they consume vast numbers of tiny (5-3000 microns) prey by filtering immense quantities of water through their oropharyngeal cavity (Smith and Sanderson, 2007; Friedland et al., 2006; Cheer et al., 2001; Sanderson et al., 1994). Mobulas

can be found world-wide in tropical and subtropical areas; however, their individual distributions are not well characterized. Mantas occur worldwide in tropical and subtropical regions and occasionally migrate into temperate waters, although they are observed primarily in near-shore environments (Last and Stevens 1994). Mantas have also been observed at seamounts and are even encountered far from shore in the open sea (Bigelow and Schroeder 1953; Last and Stevens 1994; Compagno 1999). Some of the best information available on distribution patterns within the mantas' broad geographic range comes from photo identification studies that have recorded the occurrence of individuals over time. It appears that local residence patterns are site dependent. In certain regions, the same individual mantas are observed repeatedly over long periods like in Hawaii and Bora Bora, whereas in others like New Zealand, Mexico (Baja California and Holbox), Africa, Ecuador and Southern Japan their occurrence is seasonal (Homma et al. 1997, Duffy and Abbot 2003, Dewar et al. 2008).

The whale shark is perhaps one of the most studied sharks. It is the largest known fish reaching lengths between 12 to 20 m and occurring circumglobally in tropical and subtropical areas (Compagno, 2001). Whale sharks have often been found in large scale aggregations, usually when their preferred prey are found in abundance; these aggregations have been documented in: Belize (Heyman et al., 2001), Ningaloo Reef (Taylor, 1989, 1994, 1996), the Sea of Cortez (Eckert and Stewart, 2001; Nelson, 2004), KwaZulu-Natal (Beckley et al., 1997), Kenya, the Galapagos, Veraval in India (Vivekanandan and Zala, 1994) and Mexico (personal observation). Unlike the other three lineages of filter-feeding elasmobranchs, whale sharks employ both suction feeding (Compagno, 1984) and ram suspension feeding (Taylor, 2007) to capture their prey. The particular mechanism of feeding technique in use at any given time is likely the product of how abundant the aggregation of prey is (Nelson, 2004).

The basking shark is the second largest fish reaching total lengths of up to 12 m and 4 tons (Sims, 2008). Basking sharks inhabit boreal to warm temperate waters including: coastal areas from Newfoundland to Florida and from southern Brazil to Argentina (Compagno, 1984; Tomás and Gomes, 1989; Wood, 1957), Iceland, Norway and as far north as the Russian White Sea, the Mediterranean, from the western Cape province and South Africa (Compagno, 1984; Konstantinov and Nizovtsev, 1980), in the Pacific Ocean from Japan, the Koreas, China, Australia, New Zealand, from the Gulf of Alaska to Baja California, and Peru and Chile (Compagno, 1984). Unlike the other two filter feeding sharks, the basking shark is an obligate ram suspension feeder and primarily feeds upon calenoid copepod prey (Matthews and Parker, 1950; Sims, 2008). Like whale sharks, basking sharks have been spotted in large aggregate feeding groups (up to 200 to 400 individuals) when their preferred prey is abundant (Doyle et al., 2005).

The mega mouth shark is one of the rarest species of shark with on approximately 50 specimens ever discovered (Nakaya, 2010). The mega mouth (so named because of its enormous mouth compared to its body) grows to approximately 4 m and is predicted to feed via engulfment feeding (Nakaya, 2010) or suction feeding (Compagno, 1990); however a feeding event has not yet been observed. Their distribution is unknown although specimens have been collected off Hawaii (Taylor et al, 1983), Japan (Nakaya, 2010), California (Nelson et al., 1997), Australia (Berra & Hutchins 1990 & 1991) and Mexico (personal observation).

Working with these large fishes is a challenge and the following chapters represent work based in the lab and on museum specimens, but I have also made an effort to base my investigations on the natural history of the animals and their performance in the field. To this end, I collected from whale sharks and manta rays feeding in the Yucatán as a member of

Proyecto Manta de Caribe. We shot video of whale sharks and manta rays feeding during seasonal upwelling events off Isla Holbox, Mexico, measured their cruising speeds while actively feeding in plankton blooms, and attached Pop-off Satellite Archival Tags to five manta rays (Andrea Marshall = 2, Misty Paig-Tran = 3) to determine their large scale movement patterns, temperature preferences, and depth preferences.

Study area

Isla Contoy is located between $21^{\circ} 27'$ and $21^{\circ} 32'$ latitude, and between $86^{\circ} 46'$ and $86^{\circ} 47'$ longitude. It is located in the state of Quintana Roo and belongs to the town of Isla Mujeres. It represents the last part of the reef system of the Yucatán Peninsula and is one of the Caribbean islands that preserves an intact ecosystem. The island is a refuge for marine birds and for aquatic endangered species. It is influenced by the Yucatán current and is associated with seasonal upwellings. The only humans allowed on the island are the field station managers and scientific workers.

Isla Holbox is in the Yum Balam marine protected area. It is located between $21^{\circ} 43'$ and $21^{\circ} 14'$ latitude, and between $87^{\circ} 32'$ and $87^{\circ} 07'$ longitude. It is also in the state of Quintana Roo and belongs to the town of Lázaro Cardenas. The area has a lot of endemic, rare and endangered species such as the Mexican crocodile, manatees, dolphins, turtles, whale sharks and seabirds. Holbox is also affected by the Yucatán current. In contrast to Isla Contoy there is no management plan in place.

Telemetry

At the end of the manta season (Sep), two manta rays were tagged by Andrea Marshall and Silvia Hinojosa (2010) and three mantas were tagged by myself, Nick Wegner, and Silvia

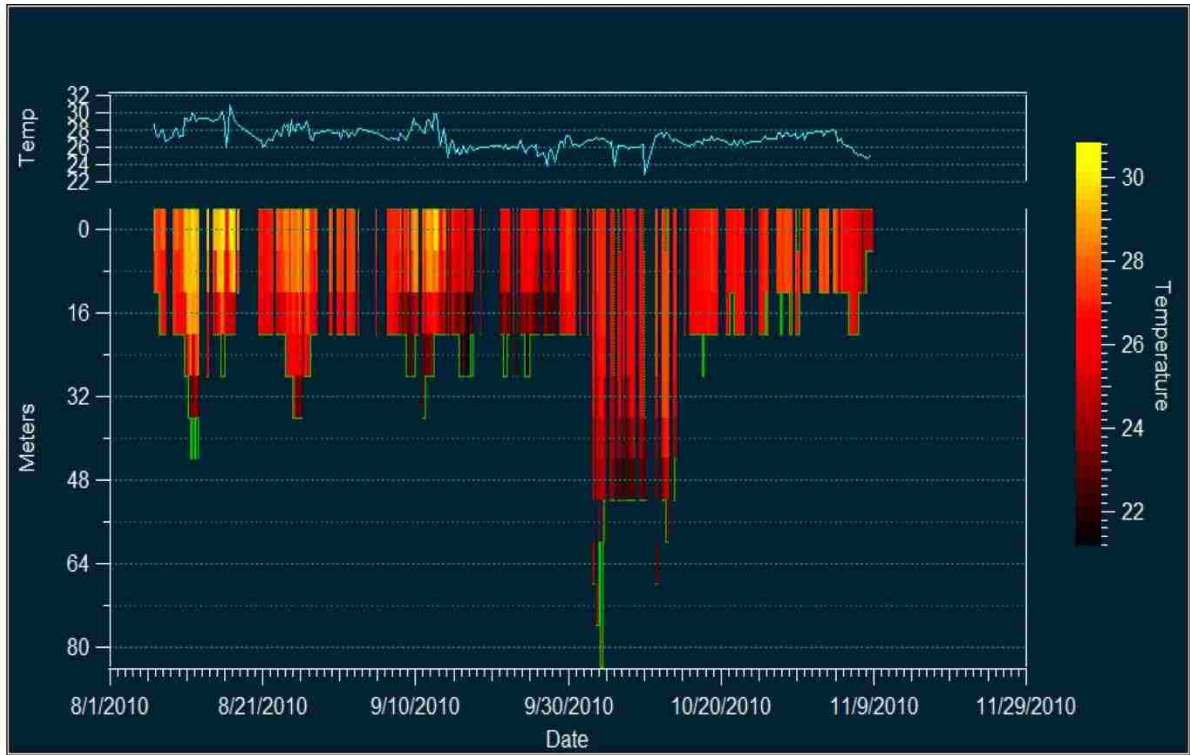
Hinojosa (2011) using Pop-up Archival Tags (PAT), model MK10 (Wildlife Computers, WA and Microwave Telemetry, MD). These tags allowed us to record measurements of physical parameters manta rays were exposed to over a six month deployment including: temperature, salinity, depth, and light based geolocation. The tags were secured to the mantas using large titanium darts that were attached to the tag using monofilament line and stainless steel crimps. The darts were inserted in the pectoral fin musculature using a modified spear gun. Once the mantas were tagged, their behavior, estimated size and other measurements were noted. The PAT tag remained attached to the manta rays for a duration of three to six months at the end of which, the tag was programmed to detach from the animal and float to the surface. Once at the surface, the tag uploaded its location to an orbiting Argos satellite. All tags successfully transmitted data but no tags were recovered following pop off.

Initial findings

We found that manta rays and whale sharks are ram filter-feeders (although whale sharks also employ suction feeding when swimming in lower density plankton patches). This means the animals swim through a plankton bloom with their mouth open, continuously filtering food particles as they go. Ram filtering is different from suction feeding where an animal will initially target its prey and then creates a negative pressure within the buccal cavity prior to opening its mouth. This creates a suction force directed into the mouth upon opening. Speed data indicated that manta rays and whale sharks swim through plankton patches at different speeds: 0.68 m/s average in manta rays and 1.1 m/s average in whale sharks.

Our manta ray tagging data showed that mantas spend the majority of their time at the ocean surface (usually in the top 20 meters) within a narrow temperature range (between 24-30°C) (Figure 1.1). They migrate in toward Isla Holbox and Isla Contoy during the summer months

(May-September) to take advantage of the productivity pulse observed during the seasonal upwelling events (CONANP, 2008). During the fall, manta rays move farther off shore into the Gulf of Mexico. Unpublished stable isotope data ($\delta^{15}\text{N}$ and $\delta^{13}\text{C}$ as well as fatty acids) and plankton towing data from Hinojosa et al. showed that although manta rays and whale sharks feed within the same planktonic patches, they are targeting very different prey: whale sharks target tunny eggs while manta rays primarily target zooea larvae and sergestids. This revelation inspired a central question: Is there a link between filter morphology and filtration performance in the cartilaginous fishes and if so, can we predict prey preferences and/or movement patterns based on their morphology?



PTT 88229

Figure 1.1 Representative temperature/depth profiles for manta rays. Temperature and depth profiles are shown for a manta tagged in 2010 during a four month deployment. The animal spends the majority of time in surface water less than 20 m deep and within a narrow temperature range (24-30°C).

Chapter 2: Bottles as models: Predicting the effects of swimming speed and morphology on size selectivity and filtering efficiency in fishes

Chapter 2 was published in the Journal of Experimental Biology in 2011

Abstract

We created physical models based on the morphology of ram suspension feeding fishes to better understand the role morphology and swimming speed play on particle retention, size selectivity, and filtration efficiency during feeding events. We varied the buccal length, flow speed and architecture of the gills slits; including the number, size, orientation and pore size/permeability of our model. Models were placed in a re-circulating flow tank with slightly negatively-buoyant, plankton-like particles (~20–2000 μm) collected at the simulated esophagus and gill rakers to locate the highest density of particle accumulation. Particles were captured through sieve filtration, direct interception, and inertial impaction. Changing the number of gill slits resulted in a change in the filtration mechanism of particles from a bimodal filter, with very small (>50 microns) and very large (>1000 microns) particles collected, to a filter that captured medium sized particles (100–1000 microns) collected. The number of particles collected on the gill rakers increased with flow speed increased and skewed the size distribution towards smaller particles (50–500 μm). Small pore sizes (105 and 200 μm mesh size) had the highest filtration efficiencies, presumably because sieve filtration played a significant role. We used our model to make predictions about the filtering capacity and efficiency of neonatal whale sharks. These results suggest that the filtration mechanics of suspension feeding are closely linked to an animal's swimming speed and the structural design of the buccal cavity and gill slits.

Key Words: Physical models, ram filter-feeding, *Rhincodon typus*, filtration efficiency, feeding selectivity

Introduction

Filter-feeding elasmobranchs are a highly migratory and large-bodied group of fishes; these combined factors make it difficult to investigate their prey capture mechanisms in a laboratory setting or *in situ*. This type of information is important, however, because the size and type of prey that are filtered are often a determinant of distribution in these poorly known fishes (Sims and Quayle, 1998; Sims, 1999). Furthermore, prey capture and food preference in pelagic elasmobranchs represent foundational data for models that predict migratory patterns, and are used to assess and maintain well-managed fisheries stocks, especially in areas where they are harvested heavily with little regulation (Coleman, 1997; Dewar, 2002; Stevens, 2007; Dewar et al., 2008).

Filter-feeding fishes consume vast numbers of tiny (5–3000 μm) prey by passing immense quantities of water through their oropharyngeal cavity (Sanderson et al., 1994; Cheer et al., 2001; Friedland et al., 2006; Smith and Sanderson, 2007). The mechanics of cartilaginous filtration are likely similar to that of smaller ram filtering fishes — swimming forward with an open mouth, ingesting food particles, and expelling water out the gill openings. Food particles may be trapped on gill rakers and transported to the esophagus. Alternatively, food particles might be entrained and concentrated without ever contacting the gill rakers. Using invertebrate filter-feeders as a model system, Rubenstein and Koehl (1977) and later LaBarbera (1984) and Shimeta and Jumars (1991) described five basic mechanisms by which particles ranging in size from 10^{-7} to 10^{-1} cm can be passively intercepted by a fibrous biological filter. These are: 1) sieving, 2) direct interception, 3) inertial impaction, 4) gravitational deposition, and 5) diffusion deposition.

In sieve filtration, particles that are larger than the pore size of the filter cannot pass through the mesh and are retained, whereas particles smaller than the pore size pass through (Fig 2.1A) (LaBarbera, 1984). In industrial dead end sieving, the filtering medium is positioned to lay perpendicular to the fluid streamlines causing particle deposition to occur either along the filter's surface or as the fluid moves through the filtering element (Sibanda et al., 2001). It had been assumed that filtering fishes sieve their planktonic prey, but this notion was refuted by gut content studies showing prey sizes smaller than the distance between gill rakers (Langeland and Nøst, 1995). In the remaining mechanisms of filtration, particles smaller than the filter's pore

size are captured by direct contact with the filtering element (LaBarbera, 1984; Shimeta and Jumars, 1991). Direct interception is the most common form of particle capture among marine invertebrate filter-feeders (Rubenstein and Koehl, 1977). This occurs when a neutrally-buoyant particle following a streamline comes within one particle radius of a filtering fiber, where it adheres to mucus or some other adhesive surface. Conversely, in inertial impaction, a sharp turn in the fluid streamline causes a negatively-buoyant particle to leave the streamline and impact a filtering surface (Rubenstein and Koehl, 1977). Gravitational deposition is similar to inertial impaction except that particles are not separated from the fluid by a sharp acceleration of the streamline, but rather by a constant gravitational force (Rubenstein and Koehl, 1977; LaBarbera, 1984; Shimeta and Jumars, 1991). Finally, in diffusion deposition, very small particles deviate from the streamlines because of random Brownian motion (Rubenstein and Koehl, 1977; LaBarbera, 1984; Shimeta and Jumars, 1991). This method captures particles smaller than those that are important for ram filter-feeding organisms.

Fishes filter-feed at higher Reynolds numbers than invertebrates, and two additional methods should be considered: cross-flow filtration and vortex filtration. Industrial cross-flow filtration takes advantage of the shear generated by fluid flow parallel to the surface of a filter to clear the filter mesh of trapped particles and concentrate them at the end of the filter chamber (Bott et al., 2000; Sibanda et al., 2001). This has been hypothesized to work in some filter-feeding fishes, when ingested food particles do not contact the gill rakers; instead, they travel parallel to the surface, eventually concentrating near the esophageal opening (Fig. 2.1B) (Brainerd, 2001; Sanderson et al., 2001, Callan and Sanderson, 2003). The final method of filtration that should be considered is vortex or hydrocyclone filtration (Fig. 2.1C). In this case, water and food particles would enter through the mouth and enter into a bilaterally symmetrical vortex near the internal gill openings. Water would then exit out the gill slits and food particles would be collected near the esophagus, or re-suspended inside the buccal cavity, increasing the chances of collision with sticky surfaces near the esophageal opening. The mechanics behind this are best appreciated by an analogy to a common household vacuum. Some bagless models use vortex filtration where dirt laden air is entrained in a vortical flow inside a cylindrical or conical chamber. The rotation of the fluid establishes a radial pressure gradient exactly sufficient to maintain a circular trajectory for a neutrally-buoyant particle. However, this pressure gradient is insufficient to maintain a circular trajectory for negatively-buoyant particles,

which subsequently accumulate near the periphery (Trakumas et al., 2001). The densest and largest particles will be expelled early in the cyclone whereas the smaller and less dense particles will only be expelled with a narrowing vortex. The clean air then passes back through the center of the vortex and exits out the top of the cylinder.

We faced an interesting challenge — a range of possible filtration types with associated differences in prey capture mechanisms and efficiencies and a set of fishes that is both morphologically diverse and experimentally intractable. We suggest that simple physical models are the best routes to investigate an initial set of predictions about filtration efficiency and prey size selectivity. We therefore tested a model of the open mouth of a ram filtering “fish” that samples particles both from an “esophagus” and from a set of “gill slits” equipped with “gill rakers”. We expected this model to give us qualitative insight into the effect that varying morphological (e.g. gill slit number, size, angle, and buccal length) and physiological (e.g. flow velocity) parameters had on efficiency and selectivity.

Our goals in this study were to: 1) show that a simplistic physical model loosely based on a filter-feeding elasmobranch allowed us to measure trends in size selectivity and efficiency of particle capture; 2) determine the effect of changing swimming speed on the size distribution of captured particles; 3) determine the effect of varying morphology, including gill slit number, gill slit orientation, gill permeability, and buccal depth on the size distribution of captured particles; 4) test the relative importance of the gill rakers and the esophagus in particle capture and 5) use measurements and inferred swimming speeds from neonatal whale sharks to predict their ability to filter different sized prey items from the water column.

Materials and Methods

Anatomy of the Filtration System

Four neonatal whale sharks, *Rhincodon typus*, were obtained from the Marine Vertebrate Collection at Scripps Institute of Oceanography. We measured each shark’s total length (TL), fork length (FL), gill width when the gill opening was fully stretched (GW), gill height (GH), distance from the opening of one gill slit to the next (DB), mouth height (MH), mouth width (MW), and total distance from the leading edge of the mouth to the esophageal sphincter, or

oropharyngeal distance (OD). We also measured the distance between the gill rakers which we refer to as pore size. Gill width, gill height and distance between gills were expressed in order from gill one (closest to the mouth) to gill five. The four neonatal whale sharks ranged in size from 533–591 mm TL and 439–468 mm FL (Table 2.1). It is important to note that the simplistic model is only loosely based on the anatomy of the neonatal whale sharks. The model's purpose is to understand how differing fish morphologies affect filtration efficiency and size selectivity. To accurately predict the prey of neonatal whale sharks, we would suggest using a model that more closely resembles this fish, e.g. a 3D rapid prototyped model based on computed tomography scans.

Predicting Swimming Speed

To determine the average swimming speed of neonatal whale sharks, we compared log-transformed length data from measured whale sharks (TL or FL) to log-transformed average swimming speeds of both sharks and bony fishes compiled from published literature (see supplemental section). The relationship between fish length and swimming speed was analyzed using a linear regression (SPSS Statistics 16). It is important to note that adult filter-feeding sharks appear to swim at slower speeds (body lengths/second \ll 0.1) compared to other sharks and bony fishes. However, since swimming speeds have never been measured on neonatal whale sharks, we based our predictions on the relationship between an organism's size and known swimming speeds, not on those of adult filtering sharks.

Filtration Models

To estimate the effects on filtration efficiency from individual parameters, we constructed models of a ram suspension feeding fish roughly based on morphological measurements of neonatal whale sharks (photos of ram feeding adult whale sharks available in the supplemental section). Our simple cylindrical models were created from 1 L soda bottles with the bottom cut off so that the mouth of our model had an 8.5 cm diameter. A cylindrical model was selected over a conical model based on both our observations of filter-feeding adult whale sharks in the Yucatan and following observations of ram filter-feeding bony fishes by Sanderson (Cheer et al.;

2001) who noted that gill arch abduction during ram feeding resulted in the oral cavity of the fish becoming more cylindrical in appearance. The length of the bottles was 23.0 cm including the neck of the bottle and 19.5 cm without the neck. We plugged the neck of the bottle with a rubber stopper to simulate a closed esophageal sphincter. A 4 mm diameter tube was inserted through the stopper so the leading edge was exposed to the posterior buccal cavity. The end of the tubing outside of the bottle was connected to a peristaltic pump to simulate particle ingestion through the tubing at a constant rate of 8.2 mL/min. Gill openings were cut with polyethylene mesh of various sizes to simulate different gill resistivities.

For the experiments we started with a standard model that was similar to the morphology measured for neonatal whale sharks with a few adjustments: four gill openings (which is intermediate between bony fishes (with a singular opercular opening and five gill slits with four gill arches on each side of the pharynx) (Harder, 1975) and the elasmobranches (with 5–7 gill slits and typically 5 gill arches on each side of the pharynx) (Butler, 1999), 90° gill orientation to the midline of the bottle (Cheer et al., 2001), gill width = 0.5 cm, gill height = 4.5 cm, buccal cavity (mouth to final gill opening) = 19.5 cm or 23 cm from mouth to esophagus, 1000 µm mesh net covering the gill openings (measured in neonatal whale sharks), and flow speed = 45 cm/s. We then systematically manipulated the gill number (1, 2, 3 and 5 gill openings) as there is some evidence that elasmobranch parabranial chambers receive varying amounts of water flow and have differing levels of oxygen extraction (Piiper and Schumann, 1967; Ballintijn, 1972; Summers and Ferry–Graham, 2001) gill orientation (0° and 55° orientation to the midline similar to Cheer et al., 2001), and permeability (no mesh, 105, 200, and 2000 µm to represent differing pore sizes of fishes. The 105 µm and 200 µm mesh sizes were similar to the width between rakers measured in smaller teleosts [e.g. herring (Gibson, 1988) *Singidia tilapia*, (Goodrich et al., 2000) Japanese anchovy, Pacific round herring, and Japanese jack mackerel (Tankaka et al., 2006)] and the larger mesh size (1000 µm) was similar to those measured from neonatal whale sharks (Motta, 2010). Gill size was increased to 1.5 cm width, representing the enlarged gill slits of the basking shark, buccal length was decreased to test for differences in ontogeny (decreased to 15 cm total, 12 cm buccal), and flow speed was increased (fish swim speed) for each gill number variation (increased to 60 cm/s).

Adjusting each feeding parameter separately allowed us to test our initial hypotheses about how differing morphologies affect filtering performance. In all treatments, we would expect that the majority of particles collected would be larger than the mesh size if direct interception is the primary mechanism of filtration and a mixture of particle sizes if other mechanisms of filtration are occurring. We would predict that if cross flow filtration is occurring, the majority of particles would be trapped close to or inside the esophagus. We hypothesized that increasing the swimming speed should increase the filtration efficiency since more particles will come into contact with the filtering elements if some form of direct interception or inertial impaction is occurring. Similarly the filtration efficiency should also increase with smaller mesh sizes. We predicted that the slanted gill orientation would affect the flow through the buccal cavity and may alter the mechanism of filtration similar by creating a vortex near the third or fourth gill slit. We predicted that reducing the buccal length would result in higher flow through the buccal cavity, creating additional turbulence near the gill slits. This additional turbulence may result in suspending the particles for longer periods of time, reducing the number of particles that come into contact with the filtering medium hence reducing the filtering efficiency. Finally, we predicted that increasing the gill slit size would increase the surface area for filtration resulting in increased filtration efficiency.

The models were based on the morphology of the neonatal whale sharks with a few key exceptions. The gill widths were measured by adjusting the gill flaps so that they were fully open during measurements. However, in all but one trial, we adjusted our bottle's parameters so that only a portion of the flap would be open during feeding since it is unlikely that these gill coverings are fully stretched during a feeding event. Mouth height and width remained fixed in all models. It is also important to note that filter-feeding sharks have a variety of mouth shapes and heights. We chose a cylindrical version to model, but adjustments to the mouth morphology may lead to differences in size selectivity and filtration efficiency.

Filtration Experiments

Experiments were carried out in an 80 cm x 28cm x 28cm re-circulating fresh water flow tank, 42 cm x 28 cm x 28 cm working area, 260 L total volume. The model was secured in the center of the tank using fishing line which was anchored above the tank. To mimic plankton,

we milled 20 mm poly(methylmethacrylate) (PMMA) cylinders to produce slightly negatively-buoyant, irregularly-shaped particles (density 1.14 g/cm^3) ranging in size from 20–2000 μm . Density for marine copepods have been estimated at 1.027 to 1.047 g/cm^3 (Knutsen et al., 2001). The size classes chosen were based on the series of meshes used during the experiments (e.g. 100 μm , 200 μm , 1000 μm , 2000 μm). These size classes also coordinate with those typically seen in plankton assemblages (e.g. $>1000 \mu\text{m}$ are the largest zooplankton, 500–1000 μm = large zooplankton and ichthyoplankton, 100–500 μm = microcrustaceans, 50–100 μm = net phytoplankton and small zooplankton, and 10–50 μm = nanoplankton) (Moloney and Field, 1991). The use of non-spherical particles does cause some complications in understanding how the particles react within the flow (e.g. their orientation), however we believe that using particles similar to those collected during an actual feeding event gives us a better understanding of how plankton would be captured along the gill rakers or at the esophagus. Sixty grams of particles were added to the flow tank and allowed to circulate for one hour prior to experimentation to approximate equal distributions throughout the tank. The initial seeding density was collected and measured so that we could compare the particle size distributions in individual experiments to the total size distribution within the tank. The tank was only seeded a single time during these experiments since the particles collected during all 64 experiments were less than 3% of the total particles within the flume.

The model was oriented with the gape facing into the flow, mimicking the conditions experienced by a ram filtering fish during a feeding event (Fig. 2.2). Particles moved through the buccal cavity and were collected either on the “gill rakers” or inside the “esophagus.” Esophageal particles were pumped through the tube and were captured in an external flask. The bottles remained in the flow for a total of three minutes, a period chosen because there was very little clogging of any mesh size during this brief exposure. During elasmobranch feeding events, raker clogging is likely prevented by periodic swallowing of the collected plankton. At the end of the experimental run, the leading edge of the bottle was covered and particles that remained on the mesh and those contained in the external flask were collected. Each experiment was replicated four times for a total of 64 experiments.

Permeability Measurements

Permeability measurements of the entire gill structures were performed on intact neonatal whale sharks. Each shark was placed in a 153 L ice chest filled with distilled water. Water was pumped out from the ice chest at a constant flow rate of 114 mL/sec, with a Flojet Model 2100–953–115 pump into a 4.41 L cylindrical (441 cm³) tank which functioned as a manometer. Water flowed gravimetrically from the cylindrical tank into the neonatal shark's buccal cavity using 1.4 cm diameter plastic tubing. The tubing was inserted into a mask that sealed within the shark's mouth (the mask was constructed from closed–cell polyurethane foam for larger individuals and molded silginate for small individuals) so that the resistance of the gill openings could be estimated by the change in water column height (pressure) in the cylindrical tank. We calculated the resistance of a neonatal whale shark's buccal cavity using the equation:

,

where R = the resistance through the gill structure, ΔP = the change in pressure estimated by measuring the change in water height of the manometer when the shark was attached to the tubing, and Q = the flow rate. These measurements helped us to determine whether the entire gill structure (including the gill filaments which were ignored during these trials) had a high level of resistance to flow. The change in pressure (ΔP) is:

$$\Delta P = \rho gh,$$

where ρ = density of water, g = gravity, and h = the average change in height of the manometer. This equation allowed us to estimate the permeability of the gill structures in preserved neonatal whale sharks (n = 3, as one shark could not be measured) within an order of magnitude. We compared the whale shark's permeability measurements to those measured from neonatal specimens of three additional filter–feeding elasmobranchs, *Mobula munkiana* (n=2) and *Mobula japonica* (n=1)

Reynold's flow (Re), the ratio of inertial to viscous forces, is an important component when attempting to quantify the effect of a filtering element on the flow around it (Shimeta and Jumars, 1991). Reynolds conditions at the level of the gill slits were calculated using the standard equation:

where Q = flow at the level of the gill slits, L = permeability of the mesh rakers, ν = the kinematic viscosity, and A = the total area of gill openings.

Data Analysis

We assessed the initial distributions particle sizes by homogenizing the milled (seeding) particles, collecting a large sub sample ($n=10,395$ particles), and determining its size distribution. Following trials, we also sub sampled from the particles collected on the gill rakers. All esophageal particles were measured because of the relatively small number collected there. We recognize that errors in plankton sub sampling are common (van Guelpen et al., 1982); however these errors are reduced by increasing sampling size. Our seeding sub sampling is based on over 10,000 particles for a total of 6 separate sub sampling events. Experimental trial data were based off of five separate sub sampling events from each replication (or 20 sub sampling events). Trial run order was chosen haphazardly except that some 45cm/s trials were run prior to 60cm/s trials and some were run after. The initial 45 cm/s trials for all replicates were as follows: 1 gill trials, 55° orientations, 3 gill orientations, 2 gill orientations, 5 gill orientations, no meshes, and 2000 μm meshes. Next we ran all 60cm/s trials in the following order: 5 gills, 1 gill trails, 3 gills, 4 gills, 2 gills. And finally we ran the final 45 cm/s trials: 4 gills, 105 μm , small buccals, 200 μm s, and increase gills.

To ensure that particle distributions within the flume remained similar over time (e.g. to ensure that larger particles did not settle out of the water column), we performed a separate sampling experiment. Once again we milled 60 g of particles, sub sampled from the initial seeding density, allowed the particles to circulate within the running flume at 45 cm/s for 1 hour prior to sub sampling, and then sub sampled particles for one minute at 30 min intervals for a total time period of 240 min (times: 0, 30, 60, 90, 120, 150, 180, 210, 240 min) using a 105 μm net. Following the same sampling techniques as the experiments, we compared the sub samples the initial seeding density distributions. We compared the distributions first excluding particles $< 100 \mu\text{m}$ and again excluding $< 50 \mu\text{m}$ to reduce errors from sampling with a net that is larger than two of our particle size categories and because we are primarily interested in understanding

how the distributions of the larger zooplankton change, not the distributions of nanoplankton and phytoplankton which is not the food sources being targeted. The differing size classes of plankton are referred to as followed: 1–50 = very small, 51–100 = small, 101–500 = intermediate, 501–1000 μm = large, >1000 μm = very large. We performed a weighted linear regression of the combined percentage of intermediate, large, and very larges collected during sub sampling events over 240 min.

All sub samples were collected, mounted on slides so that the particles didn't touch, and analyzed for size distribution using a Zeiss steREO Discovery V20 microscope (Carl Zeiss Imaging GmbH, Germany). Particles were viewed in the microscope imaging program Axio Vision and photographed using a Zeiss AxioCam HRC camera. Photos were then uploaded onto NIH Image J software (version 1.4, <http://rsbweb.nih.gov/ij/>) for analysis. We measured the total area and the mean Feret's diameter for each particle in the sub samples (n = 10, 395) of the seeding particles and the experimental trial subsamples. Although creating a continuous scale for these particles would give us a more in depth visualization of their actual size distribution, we determined that binning particles into size classes was an easier way to visualize trends in particle capture and to discuss these sizes based on actual plankton size classes. The color scheme for sizes classes will remain constant throughout all histogram figures (Figs. 4–8).

Filtering efficiency was determined by weighing air-dried particles for each replication of the trials. We expressed data as average efficiencies for all four trials. The weights of the collected particles were small compared to the seeding density, so we expressed efficiency values as an amount per thousandth (‰) rather than as a percentage. Filtration efficiency (E), or the percentage of weight-specific particle capture per three min trials, was calculated by using the equation:

,

where W_P = the weight of the particles either at the esophagus or at the gill rakers and W_S = calculated total weight of the seeded particles within the flume that are predicted to flow through the model's aperture. This allowed us to get a snapshot of the amount of particles (by weight) being filtered within a relatively short amount of time. Since we had such a small amount of

particles collected per trial, we will express the filtering efficiencies as total efficiency over the full 12 minutes. Note that filtration efficiency is used as a proxy for determining the amount of particles (by weight) collected along the gill rakers over 12 min compared to the amount of particles available in the flume. Our filtration efficiency calculation is similar to methods of industrial filtration efficiency, which is expressed as $[(1 - (\text{the number of particles concentrated downstream/upstream concentration})) \times 100]$. This is vastly different from filtering efficiencies expressed in live fishes (Drenner and Mummert, 1984; Garrido et al., 2007).

We predicted that changing the morphology (i.e., gill number, raker permeability, buccal length, gill-slit orientation, and gill size) and/or the swimming speed of the model would affect the size distribution of particles collected along the gill rakers; therefore we hypothesized that particle distributions collected during the experiments would not be the same as the seeding distribution. To test this hypothesis, four replicates of each version of the physical model were compared to six replicates of the initial seeding distribution among the five particle size categories. The various physical models were then compared to the basic model (4 gill slits, 45 sec/cm flow) in the same manner to further evaluate the effects of model alterations.

Poisson regression was used to determine if particle distributions differed significantly between the seeding distribution and the various physical models, and between the basic physical model and the other model variants. The generalized linear model (GLM) used in comparisons was of the basic form: $\log(\#particles) = \text{source} * \text{size category}$, and was analyzed using Analysis of Deviance (ANODEV; Skalski, 1996). The process of analyzing GLMs with ANODEV is analogous to analyzing linear models with ANOVA, but more appropriate for the replicated contingency table design used in this study. The scale parameter ($MDEV_{Error}/DF_{Error}$) of the interaction term was calculated from ANODEV results to determine the amount of dispersion. For overdispersed data (scale parameter > 1), F -statistics were calculated; whereas X^2 statistic were considered to be more appropriate when data were underdispersed (scale parameter < 1).

Results

Swimming speed

Swimming speed decreased significantly with length based on the available teleosts and elasmobranch data ($r^2 = 0.59$, $p < 0.001$) (Fig. 2.3). This relationship was best represented by the following equation: Swimming Speed (bl/sec) = $18.30x^{-0.78}$. Based on these results, we predict that a neonatal whale shark of approximately 50–60 cm TL swims at approximately 1 body length per second, or 45–56 cm/s.

Flume seeding

We found that intermediate, large and very large-sized particles remained suspended in the water column throughout the full 240 min trials; therefore particle settling was not a factor ($r^2 = 0.01$, $p = 0.79$) (see supplemental material). Our initial seeding distribution of particle sizes in the re-circulating flume was primarily composed of intermediate sized particles between 101–500 μm in diameter (Fig. 2.4A). Seeding distributions are represented as a percentage of the total particles \pm SD that were sub sampled ($n = 10,395$) from the 60 g of seeding particles.

Standard model

Our standard model collected particles in the intermediate to large size ranges (between 100–1000 μm) at the esophagus and large size particles (501–1000 μm) at the gill rakers (Fig. 2.4B and 2.4C respectively). Reynold's number at the level of the filtering elements was calculated to be $Re = 1.4 \times 10^5$. Compared to our seeding density, there was a three-fold increase in large particles sizes (501–1000 μm) collected at the esophagus (Fig. 2.4D) and a two-fold increase in large particles at the gill rakers (Fig. 2.4E) even though there were almost twice as many 101–500 μm particles seeded in the tank. Comparisons of the seeding distribution treatment to the standard model at all five seeding categories showed that the distribution of particles collected at the gill rakers were statistically different increase in the large and very large particles from the initial seeding morphology ($F_{(4,40)} = 4.71$, $p < 0.001$). This was characterized by a two-fold increase in very large ($>1000 \mu\text{m}$) particles collected along the rakers. The filtration efficiency for esophageal particles was very low (Total particles collected $n=135$, $E=0.006\%$) and much higher at the rakers ($E=0.56\%$). Since there was very little filtration occurring in the esophagus, we will focus on the particle capture at the gill rakers. Therefore, we

conclude that our model is not evenly collecting particles from the tank, instead, there is selective filtering.

Gill Number

The majority of particles collected in the esophagus for all permutations of the model were in the intermediate size ranges, as in the control model. Few particles were “swallowed” at the esophagus in any of the five treatments (n= 19–226 total particles over four replicates) and the average total efficiencies over all five variations was extremely low ($E < 0.01\%$ total). We did observe a very slow moving esophageal vortex during the trials that increased in speed as we increased the number of gill openings. Additionally, with four and five gill opening permutations, we noticed an increase in the number of particles collected in the esophagus (n > 100) compared to 1, 2, and 3 gill slit treatments. When we increased the experimental number of gill openings to four or five, there was turbulence near the esophageal opening; however, we could not determine whether it was a single vortex or a pair of vortices. This turbulence was rather slow-moving during one and two gill permutations and appeared to increase in speed in higher slit permutations.

Examination of the particles collected at the gill rakers showed a shift in particle distribution from the initial seeding distribution (Fig. 2.5). Reynolds numbers for 1, 2, 3, 4, & 5 gill slits were: 5.6×10^5 ; 2.8×10^5 ; 1.9×10^5 ; 1.4×10^5 ; and 1.1×10^5 , respectively. In the one gill slit model, the particles collected on the rakers were mostly small (50–100 μm) or large to very large (50–100 μm) and the distribution was statistically different from the seeding distribution ($F_{(4,40)} = 8.16$, $p = 0.003$). As we increased the number of gill openings, the size distribution of particles collected shifted to large to very large particles (>500 μm) and all permutations except 3 gills were significantly different from the seeding distribution (2 gills $F_{(4,40)} = 3.67$, $p = 0.01$; 3 gills $F_{(4,40)} = 2.40$, $p = 0.07$; 4 gills $F_{(4,40)} = 4.71$, $p = 0.003$; and 5 gills $F_{(4,40)} = 10.63$, $p < 0.001$).). The physical model transitioned from behaving as a bimodal type filter that collects particles in two narrow size ranges to an intermediate type filtration system that collects particles in a much broader size range. Although our method precluded a quantitative examination of the filtering performed at each opening, certain trends in particle deposition were evident. During the two-gill-opening trials, more particles were caught in the

first gill opening (the opening closest to the mouth of the model) than on the second opening, whereas in the three–gill trials, particles were captured primarily at the third gill opening. Particles appeared evenly distributed across all slits in the four and five–gill opening trials.

Throughout all trials we collected fewer very small ($< 50 \mu\text{m}$) and intermediate sized particles ($101\text{--}500 \mu\text{m}$) compared to the seeding distribution; however, each trial also collected more large and very large sized particles ($501\text{ to } >1000 \mu\text{m}$) than expected. Filtration efficiency decreased during the first three trials and then increased during the four and five gill trials. The total efficiencies from each trial were as follows: 1 Gill (0.34‰), 2 Gills (0.25‰), 3 Gills (0.11‰), 4 Gills (0.56‰) and 5 Gills (0.52‰).

Comparisons of the standard model to the 1,2,3, and 5 gill slit trials showed that the distributions from all but the 2 gill permutation were significantly different from the standard model (1 gill $F_{(4,30)} = 6.71$, $p = 0.001$; 2 gills $F_{(4,30)} = 1.65$, $p = 0.19$; 3 gills $F_{(4,30)} = 7.02$, $p = 0.004$; 5 gills $df = 4$, $\chi^2 = 46.28$, $p < 0.001$). The distributions of small and intermediate particles were similar to the standard model except there was a 20% increase in intermediate particles in the 2 gill morphology. The proportion of large particles was approximately 11% less than the standard model in the 2 and 3 gill slit trials.

Change in Speed

The total number of particles collected at the esophagus and at the gill rakers were more numerous at faster (60 cm/s) flow speeds. There was a more even distribution of particle sizes both at the esophagus and at the gill rakers (Fig. 2.6) compared to the standard model. Reynolds conditions at 60 cm/s were as follows for 1,2,3,4, and 5 gill rakers, respectively: 7.4×10^5 ; 3.7×10^5 ; 2.5×10^5 ; 1.9×10^5 ; and 1.5×10^5 , respectively. During these trials, increasing the number of gill openings to five slits resulted in smaller particles collected on the rakers than with fewer openings and in all but the five gill trials, had significantly different distributions from the seeding density (1 gill, $df = 4$, $\chi^2 = 6.60$, $p < 0.001$; 2 gills, $df = 4$, $\chi^2 = 5.74$, $p < 0.001$; 3 gills, $F_{(4,40)} = 8.99$, $p < 0.001$; 4 gills, $F_{(4,40)} = 5.71$, $p < 0.001$, 5 gills, $F_{(4,40)} = 1.97$, $p = 0.88$). Fewer gill openings collected particles primarily in the intermediate to large range ($101\text{--}1000 \mu\text{m}$). We noticed the same basic trends that occurred in the 45 cm/s runs (e.g., 1 gill picked up a lot of

particles within 10 to 20 s) and once again the speed of the esophageal vortex/vortices was much faster at four and five gill permutations. More large and very large particles were collected compared to the seeding distribution. At the higher speed, filtering efficiency did not increase with the number of gill slits. The 60 cm/s efficiencies were all lower than the corresponding 45 cm/s treatments (1 gill E = 0.16‰, 2 gill E=0.04‰, 3 gills E=0.02‰, 4 gill E=0.05‰, 5 gills E = 0.04‰).

The distribution of particles from all of the increased speed trials except the 1 gill trial differed significantly from the standard model (1 gill $F_{(4,30)} = 2.63$, $p = 0.621$; 2 gills $F_{(4,30)} = 31.01$, $p < 0.001$; 3 gills $F_{(4,30)} = 3.75$, $p = 0.01$; 4 gills $F_{(4,30)} = 5.65$, $p = 0.002$; 5 gills $F_{(4,30)} = 16.69$, $p < 0.001$). There was an approximately 10% increase in very small particles during the 5 gill trial compared to the standard model. The 5 gill trials collected a higher proportion of small particles (14%) compared to the standard model. There were also a higher proportion of the large particles collected in the 1 gill slit trials (~11%). Finally there was a smaller proportion of very large particles collected in each of the 60 cm/s trials, with the largest difference in the 1 gill trials (~14% less than the standard).

Gill Orientation

Adjusting the gill orientation did not change the distribution of particles collected at the esophagus; however, there was a shift from a band-pass-type filter in the 90° orientation to a notch-type filter in the 55° orientation at the gill rakers (Fig. 2.7A). Reynolds number was the same as in the 90° permutation. Particles collected were primarily very small (<50 μm) or very large (>1000 μm) and the raker distributions were significantly different from the seeding distributions ($F_{(4,40)} = 6.04$, $p < 0.001$). There was no noticeable increase in turbulence near the gill slits with this permutation; however, particle capture occurred primarily along the lower portion of the third and fourth gill openings. The total filtration efficiency for the 55° trials (0.12‰) was much lower than for the 90° trials (0.56‰). The distribution of particles in the 55° orientation model differed significantly from the standard model ($F_{(4,30)} = 17.33$, $p < 0.001$). There was an increase in very small particles collected (~18%) and a decrease in the proportion of intermediate and large-sized particles (~10%, 21% decrease respectively) compared to the standard morphology, resulting in a more even distribution of particles.

Oropharyngeal Cavity

A shortened oropharyngeal cavity did not affect the size distribution of particles collected in the esophagus. Particles collected along the rakers were primarily very small (<50 μm) or large to very large (>501 μm) and the distribution was significantly different from the seeding density ($F_{(4,40)} = 4.28$, $p < 0.001$) (Fig. 2.7B). The shortened morphology resulted in an increased the vorticity inside the buccal cavity as expected; however, we did not predict that there would also be an increased rate of particle ejection out the leading edge of the model. The total filtering efficiency (0.12‰) was much lower relative to the longer buccal cavity permutation (0.56‰). The distribution of particles in the shortened buccal model differed significantly from the standard model ($F_{(4,30)} = 4.72$, $p = 0.004$). There was a slight increase in the proportion of very small particles (~8%) compared to the standard model and the total distribution of particles collected was more even across size ranges.

Increased Gill Openings

An increased gill width decreased the relative contribution of very small particles that were collected in the esophagus from 12% to 3%. The particles collected at the gill rakers were primarily very small to small (<100 μm) or very large (>1000 μm) and the particle distributions along the rakers were significantly different from the initial seeding distributions ($F_{(4,40)} = 3.57$, $p < 0.001$) (Fig. 2.7C). Reynolds conditions were 4.7×10^4 . Filtration efficiency did not increase with increased gill size ($E = 0.21\text{‰}$). The distribution of particles in the increased gill model differed significantly from the standard model ($F_{(4,30)} = 14.09$, $p < 0.001$). There was an increase in the proportion of small (~25%) and a decrease in intermediate and large particles (~15%, 22%, respectively) compared to the standard model.

Permeability

Adjustments to the gill raker permeability did not affect the distribution of particles collected at the esophagus. Particles collected at the esophagus were in the large size range

(500–1000 μm) during all treatments. The distributions of particles collected in the esophagus for the 105 μm and 200 μm mesh were similar to the 1000 μm distribution (mostly 100–1000 μm particles). The amount of particles collected at the esophagus was low compared to those collected along the gill rakers ranging from a total of 10 particles collected over four replications in the absence of gill rakers to a total of 135 particles collected over four replications in the 1000 μm experiments. During the 1000 μm trials we noticed the presence of turbulence near the esophageal opening; however, we could not determine whether this was a bilaterally symmetric vortex or a single esophageal vortex.

Particles collected along the gill rakers at increasing pore sizes displayed a shift in size distribution. At low permeability (small pore size, 105 μm) particles were equally distributed except in the small (51–100 μm) category (105 micron, $F_{(4,40)} = 6.22$, $p < 0.001$) (Fig. 2.8A). Reynolds number was 1.4×10^3 . During these trials, particles were heavily deposited within 10–20 s of the beginning of each experiment. We collected the most particles off the gill rakers during the 105 μm experiments; however, there were almost no particles collected in the esophagus ($N = 30$). Particle deposition appeared to occur only on the first three gill openings and the fourth gill opening rarely had many particles. At 200 μm , there was a shift in the particle distribution to intermediate to large-sized particles (101–1000 μm ; $F_{(4,40)} = 6.88$, $p < 0.001$) (Fig. 8B). Reynolds number was 2.8×10^3 . Again during these runs we had almost no particle collection in the esophagus ($N = 33$ total particles over four replications), and particle capture was equal across all gill openings. During the 1000 μm mesh experiments, capture occurred only along the third and fourth gill openings. Once again there were primarily large to very large-sized particles collected (501 to $>1000 \mu\text{m}$; $F_{(4,40)} = 4.71$, $p = 0.003$), although the total distribution of all particle sizes was more uniform compared to the 200 μm experiments. We did not collect any particles during the no mesh treatment or the 2000 μm mesh trial. Reynolds number was 2.8×10^5 . Reynolds number with no-mesh was 2.5×10^6 . Particles collected in all trials were greater than expected for the large to very large particle sizes ($> 500 \mu\text{m}$) and lower than expected for the small particle sizes ($< 51 \mu\text{m}$). We saw an increase in the proportion of large particles collected compared to the seeding distribution. As expected, the lowest permeability measurements had the highest filtration efficiency of all of the trials ($E = 1.33\%$ for 105 μm and 0.85% for the 200 μm). The distribution of particles in the 100 μm differed significantly from the standard model (100 μm $F_{(4,30)} = 7.427$, $p < 0.001$) while the 200 μm trials

did not differ significantly ($200\mu\text{m } F_{(4,30)} = 1.67, p = 0.18$). There was a decrease in intermediate particles in the $105\mu\text{m}$ trials ($\sim 10\%$) compared to the standard model.

Permeability measurements of the three neonatal whale sharks (mean TL 563 ± 23.8 mm) showed very little extrinsic resistance through their buccal cavities (R ranged between 0.91 to 6.31 Pa/ml/sec) when flow rate was measured to be constant at $114\text{mL}\cdot\text{s}$ (Table 2.2). These resistance measurements were similar to other small filter feeding elasmobranchs (*Mobula japonica* = 0.99 Pa/ml/sec, *Mobula munkiana*₁ = 6.36, *Mobula munkiana*₂ = 2.27). The calculated pressure head across the filtering apparatus ranged from (106.19-171.86 Pa) similar to pressure heads calculated by Motta et al. (2010) for adult whale sharks (113 Pa).

Discussion

Gill number and swimming speed played major roles in the distribution of particle sizes collected on the gill rakers. This was unexpected since we predicted that the main form of filtration would be dead end sieving, which should only collect particles larger than the filter pore size. The particles were primarily caught along the gill rakers, which leads us to believe inertial impaction and gravitational deposition were the prominent filtering mechanisms during these trials, though we cannot rule out the possibility that cyclone filtration was occurring to some degree as we did document a bilaterally symmetrical vortex near the slits in many of the trials. In several cases we quantified a shift from a bimodal type filter to an intermediate filter or visa versa. For example, when we adjusted the number of gill openings from one to five, we saw a shift from bimodal filter (where primarily $50\text{--}100\mu\text{m}$ particles and $>500\mu\text{m}$ particles were filtered) to a filter where only intermediate and large particles were filtered. Surprisingly, we saw this same trend at increased speeds (bimodal distribution to intermediate/large size ranges) except at the five gill permutation (60 cm/s), where mostly small particles were caught. This switch to smaller particles collected was unexpected since higher velocity flow through the oropharyngeal cavity should have increased the contact rate of the most numerous particles in the flow chamber ($101\text{--}500\mu\text{m}$ particles); hence, the number of intermediate particles filtered.

Theoretical predictions of an organism's optimized swimming speeds while feeding suggest that the animals should accelerate to maximize the number of prey encountered when

feeding in low density plankton blooms and slow down when feeding in a high density plankton bloom (Ware, 1978; Sims, 2000). During the five gill slit trial, we observed that the increase in swimming speed also increased the turbulence near the gill openings within the oropharyngeal cavity. More large-sized particles appeared to remain suspended in the turbulent esophageal vortex rather than settling out on the sieve giving some evidence that the particles may have experienced some degree of cross flow filtration. This indicates that ram filter-feeders using a combination of inertial impaction and gravitational deposition, or hydrosol filtration should maintain a slower swimming speed, regardless of the plankton density, if they are targeting larger prey and increase their swimming speed if targeting smaller prey. Organisms primarily utilizing cross flow or vortex filtration would likely swim at increased speeds to concentrate larger prey in the esophageal vortex prior to swallowing.

Adjustments to the gill morphology resulted in a shift in the particle distributions at the gill rakers from intermediate-type filtration in our control group (500–1000 μm particle collected) to bimodal-type filtration. It is not surprising that increasing the size of the gill slits also resulted in an increased filtering efficiency since increasing the volume of particle laden water through this structure should result in increased opportunities for filtration. These large gills would not be necessary in pump suspension- or engulfment- feeding fishes that filter by first creating a suction force to entrain zooplankton-rich water and then subsequently close their mouths to force this water over the gill rakers. This point is illustrated nicely by comparing the smaller gill morphology of a *Megachasma pelagios*, megamouth shark, which has been hypothesized to use an engulfment feeding strategy (Nakaya et al., 2008), to that of the large-gilled basking sharks (Bigelow and Schroeder, 1953) and whale sharks (Colman, 1997) that use, at least in part, ram suspension feeding. Though we had predicted that ram filtration efficiency would increase with gill size, we did not predict that the particle distribution would shift to that of a planktonic specialist without having to adjust the pore size of the filter. These findings indicate that the morphology of the filter-feeder does play a key role in the prey size selectivity of the organism.

Perhaps the most obvious parameter affecting captured particle distribution was gill raker permeability, or pore size, which was reflected in our particle distributions. We expected the increased filtration efficiency in decreased pore size permutations (105 and 200 μm mesh sizes),

since the likelihood of a particle contacting the filtering element would be greatly increased compared to the 1000 μm and 2000 μm mesh sizes. Even with this increase in filtration efficiency at smaller pore size, the greatest average efficiency we measured was 4.54%. These seemingly low filtration efficiencies are explained by examining Stephens & Krebs (1986) optimal foraging theory which proposes that animals feeding in high density particle areas can survive well even with low filtration efficiencies, provided that their energetic needs are being met (Shimeta and Jumars, 1991). We would hypothesize that fishes with low filtration efficiencies would likely feed on plankton with high caloric/lipid values to meet their energetic needs.

In teleosts, the gill raker structures generally vary by the length of the rakers and their spacing (Nelson, 1967; Bertmar and Strömberg, 1969; Gibson, 1988; Bornbusch and Lee, 1992; van den Berg et al., 1994; Kumari et al., 2005; Vigliano et al., 2005; Friedland et al., 2006). However, the gill raker structures (sometimes referred to as filtering pads) of the filtering cartilaginous fishes exhibit substantial interspecific variation. The four basic raker morphologies are, the: 1) the bristle-like gill raker structures of the basking shark, *Cetorhinus maximus*; 2) fur-like, short gill rakers of megamouth sharks, *Megachasma pelagios*; 3) the widely spaced, flattened filtering pads of whale sharks, *Rhincodon typus*; and 4) the rigid, leaf-like, folded filtering structure of devil rays and mantas, (Mobulidae) (Fig. 2.9).

These differences in brachial filter morphology among elasmobranchs may result in differences in the basic filtering mechanics (e.g., cross flow, direct interception) and cannot be addressed using our simplistic mesh morphology. This topic would be best addressed by determining the position of the pad within the buccal cavity and by taking an in-depth look at the microstructure of the filtering pad. For example, we cannot evaluate whether a form of hydrosol filtration is occurring without performing histological techniques to determine whether a sufficient number of mucal cells are present. Rubenstein and Koehl (1977) noted that the efficiency of a filter can be altered simply by changing the diameter of the pore size or by changing the velocity of the water that passes through it. Our model's rakers were subjected to high velocity (45 cm/s) flow, and when combined with a fine mesh size (105 μm) we predicted that the primary method of particle collection would likely be a form of inertial impaction sieving. As expected, we had the greatest number of particles collected from the gill rakers

during this experiment and the particle size was similar across all size ranges. Decreased permeability (smaller pore size) at the gill rakers increased evenness of the particle sizes that were collected; however, there was no visible evidence that shear flow was moving particles from the mesh to the esophagus. We predict that basking sharks use this type of filtering and would need to either periodically clear the rakers to prevent excessive clogging or continuously transport particles through some mucous based mechanism. Organisms with a fine mesh size that utilize dead end sieving (similar to the basking shark) are likely planktonic generalists, feeding on a wide range of particle sizes. As in industrial dead-end sieving, the gill raker structures of organisms using sieve filtration would project into the buccal cavity at a perpendicular orientation to the water flow, resulting in increased filtration efficiency along their surfaces.

The unique morphology of the whale shark's filter pads open up the possibility of cross flow filtering. In whale sharks the rakers do not protrude into the buccal cavity. Instead, their morphology suggests that they lay flush with the walls of the epibranchials with sparse spacing (approximately 1000 μm pore size) between each gill raker. In our experiments, the 1000 μm rakers collected large to very large-sized particles. The very small and small-sized particles (<100 μm) did not accumulate, but rather exited easily out the mesh. Adult whale sharks appear to feed primarily through cross-flow filtration (Motta, 2010). If neonates are also utilizing some form of cross-flow filtration, we would expect that the majority of the particles collected in the esophagus should be equal to or larger than the pore size of the rakers. With the increased permeability of 2000 μm mesh, there was an increase in the size of particles that were swallowed compared to those swallowed at less permeable pore sizes; however, we could not verify whether cross-flow filtration was occurring.

The model we developed allows us to determine which parameters are important for both dead end sieving and cross-flow filtration in a way that is difficult to examine using computational models. Empirical data from live ram suspension feeding fishes is difficult to obtain in teleosts as: 1) they are generally schooling fishes that become agitated when separated from their conspecifics and, 2) they are typically small in size limiting the use of endoscopy (Cheer et al., 2001). Conversely, filter-feeding elasmobranchs are some of the world's largest fishes and are not easily acquired for experimental purposes. Physical models are an inexpensive alternative to maintaining live specimens in a laboratory and can be created by measuring the

anatomical parameters of fixed specimens from marine vertebrate collections. By focusing on how the mechanism of filtering changed with differing buccal anatomies, we were able to make predictions about the feeding mechanisms and potential prey preference of suspension–feeding fishes. Our physical model demonstrated that the filtration efficiency and particle size distribution collected during ram suspension feeding is intimately connected to both an individual’s anatomy and the swimming speed of the animal.

Acknowledgements

This research was supported by NSF Grant IOB–0616322 and by the Alliance for Graduate Education and the Professoriate Competitive Edge Summer Research Program. We would especially like to thank to H.J. Walker and Cynthia Klepadlo at Scripps Marine Vertebrate Collection for allowing us access to filter–feeding elasmobranchs. Thanks also to T. Kleinteich, S. Crofts, and two anonymous reviewers for valuable comments on earlier versions of this manuscript.

Table 2.1. Anatomical measurements of four neonatal whale sharks represented in mm. We did not * Fully extended when measured. ** Measurements did no stretch gill flap into open position.

<i>R.</i>	<i>TL</i>	<i>FL</i>	<i>GW</i>	<i>GH</i>	<i>DB</i>	<i>MH</i>	<i>MW</i>	<i>OD</i>
<i>typus</i>								
1	561	445	-	46	8.25	33*	92	105
2	566	468	4.8**	37.6	11.5	26	72	83
3	591	439	26	42.2	14.5	15	82	108
4	533	447	16.6	35.2	9.5	16	69	100

Table 2.2. Anatomical physical parameters for various bottle morphologies represented in mm.

<i>Model</i>	<i>TL</i>	<i>GW</i>	<i>GH</i>	<i>MD</i>	<i>OD</i>
Gill Number (1, 2, 3, 4, 5)	450	5	45	85	195
Increased Speed (60)	600	5	45	85	195
Permeability/Pore size (105, 250, 1000, 2000)	450, 600	5	45	85	195
Shortened Buccal length	450	5	45	85	150
Gill Orientation 55°	450	5	45	85	195
Increased Gill Size	450	15	45	85	195

Table 2.3. The calculated extrinsic resistance through the buccal cavity of three neonatal whale sharks compared to other filter feeding elasmobranchs

Specimen	ΔP	Resistance (Pa/mL/sec)
<i>R. typus</i> 2	100.73	0.88
<i>R. typus</i> 3	684.63	6.01
<i>R. typus</i> 4	449.89	3.95
<i>M. munkiana</i> 1	772.65	6.78
<i>M. munkiana</i> 2	236.69	2.08
<i>M. japonica</i> 3	101.72	0.89

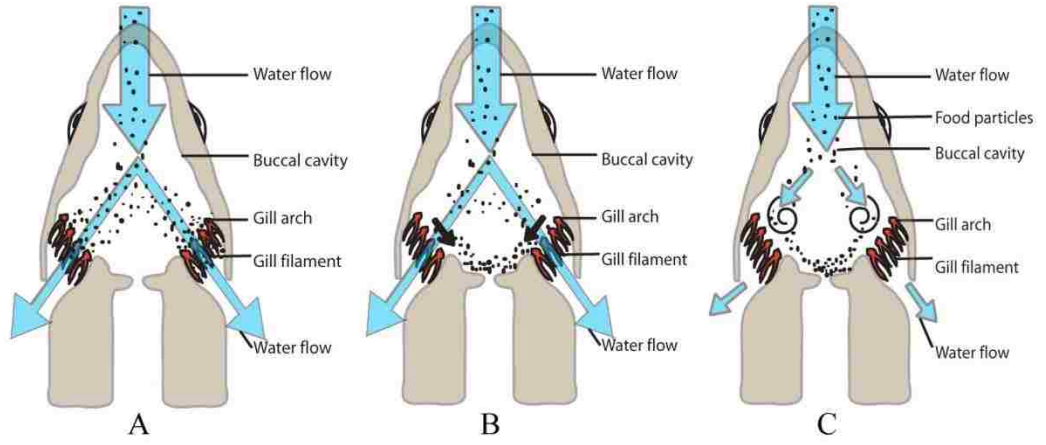


Figure 2.1. Mechanics of particle filtration for three types of filter-feeding bony fishes.

A) Illustrates sieve filtration where particles of all sizes adhere to the gill rakers by contacting the filtering element. B) Shows cross-flow filtration. Particles encounter strong shearing forces that push particles towards the esophagus. C) Illustrates vortex filtration near the gill openings where particles accumulate at the esophagus by centrifugal forces as water exits out of the operculum.

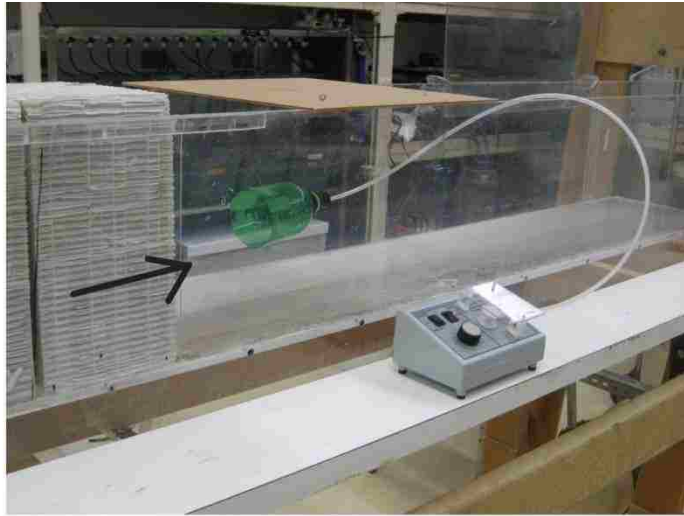


Figure 2.2. Model inserted into flume and attached to peristaltic pump, which functioned as an esophagus during trials. Water and particles move past a series of flow straighteners (direction of movement illustrated by arrow).

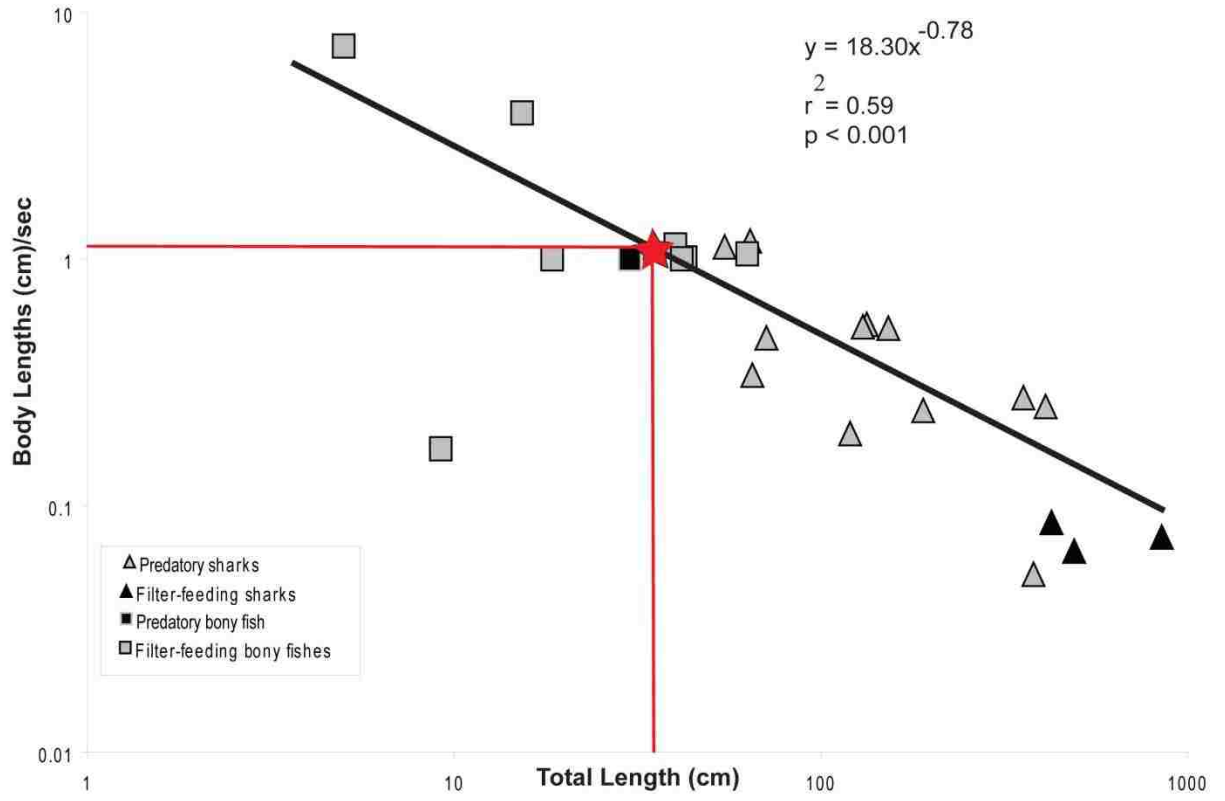


Figure 2.3. The relationship between average total length of a fish (by species) and swimming speed in body lengths (cm)/sec. Neonatal whale sharks are estimated to swim at approximately 1 body length/sec (45-60cm/s), shown as red star. The teleost outlier is *Silurus glanis*, a species of river catfish that is a sluggish swimmer. References for data can be found in the supplemental section.

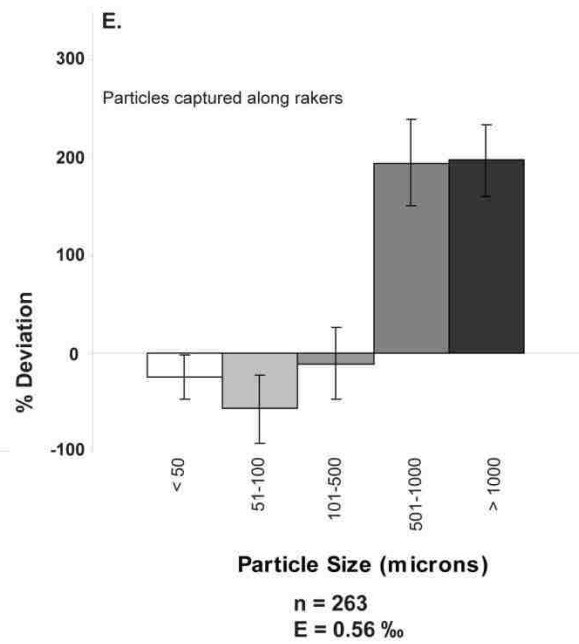
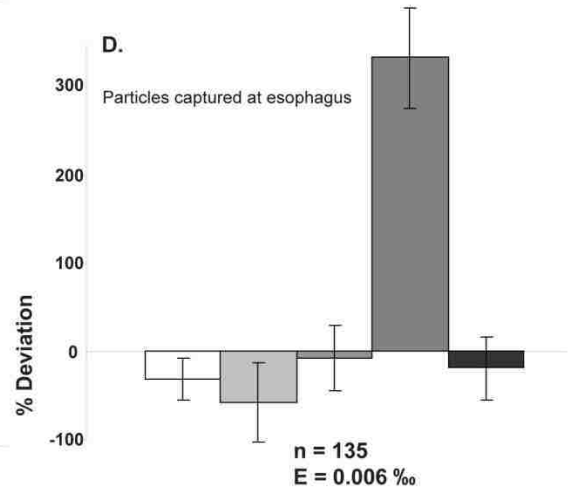
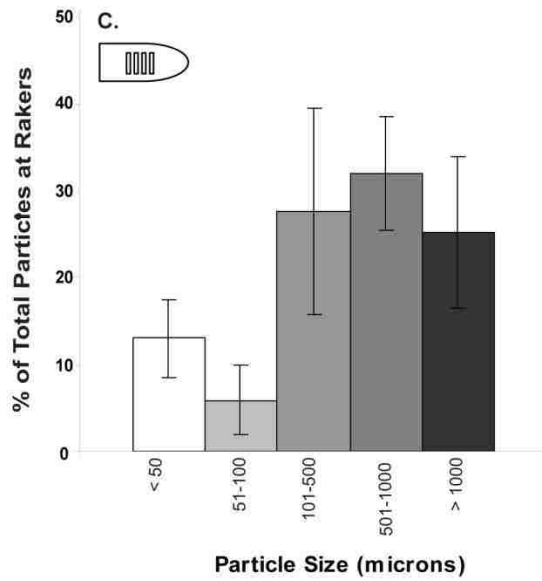
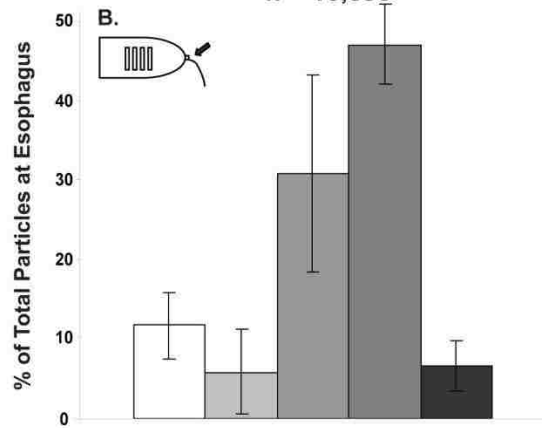
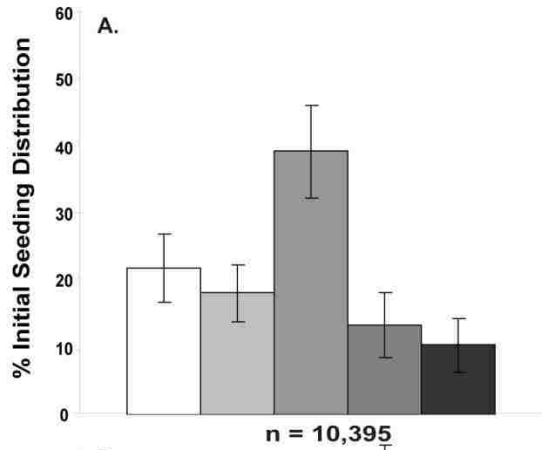


Figure 2.4. Comparison of the standard model to seeding density. n = the number of particles sub sampled, E is the average filtering efficiency. A) shows the initial seeding density of particles in flume. B) and C) are the distributions of particles collected at the esophagus and the gill rakers respectively. D and E) show the percentage of deviation of particles from the initial seeding density collected at the esophagus and the gill rakers. We will only show average percentage deviation from this point forward.

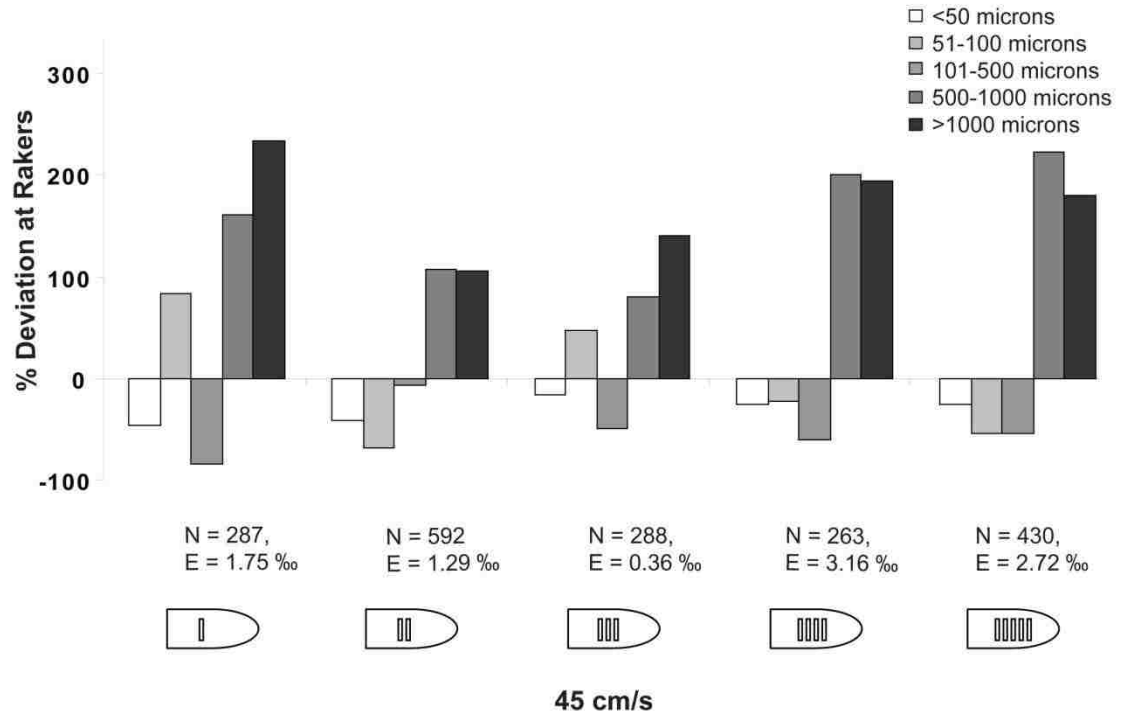


Figure 2.5. The percentage deviation from the seeding density (\pm SD) in particles collected at 45 cm/s with differing gill slit numbers.

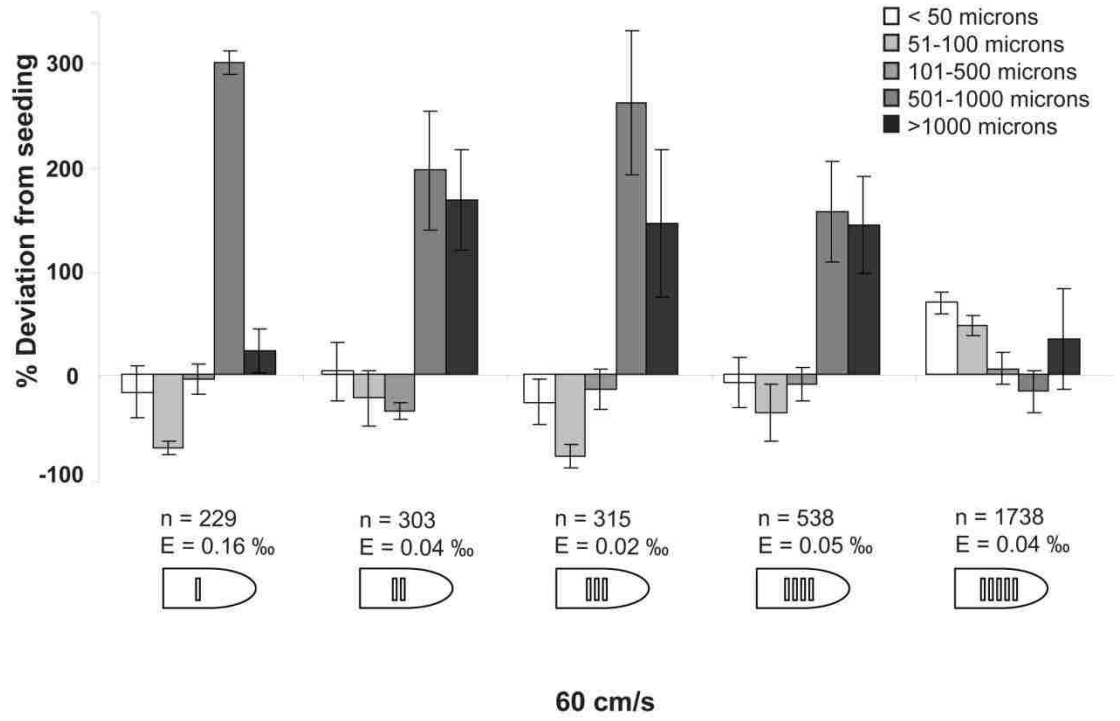
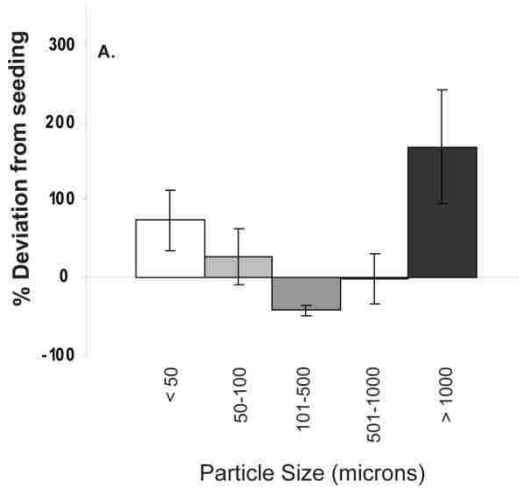
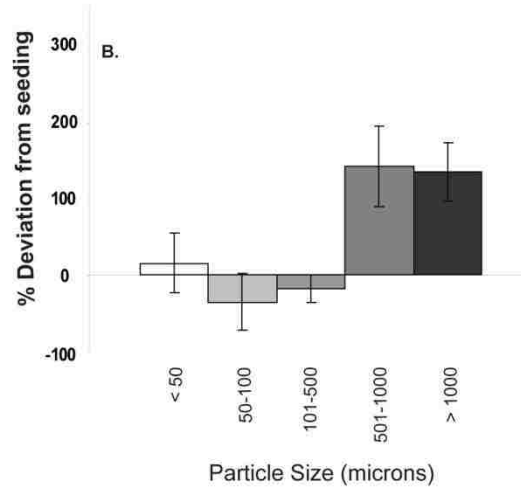


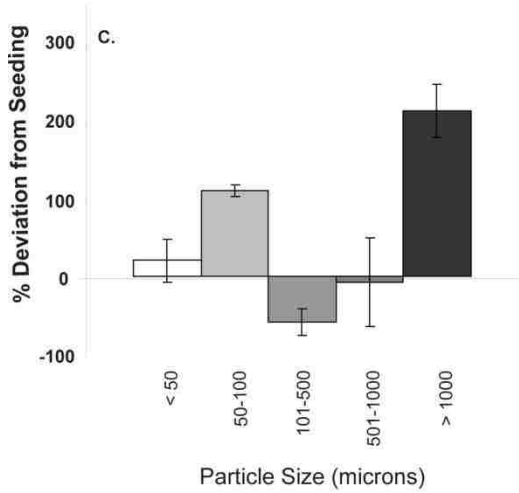
Figure 2.6. The percentage deviation from the seeding density (\pm SD) in particles collected at the rakers in an increased flow speed of 60 cm/s.



n = 510
E = 0.12 ‰



n = 364
E = 0.12 ‰



n = 510
E = 0.21 ‰

Figure 2.7. The percentage deviation from the seeding distribution for A) 55 degree gill orientation, B) shortened buccal cavity and 3) enlarged gill slits.

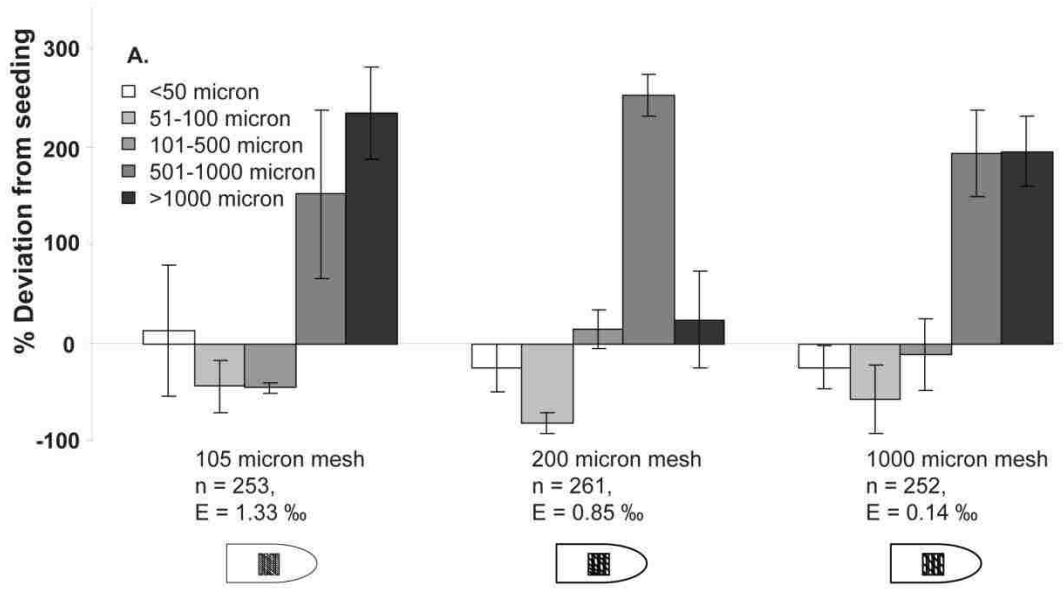
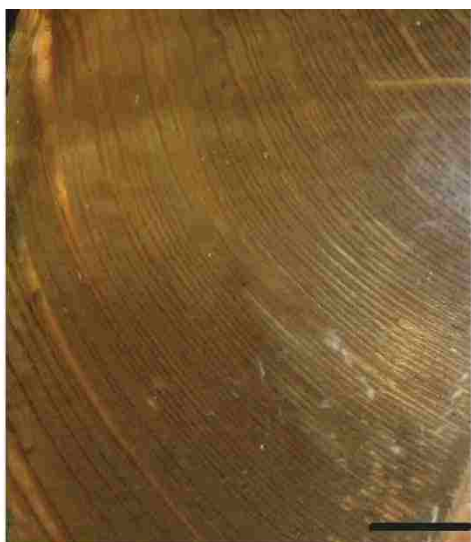


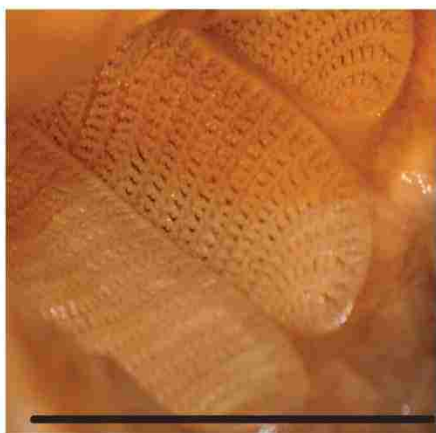
Figure 2.8. Average percentage deviation from the seeding distribution of particles collected from “gill rakers” constructed of 105 μm mesh, 200 μm mesh, and 1000 μm mesh. We did not collect any particles on 0 μm mesh or 2000 μm mesh rakers. The filtration efficiency is very high when using small raker sizes ($E = 27.56$ for 105 μm and $E = 18.16$ for 200 μm).



A



B



C



D

Figure 2.9. Gill raker morphology of A) basking shark (*Cetorhinus maximus*) rakers extracted from buccal cavity; B) megamouth shark (*Megachasma pelagios*) looking into the buccal cavity through the mouth; C) neonatal whale shark (*Rhincodon typus*) looking into the buccal cavity through the mouth; and D) *Mobula* sp. looking at rakers extracted from the buccal cavity. Scale bars show 5 cm except in C, which shows 4 cm.

Chapter 3: The filter pads and filtration mechanisms of the devil rays: variation at macro and microscopic scales

This chapter has been submitted to the Journal of Morphology

Abstract

Three lineages of cartilaginous fishes have independently evolved filter feeding (Lamiformes: *Megachasma* and *Cetorhinus*, Orectolobiformes: *Rhincodon*, and Mobulidae: *Manta* and *Mobula*); and the structure of the branchial filters is different in each group. *Rhincodon*'s filter has been described, and the Lamnids have simple filamentous filters, but the anatomy and ultrastructure of the branchial filter in the mobulid rays is varied and of functional interest. In most fishes, branchial gill rakers are elongated structures located along the anterior ceratobranchial and/or epibranchial arches; however, mobulid gill rakers are highly modified, flattened, lobe-like structures located on the anterior and posterior epibranchial elements as well as the ceratobranchials. The ultrastructure of the filter lobes can be smooth or covered by a layer of micro-cilia, and some are denticulated along the dorsal and ventral lobe surface. Flow through the mobulid oropharyngeal cavity differs from other filter-feeding fishes in that water must rapidly deviate from the free stream direction. There is an abrupt 90° turn from the initial inflowing path to move through the laterally directed branchial filter pores, over the gill tissue, and out the ventrally located gill slits. The deviation in the flow must result in tangential shearing stress across the filter surface. This implies that mobulids can use cross-flow filtration in which this shearing force serves as a mechanism to re-suspend food particles initially caught by sieving or another capture mode. These particles will be transported by the cross filter flow toward the

esophagus. We propose that species with cilia on the rakers augment the shear mediated movement of particles along the filter with ciliary transport.

Key Words: Devil rays, filter anatomy, modified branchial arch

Introduction

The devil rays, composed of 11 species in two genera (*Manta* Walbaum 1792 and *Mobula* Rafinesque 1810), are the largest of all marine rays (Nelson, 1994; Compagno, 1999; Ari and Correia, 2008; Marshall et al., 2009). They are found circumglobally in tropical and subtropical marine environments including: the Yucatan Peninsula, New Zealand, parts of Australia, Baja California, Africa, Ecuador, Southern Japan, throughout Indonesia, at cleaning stations off of Hawaii, Bora Bora, Yap, (Homma et al., 1997; Compagno & Last, 1999; Anderson 2002; Duffy and Abbott, 2003; Dewar, 2008) and even occasionally in temperate areas as far north as Southern New England (Campbell and Monroe, 1974) and New Jersey (Fowler, 1930; Bigelow and Schroeder, 1953).

Like many other large, pelagic marine vertebrates, the cartilaginous mobulids (*Mantas* and *Mobula*) are primarily filter-feeders (Gohar & Bayoumi, 1959; McEachran and Capapé, 1984; Notarbartolo-di-Sciara, 1987). Two other lineages of cartilaginous fishes have independently evolved filter-feeding - the Lamiformes: *Megachasma* and *Cetorhinus* and the Orectolobiformes: *Rhincodon* (Compagno, 1990; Cione and Reguero, 1998). Each lineage has morphologically distinct filtering structures and presumably different mechanisms for removing food particles from the water (Paig-Tran et al, 2011). The mobulids are anatomically distinct from other filter-feeding fishes (bony and cartilaginous), as their body is dorso-ventrally

compressed, their mouth is terminal, the filtering structures are on the dorso- and ventro-lateral surfaces of the oral cavity and their gill slits are on the ventral surface of the body. This flattened morphology suggests fluid flow through the oropharyngeal cavity is different from other fishes with laterally located filtering structures and lateral gill slits or opercula. The orientation of the branchial arch and structure of the filter pads is also different than suspension feeding bony fishes, baleen whales, and sharks.

This study describes the gross morphology and ultrastructure of the filter pads in 9 of the 11 species of mobulids: *Manta birostris* (Walbaum, 1792), *Mobula eregoodootenke* (Cuvier, 1829), *Mobula hypostoma* (Bancroft 1831), *Mobula japonica* (Müller & Henle, 1841), *Mobula kuhlii* (Valenciennes in Müller & Henle, 1841), *Mobula mobular* (Bonnaterre, 1788), *Mobula munkiana* (Notarbartolo-Di Sciara, 1987), *Mobula tarapacana* (Philippi 1892), and *Mobula thurstoni* (Lloyd, 1908). The aims are four-fold: (1) to provide a clear description of the filter anatomy for each species, (2) to describe the microscopic surface anatomy of the filter using scanning electron microscopy, (3) to describe the orientation of the branchial arch *in situ* so that we may assess fluid flow regimes as they move throughout the oropharyngeal cavity, and (4) to combine the anatomical information and field collected fluid flow speeds to infer the mechanism of particle entrapment.

Methods and Materials

Specimens

Mobula spp. and *Manta birostris* specimens were examined in museum collections and arches were removed for further examination in our lab - Scripps Institute of Oceanography SIO

Marine Vertebrate Collection (La Jolla, CA, USA): *Mobula japonica* (arch only; N=1), *Mobula tarapacana* (arch only; N=1), and *Mobula munkiana*; LA Natural History Museum (Los Angeles, CA, USA): *Mobula thurstoni* (N=1); Smithsonian Museum of Natural History (Washington, D.C., USA): *Mobula eregoodootenke* (N=1), *Mobula hypostoma* (N=6), *Mobula kuhlii* (N=1), *Mobula mobular/Mobula japonica* (N=1), and *Manta birostris* (filter lobe sample; N=1); additional specimens were provided by R. Rubin: *Manta birostris* (arch; N=1). We were unable to obtain specimens from *Manta afredi* (Kreffft, 1868) or *Mobula rochebrunei* (Vaillant, 1879) because of their rarity as alcohol preserved specimens.

It is unclear whether our sample of *Mobula mobular* (which is a juvenile animal) is properly identified or if it is actually *Mobula japonica*; the museum specimen was initially labeled as *Mobula diabolis*, which has been applied to several species of *Mobula* (Couturier et al., 2012). It was subsequently assigned to *M. mobular*. *M. mobular* is found in and around the Mediterranean Sea while *M. japonica* can be found circumtropically. This specimen (Smithsonian # 37391) was collected in Senegal. However, we found substantial differences in the ultrastructure between our sample of *M. japonica* and that of *M. mobular*. The possible *M. mobular* sample lacks denticles, but does have a secondary surface structure while the *M. japonica* sample lacks both features. We have treated the specimens of *M. mobular* and *M. japonica* as a single species for this paper, considering the morphological differences as possible phenotypic variation in the species.

Anatomy

Anatomical measurements were collected using the methods of Notarbartolo di Sciara (1987). These included measurements of: disc width (DW), disc length (DL), anterior projection, rostrum to rear tip of pelvic fin (P2), pre-dorsal length, dorsal base, dorsal height, rostrum to vent, tail length, first gill slit length, second gill slit length, third gill slit length, fourth gill slit length, fifth gill slit length, distance between first gill slits, distance between fifth gill slits, rostrum to first gill slit, rostrum to fifth gill slits, P2 length, tip of cephalic fin to mouth, cephalic fin width, orbit height, length between antorbitals, preoral length, tip of cephalic fin to spiracle, mouth width, inter naral width, upper tooth band length, lower tooth band length, and clasper length (Table 3.1). Following morphological measurements, we excised the right, third branchial arch from each specimen through the third gill slit. This method of extraction was necessary to preserve the integrity of the specimen. However, removing the arch without excising the surrounding epithelial tissue makes it difficult to remove the entire arch intact. The excised arches were then wrapped in alcohol saturated cheesecloth, sealed, and shipped to the University of Washington's Friday Harbor Laboratories for further examination.

Whole branchial arches, including the filter plates, were examined in the laboratory and the filter plates from each specimen were photographed and described. Lobe measurements were made by photographing the filter plates on both sides of the branchial arch with a ruler for scaling. Photographs were analyzed with NIH Image J software (version 1.4, <http://rsbweb.nih.gov/ij/>) to measure individual lobe lengths and widths. Measurements of the lobes (>20) from across the entire filter plate were combined to calculate average lobe length and height. Filter lobes were sub sampled at the medial anterior edge and sections were dehydrated gradually over 48 hours into 100% ethanol. Samples were critically point dried (Samdri 790,

Tousimis Research Corp, Rockville, MD), sputter coated (SPI Sputter 12121, SPI Supplies/Structure Pro, Inc, West Chester, PA, USA), and imaged using a scanning electron microscope (SEM) (Jeol Neoscope JCM-5000, Tokyo, Japan). We photographed the microstructure of the right, distal portion of the anterior filter lobes from each species and used NIH Image J software to measure the branchial filter pore length and width for each species from our SEM micrographs.

The entire excised third arch from each species was photographed and the filter pad areas for both the anterior and posterior filter pad were estimated using Image J software. A total of 30 filter lobes and 30 primary vanes/filter pores were selected haphazardly on the anterior arch and pooled to obtain the average filter lobe height, width, and the average filter pore area for each specimen (except in *M. japonica* where we only had four plates from a single arch). We calculated an open area ratio, β , for the entire branchial filters by calculating the ratio of pore area per paired lobe area and then extrapolated this value across the entire filter area, according to the method described in Motta et al. (2010). This allows us to estimate the total combined area for fluid flow through all of the filter pads provided that the pads themselves are not congested with food matter.

Computed tomography (CT) scans of a whole *Mobula munkiana* and the branchial arch from *M. tarapacana* were made at the UC Irvine Medical Center (Irvine, CA, USA). The specimens were wrapped in alcohol-saturated cheesecloth and sealed in extra-large ZiplocTM bags prior to being scanned using a 16 slice, Siemens RS SOMATOM Sensation (MDCT-16) with 0.75-mm slice thickness and helical-spiral scans (Dean et al., 2007). Scans were then reconstructed as 8-bit TIFF stacks and rendered as 3-dimensional images using Amira software

(v. 4.1.1, Mercury Computer Systems, Inc., USA) to visualize the branchial arches *in situ* prior to arch extraction (Figure 3.2).

Fluid flow through the filter apparatus

Manta birostris swimming speed measurements (N = 5 specimens) were made on August 6, 2011 near Isla Holbox (Cabo Catoche) and Isla Contoy, Mexico, as part of a larger *Manta* movement dataset conducted with Dr. Felipe Galván-Magaña and Silvia Hinojosa (Proyecto Manta de Caribe). *Mantas* were located feeding at the surface in plankton-rich upwelling zones at 21° 46.020'N and 87° 01.200' W (Figure 3.1). *Manta* swimming speeds were determined by pacing actively feeding animals with our boat at distance of approximately 5-7 meters laterally. We clocked the animals' swimming speeds every 15 seconds for a total duration of 2 minutes each using a GPS (Garman GPS 72, Kansas City, USA). Speed data were used only if we were able to obtain at least three speed measurements for a specimen and only if the specimen maintained a straight feeding trajectory and did not veer off course as we were pacing it. The fieldwork was conducted with knowledge and permission from the Comision Nacional de Areas Naturales Protegidas (CONANP), Mexico.

We calculated the flow rate (Q) and Reynolds number (Re) through the mouth and at the filter using:

$$Re = \frac{\rho v D_h}{\mu}$$

where ρ is fluid density, v is the velocity of the fluid, D_h is the hydraulic diameter computed from the cross-sectional geometry, and μ is the fluid viscosity. The hydraulic diameter and velocity for flow entering the mouth was calculated based on measurements of mouth width from museum specimens and swimming speeds from actively feeding *Manta birostris* in the field off Isla Holbox, Mexico. It is difficult to correctly measure the open mouth height in preserved mobulids because the fixation process stiffens the connective tissue. Instead we focused solely on measuring mouth widths. We then examined photographs we took while in the field and public domain stock photographs of actively feeding mobulids to determine the aspect ratio between mouth width to height (~2.6:1) and used these estimates to calculate the hydraulic diameter (Beebe et al., 2002) of mobulid mouths. Fluid flow through the respiratory tract of filtering fishes has been estimated to fall between 70% to 90% of the animal's swimming speed (Sanderson et al., 1994; Sims, 2000; Motta et al., 2010) based on the relatively low resistance through the branchial filters. Previous measurements of low resistance (0.99 to 6.86 Pa ml⁻¹ s⁻¹) through the respiratory tract of *Mobula spp.* indicate that 70% of the swimming speed is too conservative an estimate of fluid speed for our purposes (Paig-Tran et al., 2011). In this study, we calculated a range of biologically relevant Reynolds numbers at the mouth using fluid velocities equal to 100%, 95%, 90%, 85%, and 80% of the estimated swimming speeds. This range allows us to account for changes to the flow structure through the mouth with changing resistance, and for the differences in fluid flow for animals swimming at the surface that may not have their entire oral opening submerged, as in surface ram filter-feeding *Mantas* (Figure 3.1), and also for animals that utilize sub surface feeding (e.g. *Mobula spp.*). We used the density and viscosity of seawater at 25.5°C in the equations below (Dietrich et al., 1980; Motta et al., 2010).

Reynolds number (Re) at the filter pads where particles are collected was estimated by directly measuring the total area of anterior or posterior filter plates and the pore size of the filters. We estimated an average pore size for the anterior and posterior filter pads over the entire arch and then extrapolated these data to estimate the entire branchial filter pore area. Upon examination, we determined that filter pores composed approximately 80% of the filter area. Re at the filter were calculated with the above equation; however the D_h was calculated by taking the square root of the total open area for all the pores. Additionally, we performed a sensitivity analysis of our calculations by recalculating Re numbers with a 10% decrease and 10% increase in open pore area and also using 10% slower fluid speed (80%) through the filter pore.

To determine whether mass movement near the surface of the filter plate is subjected to convective or diffusive transport mechanisms, we calculated the Péclet number (Pé) for each species using the equation:

$$Pé = Re \times Pr,$$

where Re is the previously calculated Reynolds numbers and Pr is the Prandtl number, a ratio of viscous to thermal diffusion rates. The Prandtl number for seawater at 25°C is 7.2. Small Péclet numbers indicate mass movement by diffusion while larger Péclet numbers are indicative of mass movement by convective forces (Vogel, 2003).

Results

Anatomy

Mobulid branchial architecture consists of five pairs of chevron-shaped arches oriented along the lateral surface of the oropharyngeal cavity. The internal skeleton of the arch is composed of cartilaginous elements: the dorsally located epibranchial (EB) and the ventrally located ceratobranchial (CB), which are offset in position so that the proximal portion of the EB is angled posteriorly while the proximal portion of the CB is angled anteriorly (Figure 3.3A). This orientation makes the arch appear twisted when compared to the branchial arches of other fishes. The distal edges of the EB and CB arches articulate laterally with a secondary plate-like support structure, the lateral stay (LS) (Garman, 1913) also referred to as the extrabranchial (Compagno, 1999), articulates with both the EB and the CB portion of the distal arch and presumably provides extra support to the branchial septum (Compagno, 1999). The branchial rays (BR) project from both the EB and CB, providing support to the gill flaps (Gillis et al., 2009) and perhaps also to the gill filaments (Figure 3.3B). Water passes between the EB and the CB as it flows through the oropharyngeal cavity.

The epibranchial and ceratobranchial each support two sets of filtering plates, one oriented anteriorly (toward the mouth) and one oriented posteriorly (toward the esophagus). The anterior and posterior filter plates (AFP and PFP, respectively) are separated by the gill tissue (GT) that runs along the midline of the arch (Figure 3.4) on both the EB (not labeled) and CB. The plates are supported by highly structured supports: primary vanes (PV) which are the channels directly below the filter pore opening and secondary vanes (SV) that direct the flow of water through the filter plate toward the gill tissue. The SV opening can be seen directly beneath the terminal lobes (TL) of the filter plates.

The surface of the branchial filter is composed of a series of modified gill rakers called filtering plates (FP) along the EB and CB portions of the arch. Each plate is composed of a central cartilaginous support that runs from the central portion of the arch to the distal anterior tip of the filter at the edge of the arch. The plates resemble fronds of a bracken fern in that they are sub-sectioned into paired lobes along the entire portion of the filter (Figure 3.4). The terminal lobe of the filter plates can be rounded or lanceolate in appearance and the shape may be species-specific. However, the terminal lobe within a species varies in shape depending on whether it is located on the anterior face or the posterior face of the filter pad. The number of filter plates on an arch may also be species specific as described by Notarbartolo di Sciara (1987); however, we could not verify this as our specimens did not have all of their filter plates intact - an artifact of our method of extraction.

Some species have pronounced denticles along the anterior and posterior filter lobes. The base of the denticles are approximately 20-30 μm in diameter across all species and can be found on all surfaces of the filter lobes (anterior facing toward the flow and posterior facing into the pore as well as on the central raphe between the paired lobes) with the exception of the terminal lobe. Denticles appear to suffer heavy wear, possibly from the inertial impaction of particles suspended within the fluid as they hit the filter plate, or by masses of particles rolling over the filter surface by tangential shearing (discussed further in section 3.3). It is not clear from this study whether the denticles regenerate following wearing events. An example of heavily worn denticles and exposed pulp cavities can be seen in *Manta birostris* (Figure 3.5A & B) and *Manta thurstoni*.

Filter lobes can be described as either non-ciliated or ciliated and with or without secondary projections. The lobe surface of *Mobula tarapacana* is almost entirely covered with a

layer of cilia (Figure 3.5C & D). The surfaces of other species appear to have a raised secondary surface structure, although this structure is not as well defined and does not project as far from the surface. The surface epithelium is relatively thin with a thick layer of sub surface connective tissue between the surface epithelium and the cartilaginous skeleton (Figure 3.5E). Non-ciliated filter lobes can have a smooth surface or a rough surface epithelium (Figure 3.5F).

Individual Identification

Each species has distinctive ascending and terminal lobes (Figure 3.6). While some species are unmistakable upon a cursory examination (e.g. *Manta* lobes are fused with finger-like projections, *Mobula tarapacana* lobes are fused, *Mobula eregooteneke* has few lobes), others require closer inspection for reliable identification. The ultrastructure of the filter lobes varies among species, and the most notable differences will be discussed in the following sections. The filter plates can be separated into four main groups (Figure 3.7A-H): (1) plates with denticles and cilia/secondary projections - *Manta birostris*, *Mobula tarapacana*, *Mobula munkiana*, (2) plates with denticles, but lacking cilia and/or secondary projections – *Mobula thurstoni*, *Mobula hypostoma*, (3) plates lacking denticles with cilia/secondary projections - *Mobula kuhlii*, and (4) plates lacking denticles and cilia - *Mobula japonica*, *Mobula eregoodootenke*.

Manta birostris filter plates are notably different from those of *Mobula sp.* in that the filter lobes form finger-like projections that extend across the pore opening from the dorsal lobe, decreasing the diameter of the pore (Figure 3.8). The paired lobes on either side of the central raphe are continuous and attach to the lobes on adjacent filter plates, so there is no clear delineation between the lobes. The arch of an adult *Manta* is large; the specimen we examined

extended approximately 170 mm from the proximal to distal edge of the EB. Viewed laterally, individual filter plates are crescent shaped and extend well beyond their point of attachment to the arch (Figure 3.9). Viewed under SEM, mantas have denticles running along the anterior side of the filtering lobes. The secondary projections of mantas stem from the ventral side of their filtering lobes, though the lobe surface is smooth in appearance. The length from the medial to lateral epibranchial arch was 171 mm.

Mobula tarapacana is easily identified by the fused filtering lobes of adjacent plates, a character state unique to this species. The specimen that we examined had an unusual color gradient from tan on the medial edge to a dark grey near the terminal lobe. Adult rakers are large, rivaling *Manta* in size. The terminal lobes are highly rounded with a distinctive midline ridge. The ascending lobes are rounded near the terminal lobe, becoming a widened heart shape near the medial edge. Viewed laterally, the filter plate is straight and is attached to the arch along its entire length. Under SEM, this species has the most well defined cilia and is easily distinguished from other species. They are denticulated on both the dorsal and ventral sides of the filtering lobes, and the length from the medial to lateral epibranchial arch was 220 mm.

Mobula munkiana has rounded anterior filter lobes, similar to *Mobula tarapacana*, but with the adjacent lobes unattached. The central raphe of the terminal lobe that connects to the ascending lobes is heart shaped and the central ridge along the terminal lobe is less prominent than in *M. tarapacana*. The descending paired lobes are broad, the edges only slightly curved upwards toward the terminal lobe and becoming narrower and more heart-shaped in appearance toward the medial edge. Filter plates can be solid colored (our specimen) or have a gradient coloration similar to *M. tarapacana* (Notarbartolo di Sciara, 1987). Viewed laterally, the filter plate is shortened and appears to be angled so that only the middle 1/3 portion is attached to the

arch. Under SEM they are denticulated and have a raised, bumpy secondary structure along the surface of the filter lobes. The length from the medial to lateral epibranchial was 59 mm.

Mobula thurstoni is densely denticulated on the dorsal and ventral lobes. The terminal lobe is leaf shaped. The central raphe continues into the terminal lobe and appears to branch, leading to a vein-like pattern. Ascending filter lobes are compact and there are upwards of 20 or more. Most of the ascending plate has heart shaped lobes except very near the terminal lobe. Viewed laterally, the filter plate is straight and the majority is attached to the arch except directly beneath the terminal lobe. Under SEM, the surface of the filter lobes is smooth with no discernible secondary structures beyond epithelial ridges. The length from the medial to the lateral edge of the epibranchial was 23 mm.

Mobula hypostoma is the most highly denticulated of all the Mobulidae with denticles visible to the naked eye. We were able to obtain a total of six *Mobula hypostoma* over an ontogenetic size range and all specimens examined displayed the same characteristic/diagnostic features. The abundance of denticles ranged from < 23 denticles/mm² in juvenile *M. hypostoma* to >100 denticles/mm² in adult *M. hypostoma*. The anterior terminal lobes are broad and rounded in appearance while the posterior lobes are more leaf-shaped, similar to that described by Notarbartolo di Sciara and Seret for *Mobula rochebrunei* (pers. comm. Bernard Seret, MNHN). The central raphe is well defined along the length of the plate and extends into the terminal lobe. As in *M. munkiana*, lobes are broad near the terminal lobe and become more heart shaped toward the base; however, the lateral edges are more curved toward the terminal lobe. Viewed laterally, the terminal lobe of the arch protrudes out almost $\frac{1}{4}$ the length of the arch from the attachment point. Approximately $\frac{3}{4}$ of the lower plate is attached to the arch. The lengths from the medial to the lateral edge of the epibranchials were: 51 mm, 24 mm, and 26 mm.

Mobula japonica/Mobula mobular have a distinctive, highly structured, lancelet/point shaped terminal lobe with two small pit shaped indents along the lower portion of the lobe. The majority of the filter plate is dark grey with light beige to white colored terminal lobes. The ascending filter lobes are as wide as the terminal lobe, but not broad in appearance. The lateral lobe edges are curled toward the terminal lobe. *M. japonica* has a distinctive knob along the anterior edge of the filter lobes. Adjacent plates are packed tightly together and ascending plates are numerous. Viewed laterally, the plate is straight and connects to the arch along the entire length. The filter portion of the arch is crescent shaped. Viewed under SEM, the filter lobes of *M. japonica* are smooth and have no denticles while *M. mobular* have a bumpy, secondary structure as described previously (Figure 3.9). The length of the epibranchial from the medial to the lateral edge was 19 mm for *M. mobular*. We could not calculate an epibranchial distance for *M. japonica* as we had only a portion of the branchial arch.

Mobula kuhlii has a cushion shaped anterior terminal lobe and leaf like posterior terminal lobes similar to *Mobula hypostoma* but less pronounced. The terminal lobes are flattened in appearance and contain no discernible central ridgeline; the edges of the terminal and ascending lobes curve slightly towards the midline. Ascending lobes are broad and wide with a prominent central raphe. Viewed laterally, the plate is highly curved and only the lower ½ of the plate is attached to the arch. Under SEM the filter is ciliated, even along the terminal lobe, but no denticles are present. The length of the epibranchial from the medial to the lateral edge was 39 mm.

Mobula eregoodootenke is a distinctive species that is easily identified. The terminal lobe is elongate and the entire filter plate lacks the rigidity found in other species. There are few pairs of filter lobes ~ 5 pairs altogether (4 ascending and one terminal lobe). The central raphe is

prominent along the entire filter plate and extends into the terminal lobe. The adjacent plates are widely spaced and do not touch. Ascending lobes are circular in appearance. Viewed laterally, the plate is straight and is connected to the arch along its entire length. Under SEM, the filter lobes appear smooth with no denticles present. The length of the epibranchial from the medial to the lateral edge was 29 mm.

Fluid flow through the oropharyngeal cavity

We measured actively feeding *Mantas* swimming at an average speed of 0.68 (+/- 0.24 s.d.) m/s (n=5) and have used this value as a proxy for *Mobula sp.* swimming speeds as well. The flow rate (Q) at the mouth was estimated as 100%, 95%, 90%, 85%, or 80% of the swimming speed (Table 3.2). The average pore area for all mobulids (including *M. tarapacana*) was 1.37 mm². The average open pore area (β) for all mobulids was approximately 80% open pore area per paired lobe. Flow at the filter pore opening is laminar and Re at the filter were estimated between 10 and 300 (Table 3.3).

Our anatomical examinations of branchial arches *in situ*, suggest that fluid flow through the oropharyngeal cavity is unusual when compared to other filter-feeding fishes because the fluid does not follow a linear path from the mouth through the gill slits. Instead, the fluid flow initially follows a direct path from the mouth to the branchial arches. At each arch a portion of the fluid must turn ventrally at a near 90° angle to the antero-posterior axis of the fish. The fluid flows through the primary vanes of the anterior filter plates, through the secondary vanes which direct the flow across the gill tissue, through the parabranial chamber, and finally out the gill slits. As the fluid exits it is redirected again nearly 90° to rejoin the free stream water around the swimming fish (Figure 3.10).

Discussion

Our data suggest that filtering mechanics vary among the mobulid species but that some mechanisms of filtration are consistent across all the species. There are five mechanisms for particle sequestration by a fibrous biological filter with a pore size of the order 10^{-7} to 10^{-1} cm (Rubenstein and Kohl, 1977; LaBarbera, 1984; Shimeta and Jumars, 1991): (1) dead-end sieving, (2) direct interception, (3) inertial impaction, (4) gravitational deposition, and (5) diffusion deposition. Dead end sieving, in which particles larger than the filter mesh are retained in the buccal cavity, explains the larger planktonic prey found in mobulid guts. So, while all species can, and certainly do make use of sieving, the morphology and consequent fluid mechanics of the disparate species suggest differences in the balance of the other four methods for capturing smaller particles. Increasing the success of capturing particles smaller than the filter pore relies heavily on amplifying the probability that particles will come close enough to the filter to be retained. This can happen in several ways: 1) particles passing within one particle radius of the fiber can be retained by a sticky surface on the filter (direct interception), 2) if the fluid experiences a sharp turn in its trajectory, entrained particles will deviate from the streamline due to inertia and may make contact with the sticky filter surface (inertial impaction), 3) particles can settle out of the flow and contact the filter through gravitational forces acting on the particle (gravitational deposition), or 4) very small particles can settle out through Brownian motion (diffusional deposition). The Péclet number ($Pé$) is a dimensionless quantity that captures the ratio of advective to diffusive transport in a system. We calculated that the $Pé$ in mobulids ranges between 60-2500. This indicates that mass movement at the filter surface is primarily advective in nature ($Pé > \sim 4$); particles near the filter surface are unlikely to be caught by either gravitational deposition or diffusional deposition. But among the species there is a 40-fold

variation in $Pé$ and this suggests that *M. ergoodootenekee*, *M. kuhlii* and *M. hypostoma* are far more likely to catch particles via diffusion than *M. thurstoni*, *M. tarapacana*, *M. mobular* and *M. japonica*. We propose that the mechanisms of small particle capture occur in conjunction with a sticky sieve mechanism for particle retention. This leads to the prediction that mobulid filter surfaces contain a high concentration of mucus producing cells that coat the filter lobes for particle retention.

After capture, particles must travel from the filter to the esophagus for ingestion. Unlike the rakers in bony fishes, mobulid filter pads are rigid and cannot contact additional sticky surfaces along the arches during oropharyngeal contraction. We propose that the cilia in some mobulid species serves as a mechanism for particle and mucus transport. Denticles protect against damage of this delicate ciliated region from particles impacting the filter surface. In addition to ciliary transport, a second form of particle transport, cross-flow filtration, moves particles from the capture site to the esophagus. Cross-flow filtration takes advantage of tangential sheering generated by fluid flow parallel to the surface of a filter to continuously clear the filter mesh (Bott et al., 2000; Sibanda et al, 2001, Hung et al, 2012). This mechanism has already been proposed as a biological filtration mechanism in bony filter-feeding fishes (Sanderson et al, 2001; Callan and Sanderson, 2003) and also in elasmobranchs (Motta et al, 2010; Paig-Tran et al., 2011). The $Pé$ at the filter surface in the mobulids are high enough, especially in the large mobulids (*Manta birostris* and *Mobula tarapacana*), to support particle transport to the esophagus through cross-flow filtration. Cross-flow filtration solves two filtering problems: 1) clogging at the filter, which decreases permeability, increases the pressure differential across the filter, and changes its size selectivity; and 2) interruption of filtration

during filter cleaning events, which in other fishes require mouth closure and gill arch adduction and abduction.

The Reynolds number (Re) for flow entering the mouth of mobulids indicates that flow is turbulent and dominated by inertial forces ($Re > 2000$). The Re at the filter is in the transitional range between laminar and turbulent flow, although we predict that the flow through the filter pore and through the primary vanes is laminar. This could be demonstrated through modeling, but would be difficult to show experimentally. The Re at the filter mesh in mobulids (10-350) is similar to that calculated by Motta et al. (2010) ($Re \sim 300$) in whale sharks. In large mobulids (*Manta*, *M. tarapacana*, and *M. japonica*/*M. mobular*) the total filter area is smaller than in *Rhincodon typus* [*Rhincodon typus* average (3 specimens) filter area = 11,303 cm²; TL average = 486 cm (Motta et al. 2010), *Manta* (1) filter area = 2,230 cm²; DW = unknown, *M. tarapacana* (1) filter area = 2,670 cm², DW = 301 cm]. The difference in the total size of the filter area reflects a difference in the amount of fluid being filtered, which is directly related to open mouth area and swimming speed. Mobulids have considerably smaller gape than the filter feeding sharks. *Rhincodon typus* had open mouth areas of 914 cm² and 1724 cm² – which is 84.7% of the total open mouth area since the animal feeds with part of its mouth above the water. Basking sharks have an even larger total mouth area measured at 4000 cm² (Parker and Boeseman, 1954; Sims, 2008); nearly four times larger than whale sharks. Adult *Mobula tarapacana* has an average total open mouth area an order of magnitude smaller 57 cm² (average width = 12 cm), and *Mantas* have approximately half the open area as *Rhincodon typus* at 406 cm² for *Manta alfredi* (mouth width average = 32 cm) and 419 cm² for *Manta birostris* (average mouth width = 33 cm) (Marshall et al., 2009). *Mantas* (swimming speed = 0.68 m/s) are swimming at approximately 70-80% of the speed of filter feeding sharks; whale sharks = 0.99 m/s (Motta et

al., 2010) and basking sharks = 0.85 m/s (Sims, 2000). We can therefore calculate *Mantas* and *Mobula spp.* total filtration per hour (fluid flow at 90% of swimming speed x total area of mouth) is approximately 10.8 m³ hr⁻¹ for *M. tarapacana*; 86.4 m³ hr⁻¹ in *Manta alfredi*; 90 m³ hr⁻¹ in *Manta birostris*). The filtering sharks filter between 4 to 12 times more water per hour than even the largest mobulids; whale sharks = 326 m³ hr⁻¹ (Motta et al., 2010) and basking sharks = 1100 m³ hr⁻¹.

The distinctive differences in the anatomy of the filtering lobes in mobulids is useful for taxonomic identification in the field or when identifying museum specimens. However, caution should be taken when using the filter plates to distinguish between certain species as some filter pads are almost identical (e.g. *Mobula japonica* and *Mobula mobular*). In other species, the anterior and posterior terminal lobes are different from one another and may resemble the terminal lobe of another species. This may be the case with *Mobula hypostoma* and *Mobula rochebrunei* (not described in this study). Unpublished specimen identification guides by Notarbartolo-di-Sciara and Seret describe useful morphological differences between these two species; however, upon our examination of *M. hypostoma* we found that the same morphological descriptions could be used when describing the differences between the anterior and posterior terminal lobes within this same species. The marked differences between the filtering plates of most species (especially in unmistakable specimens like *Manta birostris*, *Mobula tarapacana*, and *Mobula eregoodootenke*) could lead to more accurate mobulid identification in the field, especially in fishing operations where the branchial filters are the only remaining/available portion of the fish. For example, *Manta* and *Mobula* fisheries are currently on the rise in response to increasing demand for their gill arches (Booda, 1984; Dewar, 2002; Rubin, 2002; White et al., 2006a; Rajapackiam et al., 2007a; Mohanraj et al., 2009, Courier et al., 2012) which

are used in the Chinese medicinal trade (IUCN, 2011). The meat is generally discarded, resulting in difficulty when attempting to identify to which species the filters belonged. The morphological descriptions provided in this manuscript can serve as a useful guide to key out what species an extracted branchial filter came from by identifying characteristic ascending and terminal filter lobes.

Acknowledgements

We are greatly indebted to HJ Walker (SIO Marine Vertebrate Collection at Scripps Institute of Oceanography), Lynne Parenti, Jeff Clayton, Jerry Finan (Smithsonian Museum of Natural History), Jeff Seigel (LA Natural History Museum), and Robert Rubin for graciously allowing us to examine and sample from their *Mobula* and *Manta* collections. Thanks also to our collaborators Dr. Felipe Galván-Magaña, Silvia Hinojosa, and Dr. Nick Wegner who helped us collect *Manta* speed data as a part of a larger *Manta* movements project as a collaborative effort through Proyecto Manta de Carribe. Dr. Katie Staab, Joseph Bizzarro, Timothy Dwyer, and Dr. Megan Dethier provided helpful comments on this manuscript. Thank you to Dr. Mason Dean for help with CT scanning and anatomy, Dr. Dave Ebert for discussing mobulid systematics, and especially to Dr. Tomasz Owerkowics for providing additional lab space and helpful discussions on morphology. We are grateful for funding from a variety of sources including: the Smithsonian Museum of Natural History and the University of Washington Sargent Fellowship for student travel funding to museums; The University of Washington WRF-Hall fellowship, the Richard and Megumi Strathman Fellowship, UC-Mexus Collaborative Grant (440763-19900), and a National Geographic's Waitt Grant.

Table 3.1. Morphometrics of *Mobula sp.* measured from preserved museum specimens. *M. munkiana* (SIO 85-34, 85-35), *M. japonica* (SIO 82-9) reported in Notarbartolo-di Sciara 1987a.
 ** Tail broken or not fully intact.

Species	<i>M. kuhlii</i>	<i>M. mobular</i>	<i>M. eregoo</i>	<i>M. hypo</i>	<i>M. thurstoni</i>					
Sex	M	M	F	M	M	M	M	F	M	F
Spec #	205268	37391	170365	197409	205397	75873	73872	73871	78874	38433-1
Disc width (mm)	779	419	722	696	705	1048	1260	1052	1105	612
Disc Length	421	233	378	301	345	602	585	614	502	344
Anterior projection	280	264	288	247	208	447	N/A	473	376	261
Rostrum to P2	406	258	399	353	386	661	693	649	527	288
Predorsal length	352	230	334	310	333	548	534	546	464	N/A
D base	19	20	50	cut off	26	80	78	70	40	43
D height	45	22	33	cut off	27	52	52	58	52	10
Rostrum to vent	329	200	356	301	312	481	58	475	480	302
Tail length	620	733	551	broken	510	172*	303*	56**	138*	165
1st gill slit	42	24	28	30	42	56	59	56	53	29
2nd gill slit	39	22	31	32	41	65	68	58	55	33
3rd gill slit	40	22	35	30	40	65	66	57	56	32
4th gill slit	38	24	32	32	39	64	65	55	53	26
5th gill slit	30	18	26	28	29	43	51	46	41	20
Between 1st gill	98	63	97	92	98	158	171	57	53	76
Between 5th gill	37	27	33	22	27	44	147	46	43	25
Rostrum to 1st gill	81	55	99	79	81	132	84	127	126	67
Rostrum to 5th gill	153	102	187	161	69	275	232	261	250	N/A
P2 length	52	39	59	48	60	112	101	117	142	54
Tip of cephalic to mouth	87	51	111	77	78	125	144	140	123	82
Cephalic width	52	24	50	32	33	73	49	59	40	73

Orbit height	19	20	20	18	19	21	21	24	20	22
B/w antorbitals	123	92	85	116	90	141	150	143	128	103
Preoral	35	20	43	27	25	46	46	42	39	26
Tip of cephal to spiracle	111	73	115	92	100	160	140	162	120	83
Mouth width	86	60	82	80	85	132	147	134	114	74
Internaral	71	47	70	67	78	121	129	120	114	62
Upper toothband length	65	46	57	31	29	75	68	72	68	38
Lower toothband length	68	45	59	40	39	76	67	75	70	47

Species	Re x 10 ⁴ 100% (Q = 0.68 m/s)	Re x 10 ⁴ 95% (Q = 0.65 m/s)	Re x 10 ⁴ 90% (Q = 0.61 m/s)	Re x 10 ⁴ 85% (Q = 0.58 m/s)	Re x 10 ⁴ 80% (Q = 0.54 m/s)
<i>Manta birostris</i>	N/A	N/A	N/A	N/A	N/A
<i>Mobula tarapacana</i>	N/A	N/A	N/A	N/A	N/A
<i>Mobula munkiana</i>	2.9	2.8	2.7	2.5	2.4

Table 3.2. Calculation of Re at the mouth of a fish swimming at 0.68 m/s. Estimates of flow at the mouth were not available for *Manta birostris* and *Mobula tarapacana* because we did not have morphometric data (TL, Mouth width) from these species. Q = fluid speed.

<i>Mobula thurstoni</i>	1.8	1.7	1.7	1.6	1.5	
<i>Mobula hypostoma</i>	3.0	2.9	2.7	2.6	2.4	
<i>Mobula japonica/mobular</i>	1.6	1.5	1.4	1.3	1.2	
<i>Mobula kuhlii</i>	2.2	2.1	2.0	1.9	1.8	
<i>Mobula eregoodootenke</i>	2.1	2.0	1.9	1.8	1.7	
Species	Calculated filter pad open area m ²	Average pore area mm ² (+/- stdev)	Re/Pé at pore (80% flow)	Re/Pé at pore (90% flow speed)	Re/Pé with 70% open pore area	Re/Pé with 90% open pore area

Table 3.3. Calculations of the total filter area, the average filter pore size (>20 pore measurements each), and Re number at the filter pore (80% and 90% of swimming speed; 80% open pore area) with sensitivity analysis -70% open pore area and 90% open pore area (at 90% swim speed).

			speed)			
<i>Manta birostris</i>	0.179	1.18 (0.29)	-	-	-	
<i>Mobula tarapacana</i>	0.267	3.34 (0.97)	309/2232	350/2521	331/2386	292/2104
<i>Mobula munkiana</i>	0.027 (+/- 0.01)	1.37 (0.23)	14/104	16/117	15/111	14/98
<i>Mobula thurstoni</i>	0.072	0.36 (0.11)	27/195	31/195	32/209	29/184
<i>Mobula hypostoma</i>	0.011(+/- 0.004)	3.24 (0.1) adult & 0.53 (0.19) juv	8/64	10/60	9/65	8/57
<i>Mobula japonica/mobular</i>	0.004	0.27 (0.07) juv	30/233	34/218	32/233	29/206
<i>Mobula kuhlii</i>	0.012	0.66 (0.14)	26/201	29/118	28/201	25/177
<i>Mobula eregoodootenke</i>	0.006	0.99 (0.22)	20/146	23/146	22/157	19/138

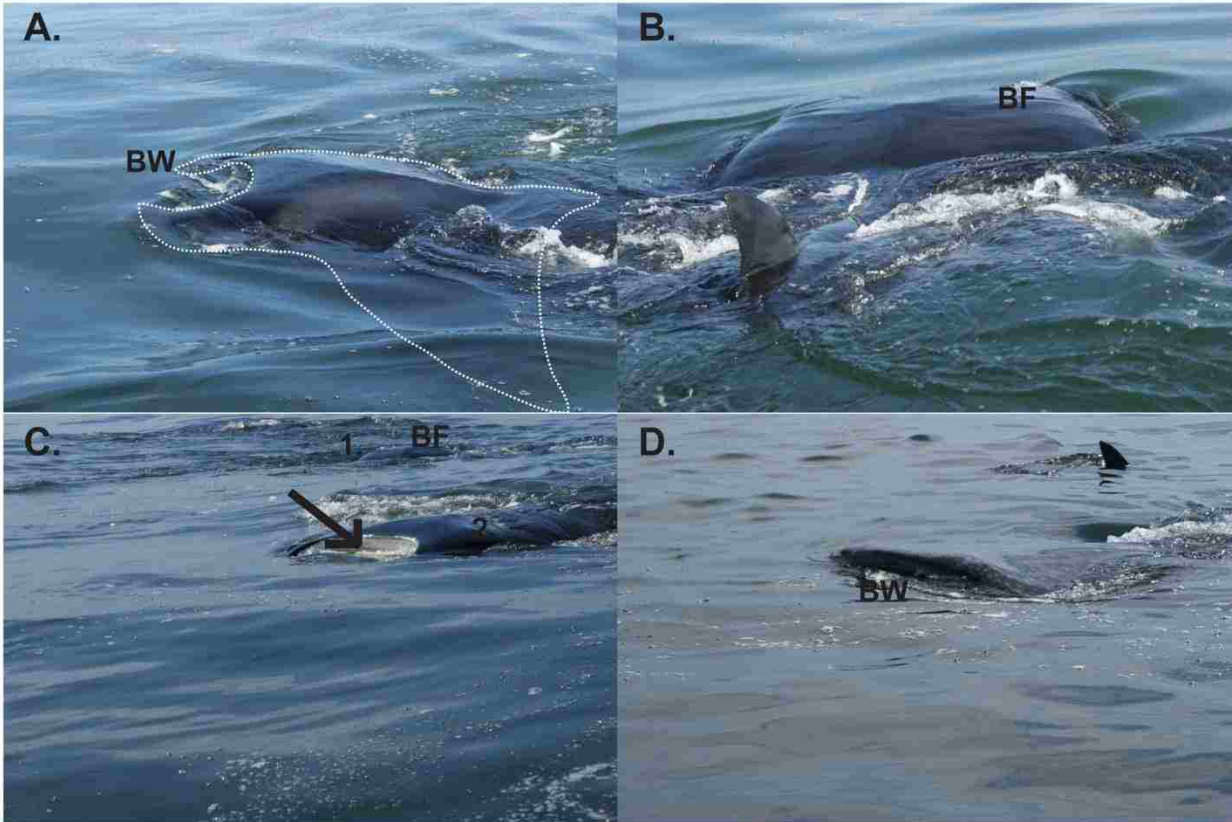


Figure 1

Figure 3.1. *Manta birostris* ram surface feeding in A) lateral view, B) posterior view, and C) anterolateral view. A) Shows the slight bow wave (BW) in front of the mouth. We have outlined the body of the manta. B) The posterior view shows the indentations on the dorsal surface where the branchial filters (BF) reside within the pharyngeal cavity. C) The antero-lateral view arrow shows that the mouth is not fully submerged when the animals are feeding at the surface. Two mantas are labeled in this photograph. All three images also illustrate how close we can maneuver to the animal to measure swimming speeds. D) Shows antero-lateral view of whale shark swimming in the same plankton bloom. Note that more of the mouth is exposed out of the water and there is a larger bow wave in front of the upper jaw.

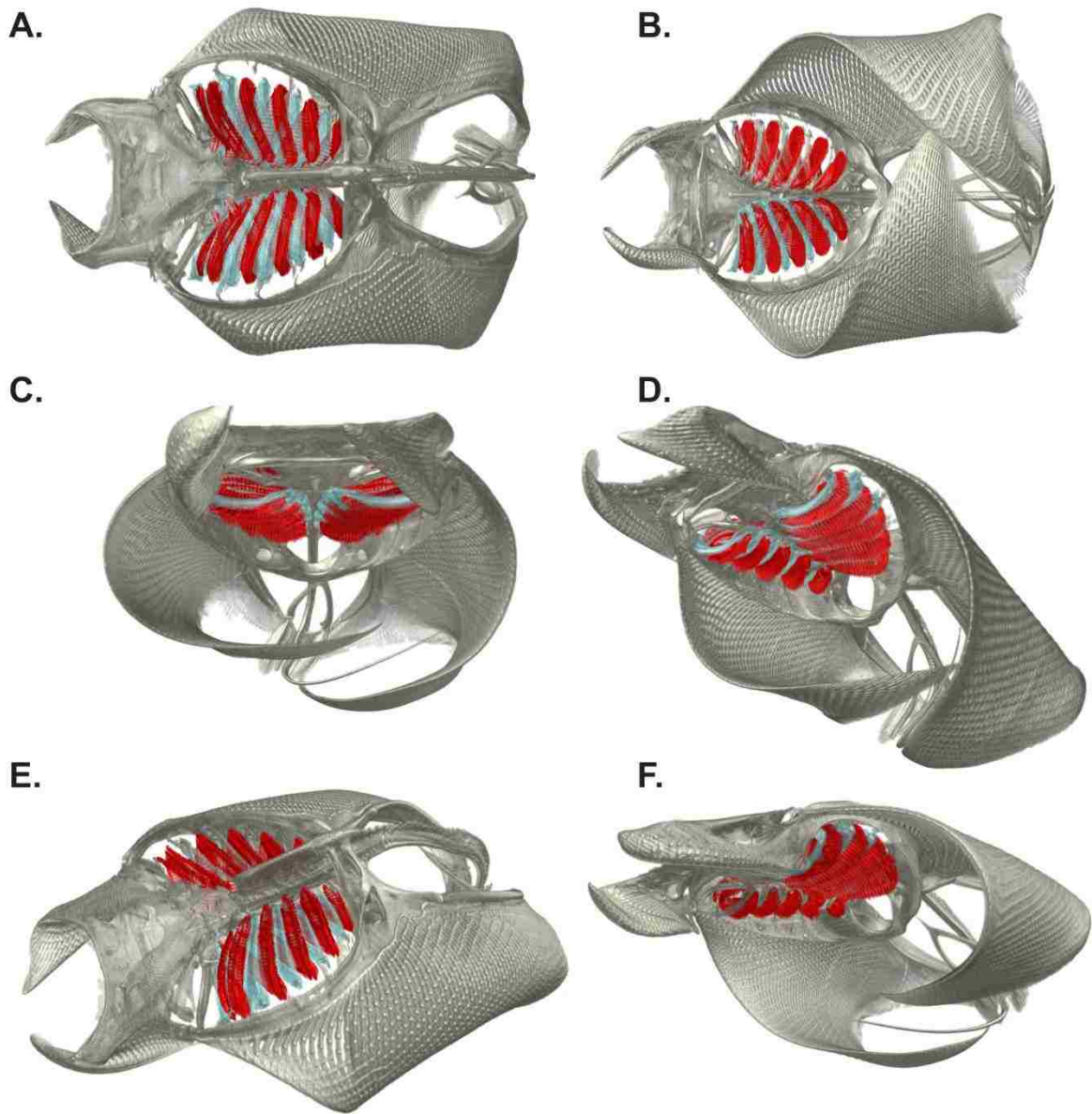
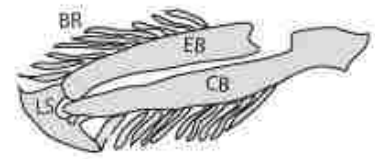
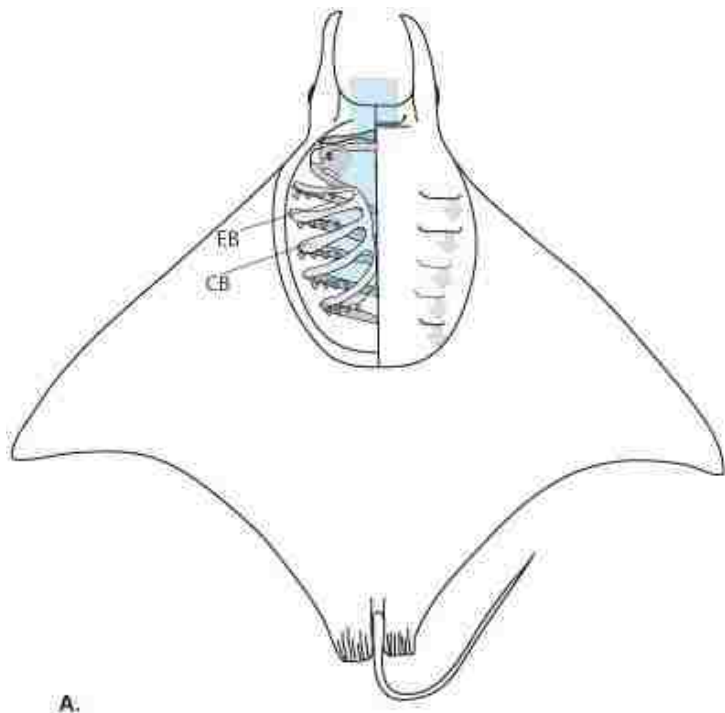


Figure 2

Figure 3.2. Computed tomography scans of *Mobula munkiana* showing branchial filters *in situ* from (A) dorsal view (B) ventral view, (C) anterior view, (D) ventro-lateral view, (E) dorso-lateral view, and (F) a rotated ventro-lateral view. Filter lobes are displayed in red and cartilaginous arch in blue.



B.

Figure 3.3. The architecture of the offset gill arch in a *Mobula* (ventral view). (A) shows the orientation of the branchial gill archs: EB = epibranchial, CB = ceratobranchials. Water flows between the EP and CB and exits out the pharyngeal cavity through the ventral gill openings. Note the medial EB is posterior to the medial CB. (B) The architecture of individual gill arches in dorsal ventral view and rotated 90 degrees. The top diagram illustrates the offset morphology of the branchial arches. The medial EB attaches posterior to the medial CB. The middle diagram shows the cartilaginous skeletal structure of the arch including the supportive branchial rays (BR) and the lateral stay (LS) common to myliobatoid rays (not shown in A). The bottom diagram illustrates the actual surface structure of the arch including the filter plates (FP) composed of many repeating filter lobes and the gill tissue (GT) used for respiration.

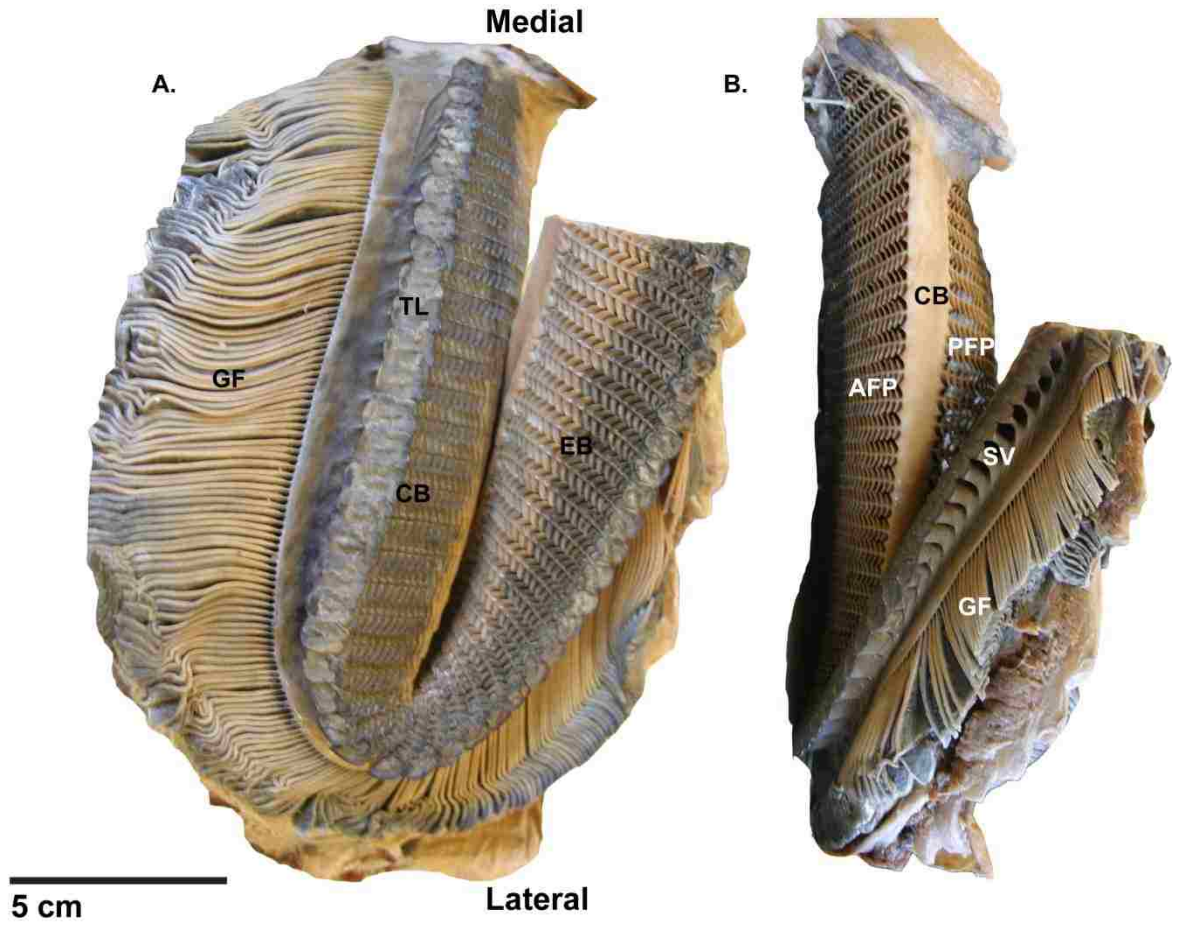


Figure 4

Figure 3.4. Gross anatomy of *Mobula tarapacana* gill arch with filter plates attached. A) Anterior view showing terminal filter lobes (TL) and Gill tissue (GT) on the epibranchial (EB) and ceratobranchial (CB) arch. B) Lateral view showing GT, secondary vanes (SV), posterior filter plates (PFP), ceratobranchial (CB), and the anterior filter plates (AFP).

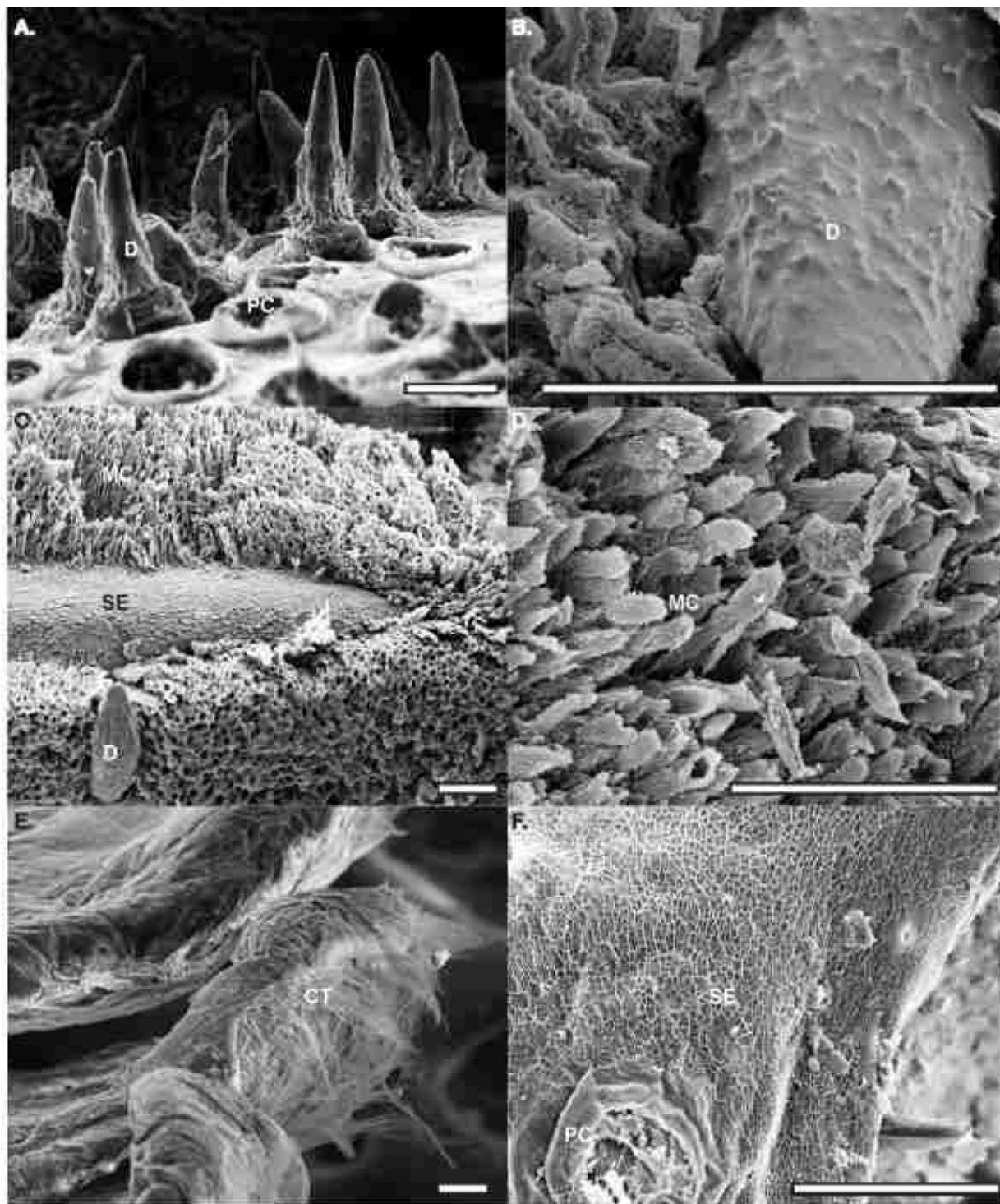
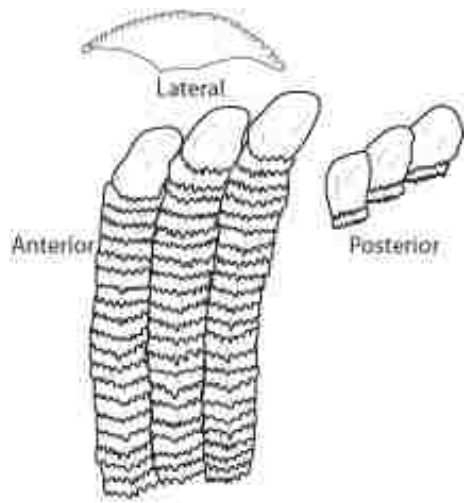
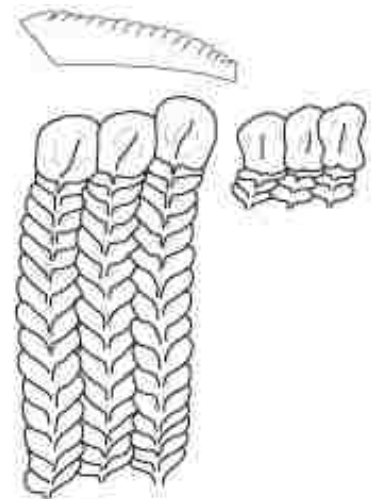


Figure 3.5. Microstructures of *Mobula* filter pads. A) Denticles (D) and pulp cavities (PC) of *Mobula munkiana*, B) surface of a *M. tarapacana* denticle, C) micro cilia (MC), surface epithelium (SE), and denticle of *M. tarapacana*, D) microcilia *M. tarapacana*, E) fibrous connective tissue (CT) in *M. kuhlii*, and F) filter surface epithelium and a pulp cavity in *M. thurstoni*.

Scale bars = 50 microns.



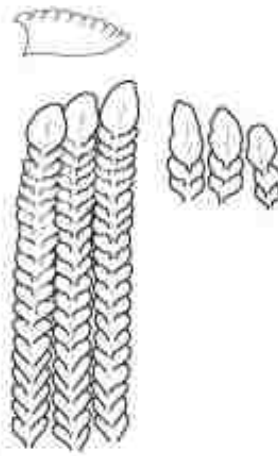
Manta birostris



Mobula tarapacana



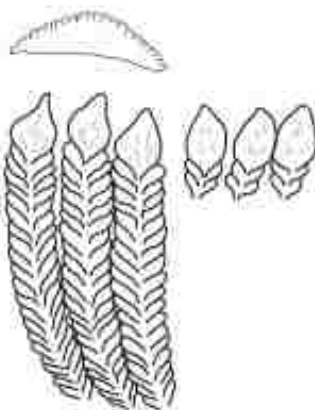
Mobula munkiana



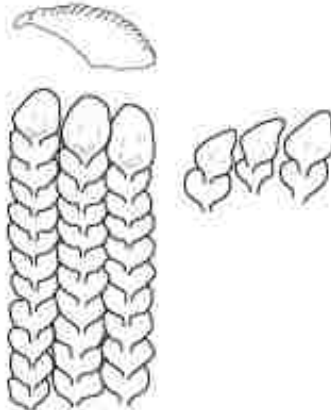
Mobula thurstoni



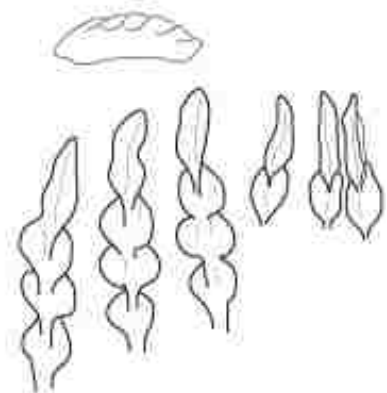
Mobula hypostoma



Mobula japonica
Mobula mobular



Mobula kuhlii



Mobula eregoodootenke

Figure 6

Figure 3.6. Morphology of mobulid filtering lobes in 8 species from lateral, anterior, and posterior perspective.

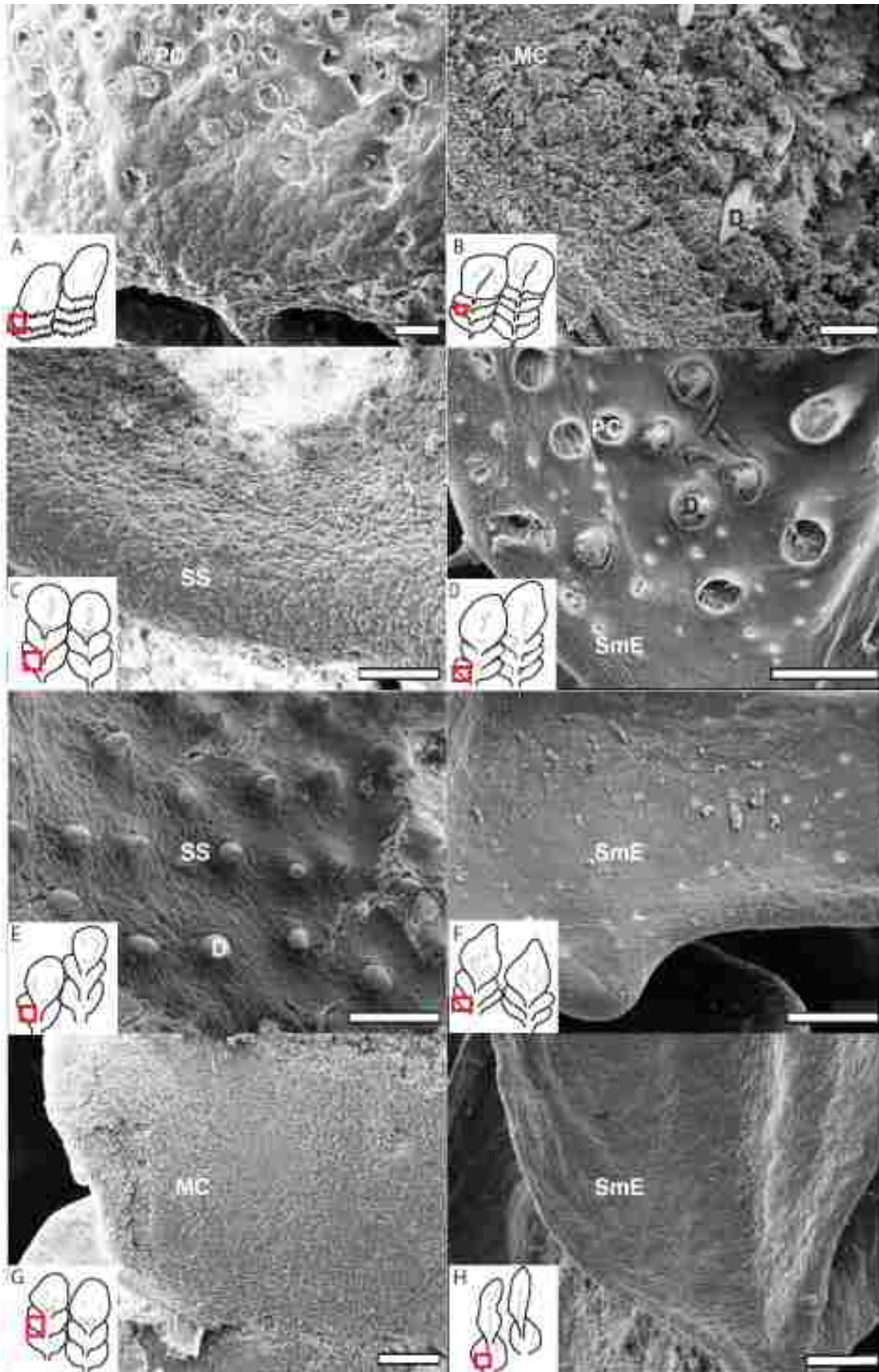


Figure 7

Figure 3.7. Scanning electron microscopy (SEM) of the filter surface in: A) *Manta birostris*, B) *Mobula tarapacana*, C) *Mobula munkiana*, D) *Mobula thurstoni*, E) *Mobula hypostoma*, F) *Mobula japanica*, G) *Mobula kuhlii*, and H) *Mobula eregoodootenke*. PC= pulp cavity, Cil=cilia, SS=secondary structure, Den = denticles, SmE= smooth epithelial surface. Scalebars = 50 microns.

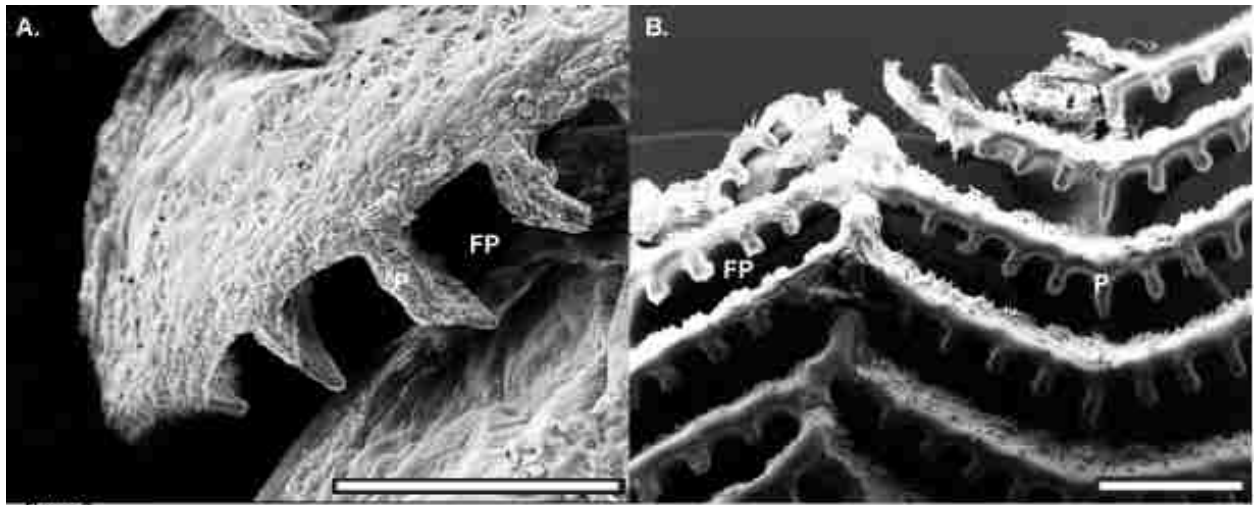


Figure 8

Figure 3.8. SEM of *Manta birostris* filter pad. A) Surface structure showing finger-like projections (P) at the filter pore (FP) and B) several filter lobes illustrating the projections across the filter pores. Scalebars = 1 mm.

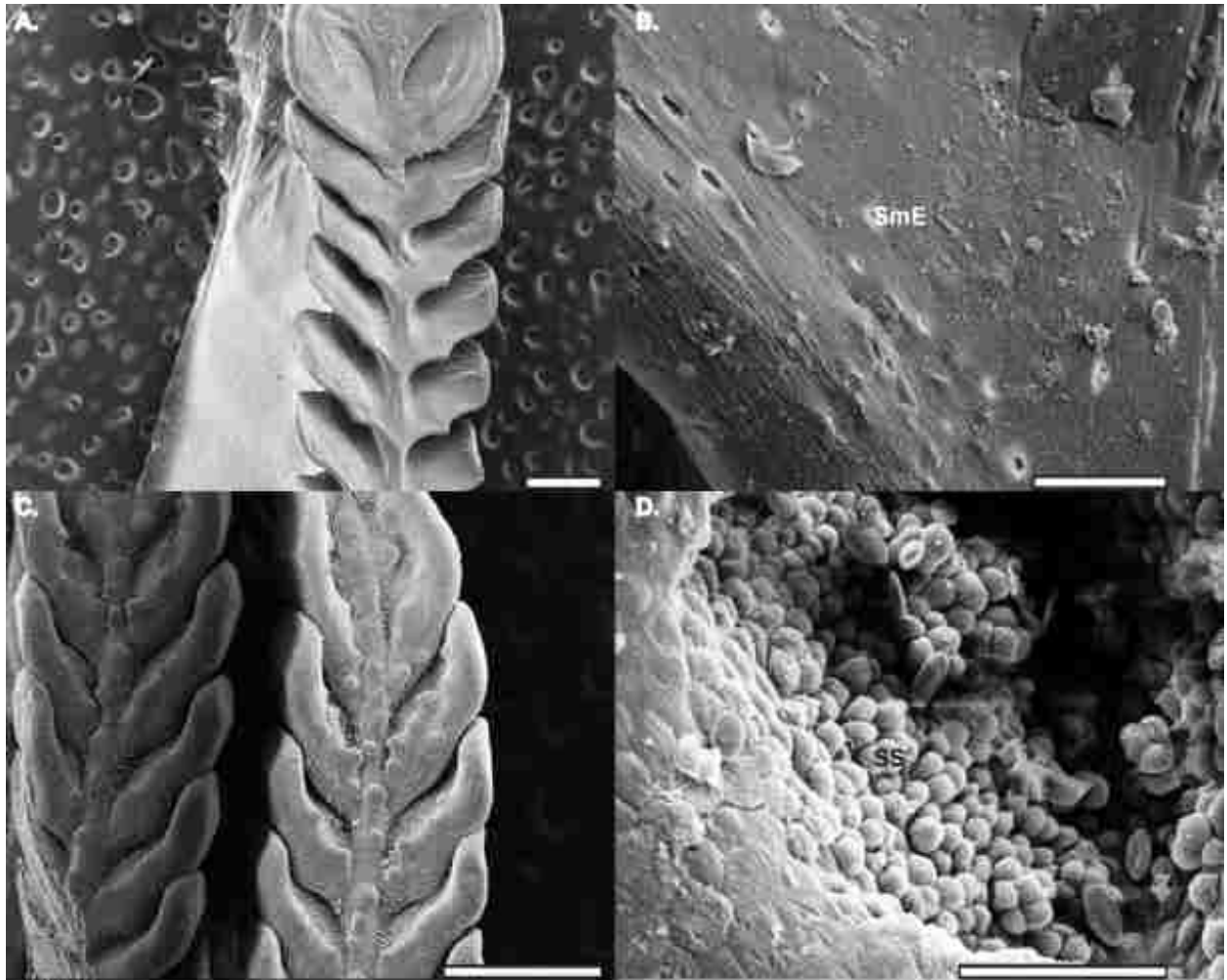


Figure 9

Figure 3.9. Surface structure of *Mobula japonica* (A & B) and neonatal *Mobula mobular* (C & D). A) Ascending filter lobe of *M. japonica*, B) surface of *M. japonica* is smooth (SmE), C) ascending filter lobe of *M. mobular*, and D) surface of *M. mobular* appears to have a secondary microstructure (SS). These differences may be attributed to the age of the animals sampled.

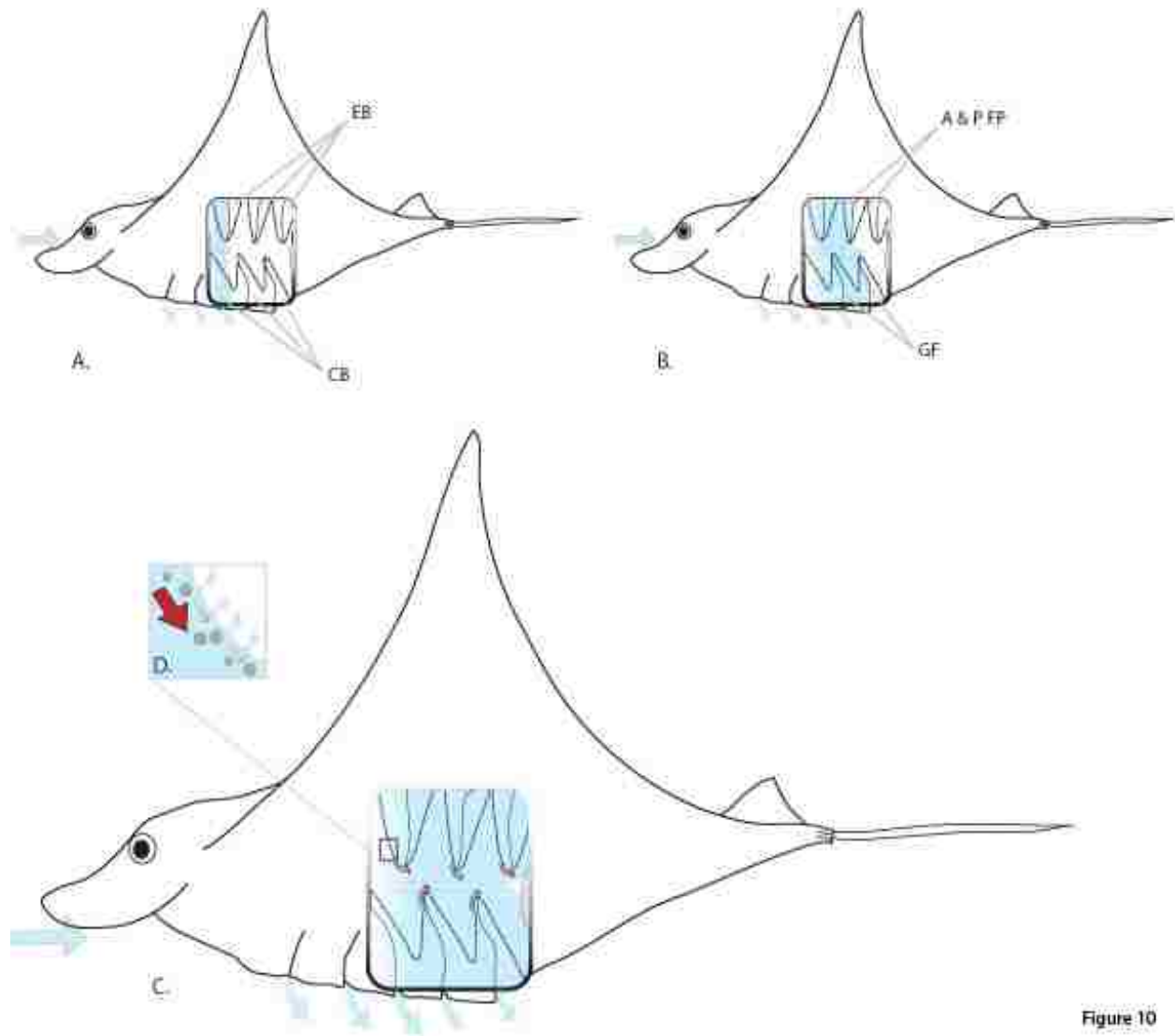


Figure 10

Figure 10. Water flow through the bucco-pharyngeal cavity. Diagrams A-D illustrate a time series of water flow through the bucco-pharyngeal cavity. Water moves in through the mouth and exits out the gill slits on the ventral surface of the ray. The branchial arch is arranged so that the epibranchial (EB) and ceratobranchials (CB) are slightly offset. Water passes between the anterior and posterior filter plates (A & P FP) located on both the upper EB and lower CB while food particles are retained on the filter. Water then passes through the filter's primary and secondary vanes (not shown) before flowing over the gill filaments (GF) and out the gill slits. (A) Illustrates water as it moves through the third branchial arch. (B) Water passing the fourth branchial arch and anterior portion of the ceratobranchial on arch V. (C) Water moves through the entire bucco-pharyngeal cavity. Water pressure is higher near the first branchial arches and lower near the esophageal opening. Red arrows indicate a shearing force created tangential to the filter plates which may act as a mechanism to clear particles from the FP. (D) Indicates the movement of water and food particle entrapment along the filter plate of arch III. Particles are trapped on the filter plate likely by a combination of sieving and hydrosol filtration as the water flows through the FP.

Chapter 4: The structure of suspension feeding elasmobranch filters

Abstract

The four independent evolutions of filter-feeding in the cartilaginous fishes led to four structurally different branchial filters. While some filters are robust, flattened filter pads (whale sharks, manta rays and devil rays), others more closely resemble gill rakers in bony fishes (basking sharks and mega mouth sharks). We used histology and scanning electron microscopy to investigate the composition of the branchial filters in 12 of the 14 species of cartilaginous filter-feeding fishes. We hypothesized that mucus producing cells would be abundant along the filter epithelium and perform as a sticky mechanism to retain and transport particles to the esophagus. We found that 11 of the cartilaginous fishes' branchial filters are composed of a hyaline cartilage core surrounded by a layer of highly organized connective tissue. In mobulids, the keratinized squamous epithelial tissue may contain mucus cells, denticles, and/or cilia. Whale sharks have loose connective tissue and a thin epithelial layer that lacks mucus cells, denticles, and cilia. Mega mouth sharks' hyaline cartilage core is surrounded by a dense, organized connective tissue layer and a thin epithelium that is completely covered by a layer of denticles. Basking sharks' filters lack a cartilaginous core and instead are composed entirely of smooth keratin. Mucus producing cells were present in only three of the 12 species examined which indicates that most cartilaginous filter-feeders do not use sticky sieving mechanisms to retain and transport particles.

Key words: Branchial filter, histology, *Mobula*, suspension feeding

Introduction

Suspension feeding in the cartilaginous fishes evolved approximately 66-22 million years ago (Cione and Reguero, 1998; Friedman et al., 2010) and includes four independently evolved lineages of fishes (Cetorhinidae, Megachasmidae, Rhincodontidae, and Mobulidae) (Sanderson and Wassersug, 1993). The mechanisms of filtration used by fishes are reflective of the morphology and composition of the filtering tissues. Most suspension feeding bony fishes have one or two rows of elongated gill rakers protruding anterolaterally (and also medially or posteromedially if there is a secondary row) from the epibranchial and ceratobranchial gill arches (Sanderson and Wassersug, 1993). The arches are composed of a cartilaginous or bony core covered by an epithelial layer which may contain mucus producing goblet cells, taste buds, and/or cuticle secreting cells (Friedland, 1985; Sibing and Uribe, 1985; Sanderson and Wassersug, 1993). The elongated rakers can be smooth or they may contain denticles or branchiospinules attached to the surface that assist with particle sequestration during feeding events (Collette and Nauen, 1983; Friedland, 1985; Bornbusch, 1988; Gibson, 1988; Sanderson et al., 1996; Ross et al., 2005).

The cartilaginous (elasmobranch) fishes have structurally different rakers than the bony fishes; some do resemble a modified version of the anteriorly protruding gill raker structure of bony fishes (*Cetorhinus maximus*, *Megachasma pelagios*) while others are dorsoventrally flattened filtering pads/plates [*Rhincodon typus* (Motta, 2010); *Mantas* and *Mobulas* (Notarbartolo di-Sciara, 1987; Paig-Tran et al., 2011)]. The surface of the filter can be smooth and bristle-like (*Cetorhinus maximus*: Matthews and Parker, 1950; Paig-Tran et al., 2011) or it can have varying degrees of coverage by denticles (*Megachasma pelagios*: Oikawa and Kanda, 1997; *Rhincodon typus*: Sanderson and Wassersug, 1993; *Manta* and *Mobulids*: Paig-Tran et al., in review).

Early predictions for particle capture and retention in the bony fishes speculated that direct sieving (collecting food particles bigger than the pore size of the filter) is the dominant mechanism of particle filtration (LaBarbera, 1984); however, more recent studies have shown that additional mechanisms including sticky sieving and cross-flow filtration may also be occurring in some species (Northcott and Beveridge, 1987; Goodrich et al, 2000; Callan and Sanderson, 2002; Smith and Sanderson, 2007). Work by Langeland and Nøst (1995) showed that particles in fish guts are often smaller than the pore size of the filter and therefore, additional mechanisms of particle sequestration must occur besides simple direct sieving. These mechanisms include direct interception, inertial impaction, gravitational deposition, and diffusional deposition (Rubenstein and Kohl, 1977). However, these mechanisms only solve the problem of how a particle comes into contact with a filter fiber and neglects the mechanism for retention at the filter. Sanderson et al. (1996) demonstrated that in Nile Tilapia, particles hitting the filter are retained by adhesion to sticky surfaces (e.g. mucus entrapment). Sticky sieving requires an abundance of mucus producing cells along the epithelial surface of the filter. This provides an adhesive coating along the filter so that any particles that come within one particle radius of the filter are retained. Work by Paig-Tran et al. (*in review*) examined the ultrastructure of the branchial filters in the mobulid - devil rays (*Mantas* and the *Mobulas*) and found that some species' filter lobes were covered with epithelial cilia. The presence of cilia along the surface of the filter lobe indicated that some form of sticky sieving is likely occurring as either a mechanism of particle retention, or as a mechanism of transport for food particles following initial capture events. Verification for whether sticky sieving is actually occurring relies heavily on the detection of high concentrations of mucus producing cells present along the filter lobes.

How then are mucus laden particles transported to the esophagus for ingestion? Goodrich et al. (2000), Callan and Sanderson (2002), and Smith and Sanderson (2007) demonstrated that cross-flow filtration is used as a filter mechanism in bony fishes and Motta et al. (2010) predicted that whale sharks may also take advantage of cross-flow. Cross-flow filtration makes use of tangential shearing to clear the filter following initial particle collection events, prevents clogging of the filter, and serves to move food particles toward the esophagus for ingestion. It is difficult to test whether cross-flow filtration is actually occurring in the elasmobranch fishes since they are large bodied, fast moving fishes that are difficult to keep in aquaria. Although these mechanisms are difficult to explore *in situ*, they have been demonstrated theoretically (Hung et al., 2012) and experimentally with simplistic models (Paig-Tran et al. 2011).

The present study uses histology to examine the composition of the filter pads/rakers in 12 of the 14 species of filter-feeding elasmobranchs: *Manta birostris* (Walbaum 1792), *Mobula eregoodootenke* (Cuvier, 1829), *Mobula hypostoma* (Bancroft 1831), *Mobula japonica* (Müller & Henle 1841), *Mobula kuhlii* (Valenciennes in Müller & Henle 1841), *Mobula mobular* (Bonnaterre 1788), *Mobula munkiana* (Notarbartolo-Di Sciara 1987), *Mobula tarapacana* (Philippi 1892), *Mobula thurstoni* (Lloyd 1908), *Rhincodon typus* (Smith, 1828), *Cetorhinus maximus* (Gunnerus, 1765), and *Megachasma pelagios* (Taylor et al., 1983). The aims of this study are: (1) to provide a clear description of the composition of the branchial filter for each species and (2) to verify the presence of mucus producing cells in the branchial filter epithelium - evidence for sticky sieving filtration.

Methods and Materials

Specimens

Samples of the filter pad/raker tissue were collected from preserved museum specimens [Smithsonian Museum of Natural History (Washington D.C., USA): *Manta birostris* (N =1), *Mobula hypostoma* (N= 6), *Mobula eregoodootenke* (N=1), *Mobula mobular/M. japonica* neonate (N=1), *Mobula kuhlii* (N=1); LA Natural History Museum (Los Angeles, CA, USA): *Mobula thurstoni* (N=1), *Cetorhinus maximus* (N=1); Scripps Institute of Oceanography SIO Marine Vertebrate Collection (La Jolla, CA, USA): (*Mobula tarapacana* (N=1), *Mobula munkiana* (N=2), *Mobula thurstoni* (N=1), *Mobula japonica* (N=1), *Rhincodon typus* neonate (N=2), *Megachasma pelagios* (N=1); R. Rubin: *Manta birostris* (N=1)]. *Manta alfredi* and *Mobula rochebrunei* were not available for this study.

In *Manta* and *Mobula* spp., we excised the right, third branchial arch through the third gill slit following methods described by Paig-Tran et al. (*in review*). In *Rhincodon typus*, a 1cm x 1cm subsection was extracted orally from the right, third filter pad. All specimens were wrapped in ethanol soaked cheesecloth, sealed, and sent to the University of California, Irvine for histology and the University of Washington for SEM. In *Megachasma pelagios*, the entire right gill structure (arch 1-5) was removed from a thawed specimen at Scripps Institute of Oceanography, preserved in 10% neutrally buffered formalin, stored in 70% ethanol, and only rakers extracted from the third branchial arch were analyzed using histology and SEM. *Cetorhinus maximus* gill rakers were already extracted from the arch and stored as dried samples at the LA Natural History Museum. We were unable to verify which arch the rakers were originally extracted from.

Histology Preparation

Specimens were dehydrated using one of the following treatments over 48 hours: 1) an ascending ethanol dehydration series to 100% (*Manta birostris*, *Mobula tarapacana*, *Mobula thurstoni*), or 2) an ascending t-butyl alcohol dehydration series (all remaining specimens).

Following dehydration, samples were infiltrated three times (3 hr per infiltration, at 60°C, -25 Pa) with hard paraffin (Paraplast type I melting point 55-57°C, Richard-Allen Scientific, Kalamazoo, MI, USA), embedded, and sectioned transversely at 10 µm (*Manta birostris* and *Mobula tarapacana*) for large samples or 5 µm for smaller samples using disposable blades on a manual rotary microtome (model 815; American Optical Company, Buffalo, NY, USA). *Manta birostris* and *Mobula tarapacana* specimens were large and required an additional treatment to soften the specimen prior to sectioning. These embedded samples were soaked for 30 min in Nair™ Hair Removal (Church and Dwight Co, INC, Princeton, NJ, USA) after every 10 sections to reduce tissue separation from the paraffin during sectioning. Serial sections were mounted, dried for 1 week, and alternately stained with Harris Hematoxylin (Mallory, 1944) and Eosin (Putt, 1948) stain, Dane's stain (Dane and Herman, 1963), and a modified version of Masson's Trichrome (Gurr, 1956). Hematoxylin and Eosin stain is a general stain used for visualizing tissue samples. Dane's stain is used to visualize prekeratin (orange), keratin (red), and mucopolysaccharides (turquoise). Masson's trichrome is useful when visualizing collagen (blue-green), mucus (blue-green), nuclei (blue to black), and cytoplasmic elements (red/mauve).

Histology slides were viewed using a Zeiss steREO Discovery V20 microscope (Carl Zeiss Imaging GmbH, Jena, Germany) using the microscope imaging program Axio Vision (Carl Zeiss) and photographed using a Zeiss AxioCam HRC camera. Images were viewed and measured using NIH Image J software (version 1.4, <http://rsbweb.nih.gov/ij/>).

Scanning Electron Microscopy

We performed scanning electron microscopy (SEMs) on the three shark species (*Megachasma pelagios*, *Rhincodon typus*, and *Cetorhinus maximus*). In depth SEMs for *Mobula* can be found in Paig-Tran et al. (*in review*). Samples of *M. pelagios* and *R. typus* filter pads/rakers were dehydrated into 100% ethanol over a 48 hour period. The samples were then critically point dried (Samdri 790, Tousimis Research Corp, Rockville, MD, USA) using a liquid CO₂ method, sputter coated (SPI Sputter 12121, SPI Supplies/Structure Pro, Inc, West Chester, PA, USA), and scanned using a bench top scanning electron microscope (Jeol Neoscope JCM-5000, Tokyo, Japan). *Cetorhinus maximus* rakers were not dehydrated or critically point dried; however, they were sputter coated prior to scanning. We photographed the ultrastructure for the three species of sharks and used NIH Image J software (version 1.4, <http://rsbweb.nih.gov/ij/>) to measure the pore size in neonatal *R. typus* filter pads.

Results

General Filter Structure in Mobulids

Mobulid filter pads are different from both the gill rakers in bony fishes and from the gill rakers and flattened filter pads filter-feeding sharks (Paig-Tran et al., *in review*). The branchial arch is cartilaginous and covered by modified filter structures (filter lobes) that are attached to the anterior and posterior epibranchial and ceratobranchial arches. The arches are offset from one another so that the medial epibranchial arch attaches posterior to the medial ceratobranchial attachment. The filter structures run along the length of the arch and are composed of ascending rows of individual filtering lobes (AL) ending in a terminal lobe (TL) (Figure 4.1A). The innermost skeletal support system runs the length of the lobe and is composed of a central

hyaline cartilaginous core that branches into paired filtering lobes (4.1B & 4.1C). The hyaline cartilage skeleton is surrounded by a well-defined perichondrium (P). Lacunae (spaces surrounding the chondrocytes) are visible throughout and are a product of histological slide preparation.

Surrounding the cartilaginous core is a highly regular, connective collagenous tissue which can either be dense (DCT) or loose (LCT) (Figure 4.1D). The connective tissues in the medial portion of the filter lobe (near the central ascending ridge) contain blood vessels (Ves) supplying the filter lobe tissues. The epithelial layer is substantial and is composed of stratified squamous keratinized epithelium (SQET) (Figure 4.1E); not all of the epithelial cells contact the basement membrane and in some areas the cells are several layers thick. In some mobulids there is a layer of cilia lining the outermost epithelium (Cil). Goblet (mucus producing) cells occur in abundance within the epithelial layer (MC) (Figure 4.1B & 4.1F) and in some, denticles are also present within the epithelial layer (Dent). The terminal filtering lobes are rounded or lancelet. The distal edge contains the highest concentration of mucus producing cells (Figure 4.2) and the epithelial tissue at the distal lobe is thick.

The tissue surrounding the hyaline cartilage can be either dense connective collagenous tissue or loose connective tissue, is highly organized/structured, and is birefringent under cross polarized light. Here we have shown the birefringence in our largest *Mobula* filter pad specimen: *Mobula tarapacana* (Figure 4.3A-4.3C). A series of photographs under differing degrees of polarization in *Mobula tarapacana* illustrates the fiber angles of the connective tissue under a polarizing lens at 4x magnification, under partial cross polarization, and under cross polarization.

Individual mobulids

Manta birostris is the largest of the mobulids and has one of the most distinctive filtering pads. Adjacent ascending lobes are fused together and there are characteristic finger-like projections extending from the ventral portion of the lobe across the filter pore (Figure 4.4A), which effectively decreases the diameter of the filter pore opening. The hyaline cartilage is surrounded by ordered loose connective tissue; no dense connective tissue is present. The epithelium in *M. birostris* is highly keratinized and includes dermal denticles along the dorsal and ventral portion of the filter lobes. Mucus producing cells are not evident within the epithelium. The dorsal epithelium is substantially thicker (90-170 μm) than the ventral epithelium (25-35 μm).

Mobula tarapacana's filter pad is also highly distinctive from all other *Mobulas*. The ascending lobes also are fused together so that the epithelial tissue and dense connective tissue from adjacent lobes are connected to each other, forming a more rigid filter plate (Figure 4.5). Although close in filter lobe size, it is easy to distinguish between *Manta birostris* and *Mobula tarapacana* filter pads because *M. tarapacana* lacks the finger-like projections seen in *M. birostris*. *M. tarapacana* is highly ciliated, has one of the thickest layers of stratified squamous epithelium (80-125 μm dorsal lobe and 50-80 μm ventral lobe), and includes both mucus producing cells and denticles along the dorsal and ventral portion of the filter lobes.

Mobula munkiana is denticulated along the medial dorsal filter lobe with a high presence of mucus producing cells along the entire epithelial layer; the epithelium lacks cilia (Figure 4.6). The epithelium is the thickest of all the mobulids and is substantially thicker on the dorsal surface (88-178 μm) and on the lateral edges of the filtering lobe (~260 μm) than on the ventral surface (35-50 μm). A layer of loose connective tissue surrounds the hyaline cartilage core.

Mobula thurstoni is highly denticulated along the dorsal and ventral lobe however this is difficult to determine in our samples; however it is well documented under scanning electron microscopy (Paig-Tran et al., *in review*). The connective tissue surrounding the hyaline cartilage is loose and forms a connective sheath between the ascending lobes (Figure 4.7). We could not determine the presence of mucus producing cells along the epithelial surface. The dorsal epithelium is between 40-70 μm thick while the ventral epithelium is 19-30 μm thick.

Mobula hypostoma has the greatest number of denticles along the dorsal and ventral surface of the filter plate per unit area and is easily recognized by its rough exterior. The DCT was approximately 30-80 μm thick. There is a substantial loose connective tissue layer in *M. hypostoma* forming a connective sheath between the ascending lobes (Figure 4.8) which is between 50-240 μm thick on the ventral surface. The epithelium is thin in comparison to *M. tarapacana* (13-17 μm).

Mobula japonica/Mobula mobular (juvenile) is lacking in denticles and cilia; however, the squamous epithelial tissue is highly keratinous (Figure 4.9). The epithelial tissue is thickest in between adjacent filtering lobes (120-145 μm) and thinner at the filter lobe tip (~30 μm). The hyaline cartilage is surrounded by a thick layer of dense connective tissue. There are no visible mucus producing cells along the epithelial surface.

Mobula kuhlii lacks denticles, but has cilia along the surface epithelium. Mucus producing cells are abundant, especially near the medial edge of the pore where tissue in-folds (Figure 4.10). Loose connective tissue surrounds the hyaline cartilage. The squamous epithelium is thickest near the pore opening (88-166 μm) and thinnest near the lateral lobe edge (19-25 μm) and on the ventral surface (56-60 μm).

Mobula eregoodootenke has another highly distinctive filter. The ascending lobes are few (approximately 4 paired lobes) and lobes are pliable unlike the rigid lobes of other *Mobulas*. Loose connective tissue surrounds the hyaline cartilage (Figure 4.11) and is between 65-88 μm thick. *M. eregoodootenke* lacks denticles and cilia. The epithelial layer is thin (33 μm) yet highly keratinized. The cartilaginous core is between 122-167 μm in thickness.

Sharks

The filter lobe of *Rhincodon typus*, whale shark, closely resembles the filter lobe structure of the mobulids. The gross morphology of *Rhincodon typus* flattened filter pad has been previously described by Motta et al. (2010). Upon close examination, the pad is similar to that of mobulids in that there are repeating filtering elements that are composed of a central ascending core which branches into paired, secondarily branching filtering lobes forming a filter “mesh” (Figure 4.12A and 4.12B). In our specimen (juvenile) the filter pad is composed primarily of hyaline cartilage (Figure 12C). The connective tissue surrounding the cartilage is loose and the epithelium is also thin with no apparent mucus producing cells present.

Megachasma pelagios has a filter that more closely resembles the rakers of bony fishes than the flattened filtering pads of the mobulids and *Rhincodon typus*. The filter is composed of many repeating denticulated rakers (Figure 4.13A & 4.13B). The modified rakers are composed of a hyaline cartilage core surrounded by a dense connective tissue and a thin epithelial covering (Figure 4.13C-E).

Cetorhinus maximus has a smooth keratinous bristle like structure described by Matthews and Parker (1954) and Sims (2008). The rakers lack any type of denticulation, cilia, or mucus cells (Figure 4.14). Unlike the other filter feeding cartilaginous fishes, *Cetorhinus* rakers do not

have a cartilaginous skeleton. The medial edge of the raker that connects to the epithelium along the branchial arch is curved while the distal portion of the raker becomes more narrowed as it extends away from the arch.

Discussion

We proposed that the filter-feeding cartilaginous fishes use sticky sieving to retain food particles along their branchial filters prior to particle transport to the esophagus. However, we only verified that mucus producing cells are present along the ascending filter lobes in 3 of the 12 species examined. This means that the majority of the suspension feeding cartilaginous fishes do not use a sticky sieving mechanism to retain and transport particles along the filter following initial collection events. How then are particles 1) separated from the fluid streamline and 2) transferred to the esophagus for ingestion when there are no sticky surfaces for particles to adhere to?

The possible mechanisms by which particles come into contact with a filter fiber (Rubenstein and Kohl; 1977; LaBarbera, 1984; Shimeta and Jumars, 1991) predicted that fishes primarily use sieving mechanisms to filter particles from the fluid streamline. Recent work (Goodrich et al., 2000, Friedland et al., 2006; Smith and Sanderson, 2007) demonstrated experimentally that direct sieving is not the only mechanism for particle sequestration and that particles smaller than the pore size of the filter are also ingested. Paig-Tran et al. (*in review*) showed that in the devil rays, low Reynolds numbers (dimensionless number used to illustrate the ratio of inertial to viscous forces) and high Péclet numbers (dimensionless number used to illustrate the ratio of advective to diffusive forces) at the surface of the filter create ideal

conditions for particles (both larger and smaller than the pore size) to contact the filter via three mechanisms: direct sieving, inertial impaction, or direct interception. Some fishes make use of sticky mechanisms along the branchial filter to retain food particles smaller than the filter (Northcott and Beveridge, 1988; Sanderson et al., 1996). The presence of mucus producing cells along the filter lobe supports sticky sieving as a likely mechanism of particle retention and transport to the esophagus in *Mobula tarapacana*, *Mobula munkiana*, and *Mobula kuhlii*. However, the mobulids that lack mucus cells must employ other mechanisms. Cross-flow filtration may serve to circumvent the need for retaining particles along adhesive surfaces by making use of tangential sheering parallel to the filter surface to push particles from the filter elements toward the esophagus for ingestion.

It is interesting to note that the whale shark and the devil ray lineages evolved filter-feeding separately yet both make use of a modified, flattened filter pad structure and are likely using cross-flow as a means of transporting particles to the esophagus. Despite obvious differences between the branchial arches in these two lineages of fishes [e.g. *Mantas* and *Mobulas* have offset epibranchial and ceratobranchial arches that form a twisted arch structure (Paig-Tran et al., 2011, Paig-Tran et al., *in review*) while whale sharks display the more characteristic c-shaped branchial arches seen in most fishes (Motta et al. 2011; Paig-Tran et al. 2011)] the basic structures of the filter pads are similar. The devil rays have numerous, repeating rows of elongated, paired filter lobes that end in a rounded, terminal lobe at the edge of the branchial arch (Notarbartolo di Sciara, 1987; Paig-Tran et al. *in review*). Each filter lobe is attached to the arch by a cartilaginous support structure and the open area between these supports forms the secondary vanes, channels through which water passes from the filter pore to the gill tissue. Whale sharks also have numerous repeating filter lobe rows which contact the adjacent

rows, in turn forming a “reticulated mesh” for filtering (Motta et al., 2010). Each of these filter rows is also supported by cartilaginous support structures which, as in the mobulids, connect the filter to the branchial arch. Once again, the spaces between these support structures form a series of secondary vanes through which water is tunneled toward the gill tissue. The buccopharyngeal length and filter morphology in these two lineages are easily compared to the flattened, permeable filter mesh used in industrial cross-flow filter systems. When whale sharks and mobulids feed, the rakers along the arches are positioned such that the buccopharyngeal cavity resembles an elongated “pipe” lined by numerous flattened filter structures. Water deviates from the initial incoming streamline to exit through the filter pores, leaving behind a slurry of food particles which must then make use of cross-flow to travel to the esophagus for processing.

The filter pads in whale sharks and devil rays are very different from the architecture of the two lamniform lineages (basking sharks and mega mouth sharks) of filter-feeding sharks and also that of bony fishes. The rakers in these sharks extend off the epibranchial and ceratobranchial arches and project anterolaterally into the buccopharyngeal cavity (i.e. oriented towards the incoming flow). The mega mouth’s rakers are shortened and robust, composed of a hyaline cartilage core, and externally covered with denticles while the basking shark’s rakers are elongated and brittle, smooth, and composed entirely of keratin. However, these two sharks do have very different feeding modalities and likely use their rakers in differing ways. Basking sharks are continuous ram suspension feeders; like the devil rays, these sharks swim with an open mouth continuously filtering plankton (Sims, 2000). Presumably basking sharks are using direct sieving, inertial impaction, and/or direct interception to capture their prey along their elongated, keratinous rakers; however, once again there are no mucus producing cells along the length of the filtering elements to help retain and transfer food particles following capture events.

It is entirely possible that cross-flow filtration also plays a role in basking shark filtration. The mega mouth shark uses engulfment feeding to capture its prey; a feeding mode more similar to that of the balaenopterid whales than any of the other suspension feeding sharks (Nakaya et al. 2008). This mode relies on rapid expansion of the buccopharyngeal cavity to hold large quantities of water prior to closing the system and processing the water through the filtering elements. Once again, there are no discernible mucus producing cells along the mega mouth shark's filtering elements. However, the irregular flow through the buccopharyngeal cavity would not support cross-flow as a means of clearing the filter. The mega mouth does have a large fleshy tongue that may aid in clearing the filter following water expulsion.

When comparing other feeding parameters, we find that the gill openings in the mega mouth shark are only $\frac{1}{4}$ to $\frac{1}{3}$ the size of basking sharks (Nakaya et al. 2008) measuring 4-6% of the total length (TL) in mega mouth (Taylor et al., 1983; Berra & Hutchins, 1990; Nakaya et al., 1997; Yano et al., 1999) compared to 15-20% TL in basking sharks (Bigelow & Schroeder, 1948; Bass et al., 1975). However, mega mouth has the longest buccopharyngeal cavity of all the filter-feeding sharks (mega mouth ~24-29% of the TL; basking shark ~ 16-18% of the TL; whale shark ~ 18-25% of the TL) (Nakaya et al., 2008). What then is the benefit for an animal to have such small gill slits when processing large volumes of water during each feeding event? Presumably, the short gill slits in mega mouth act as a Hagen-Poiseuille flow restricting system, dropping the speed of the fluid as it exits out the gill slits and allowing for food particles to stay in contact with the filtering elements for longer periods of time. Using the morphometrics reported in Taylor et al. (1983) and Nakaya et al. (2008), the extended gape of a mega mouth while feeding is approximately 18.5% of its TL (TL 5440 mm; 1006 mm mouth width and 700 mm mouth height ; gape area = $704,200 \text{ mm}^2$ in the reported specimen). In order for the inlet

and outlet flow to be equal, we would assume that the outlet must be the same area as the inlet (disregarding the addition of gill rakers and any pressure drops thus associated). We can calculate the width size that the gill slits must be in order for the “pipe” to have the same inlet and outlet flows. By assuming that the heights of the gill slits are constant at 6% of the TL (or 326.4 mm in a 5440 mm TL fish) then we calculate that the width of each gill slit must be equal to 21.6 mm. However, this would only hold true if mega mouth shark was a continuous ram filter feeder, not an engulfment feeder. In this case the initial intake of water is much larger, spanning the entire buccopharyngeal cavity. Nakaya et al. (2008) calculated that the entire area of the buccopharyngeal chamber can hold 565 liters (or 565,000,000 mm²) – hence the outlet (total area = 704,200 mm²) would be far too small to process such a large volume of water without restricting the exiting flow considerably.

Acknowledgements

We sincerely thank HJ Walker (SIO Marine Vertebrate Collection at Scripps Institute of Oceanography), Lynne Parenti, Jeff Clayton, Jerry Finan (Smithsonian Museum of Natural History), Jeff Seigel (LA Natural History Museum), and Robert Rubin for graciously allowing us to examine and sample from their *Mobula* and *Manta* collections. We would like to express many thanks to Dr. Tomasz Owerkowics for providing lab space and for helpful discussions on histology techniques. Thank you to Dr. Jacqueline Webb for providing t-butyl dehydration protocols. We thank the Smithsonian Museum of Natural History and the University of Washington Sargent Fellowship for providing student travel funding to museums. The University of Washington WRF-Hall fellowship provided one quarter of student support. Thank you to the Richard and Megumi Strathmann Fellowship for providing housing support at FHL labs.

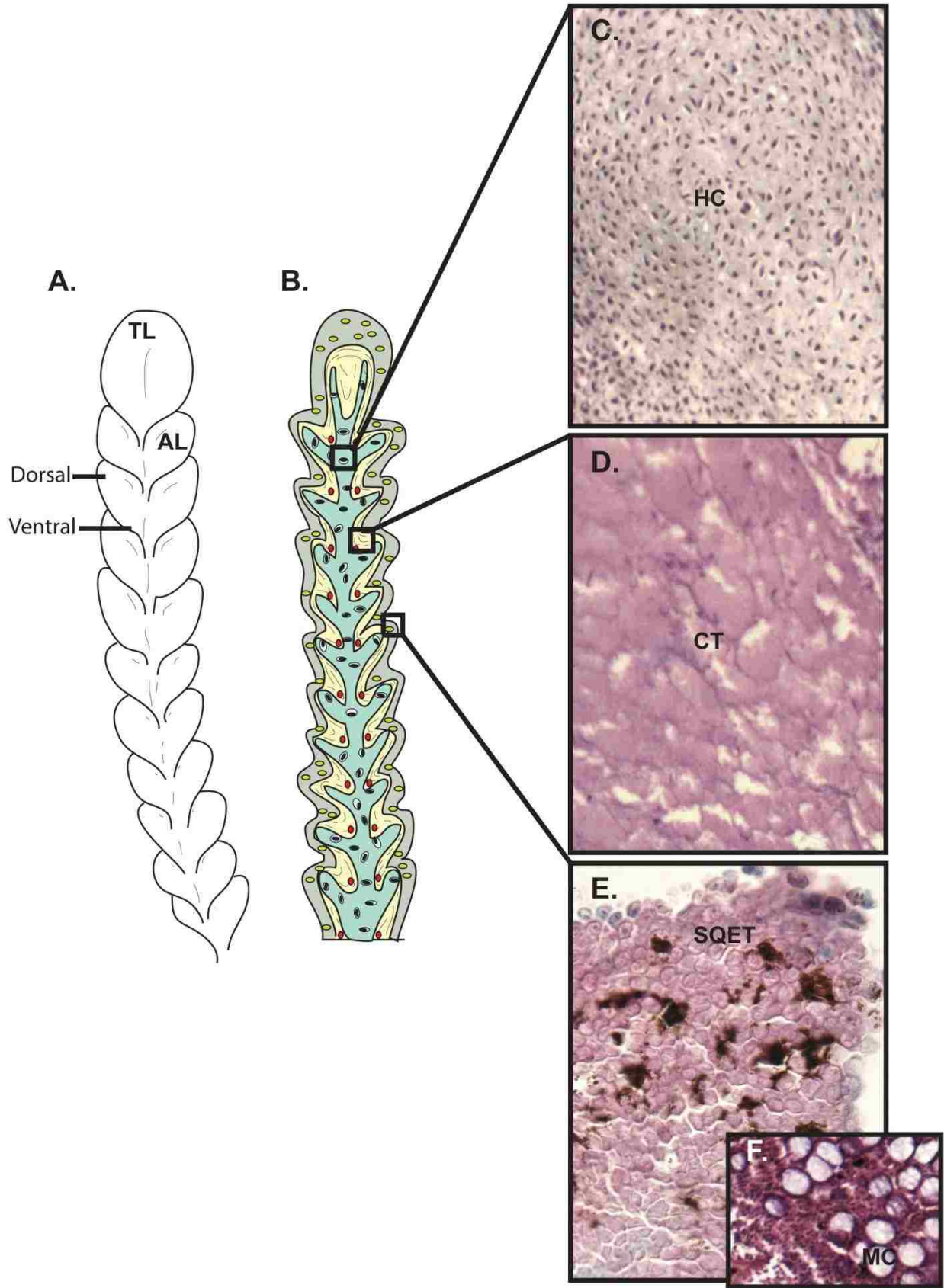
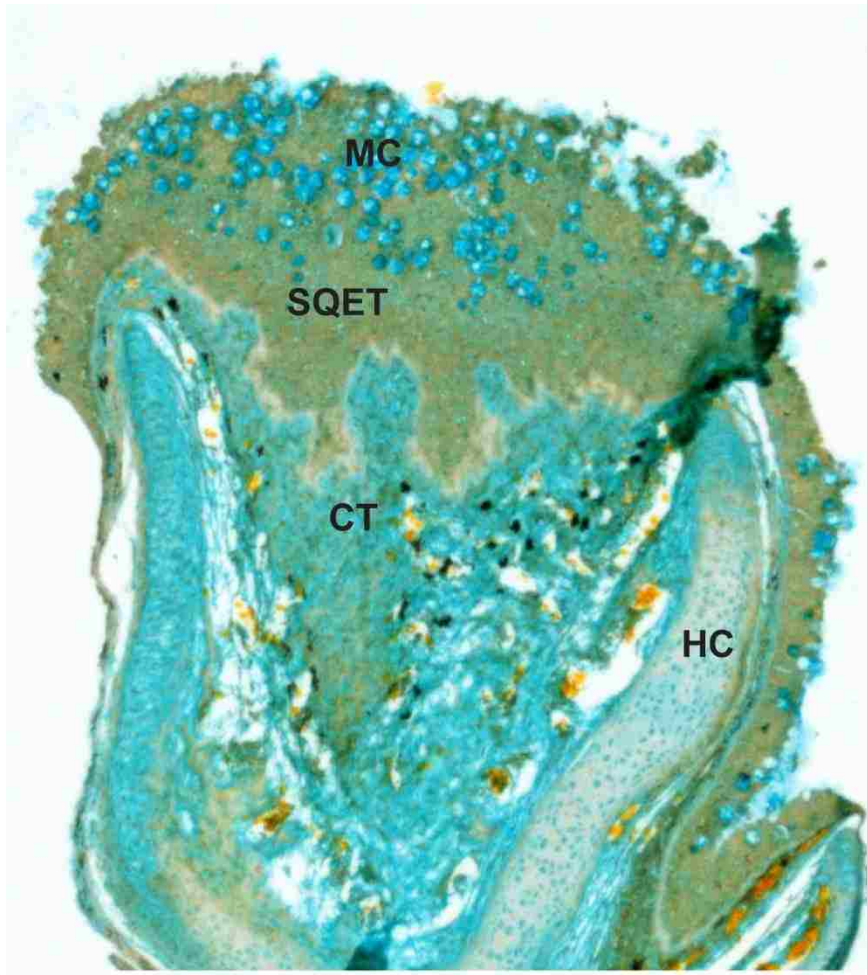
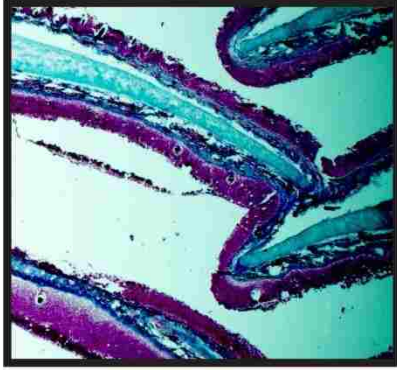


Figure 4.1. Generalized *Mobula* filter lobe. A) Illustrates one ascending filter lobe (AL) ending in the terminal lobe (TL). Each paired filtering lobe has a dorsal surface, which forms the bottom edge of the filter pore opening, and a ventral surface, which forms the top of the filter pore opening. B-F) Illustrates the composition of the filter lobe. The central support system is composed of hyaline cartilage (HC). Organized connective tissue (CT) surrounds the cartilage and can be either loose or dense in consistency. The keratinized epithelium is composed of many layers of stratified squamous cells (SQET). The epithelium may contain mucus producing goblet cells (MC) and/or denticles (not shown) that extend out into the filter pore.

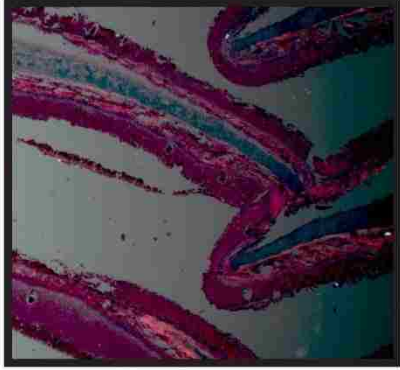


100 microns

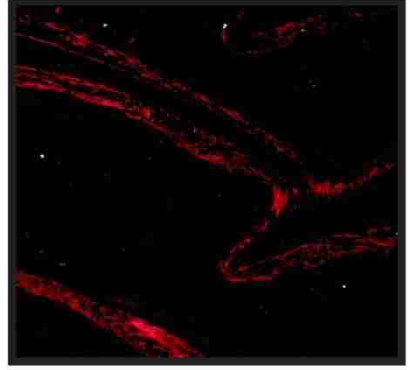
Figure 4.2. Mucus producing cells in the terminal lobe. The terminal lobe of the filter lobe (*M. kuhlii* shown stained with Dane's stain) is supported by two cartilaginous supports (HC) with a dense layer of connective tissue (CT) in between. The keratinized epithelium is the thickest at the distal edge of the terminal lobe and is often covered by an abundance of mucus cells (MC).



A.

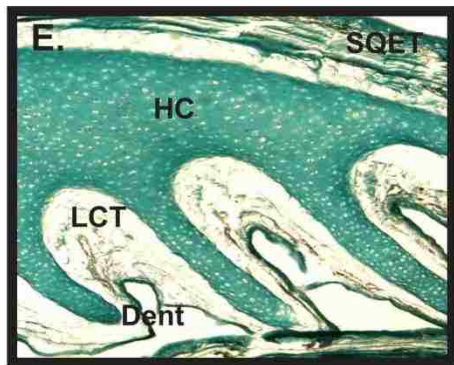
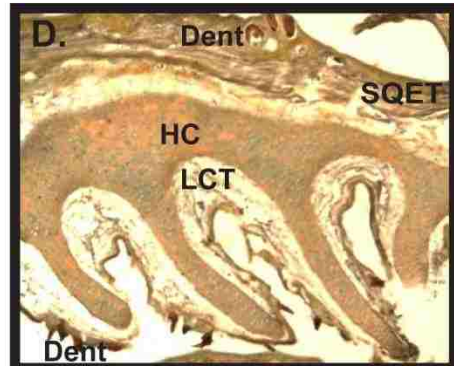
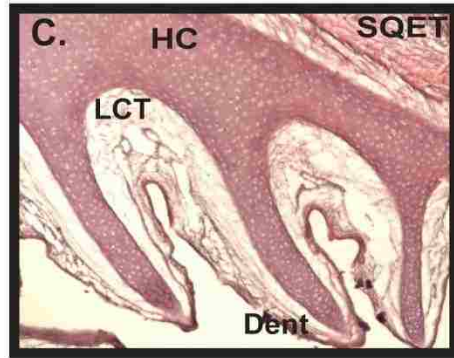
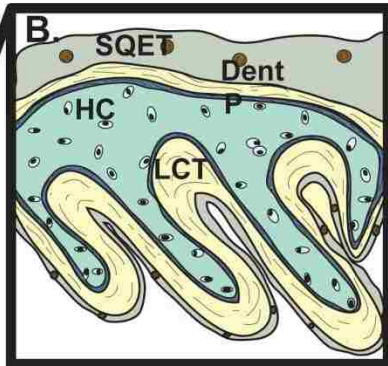
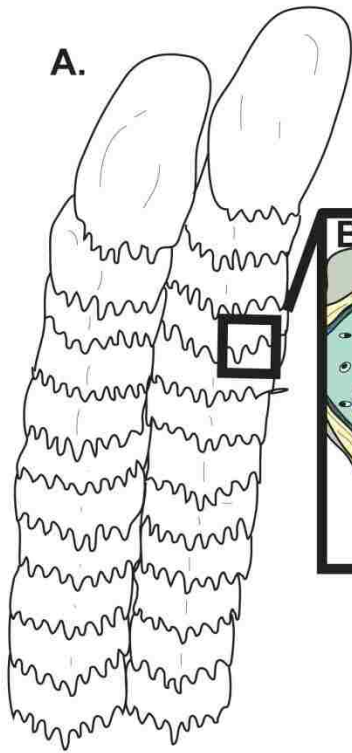


B.



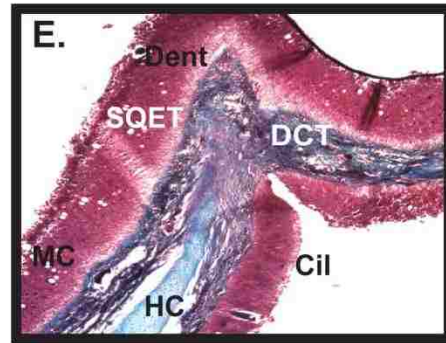
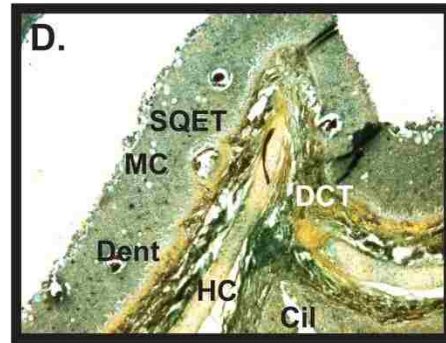
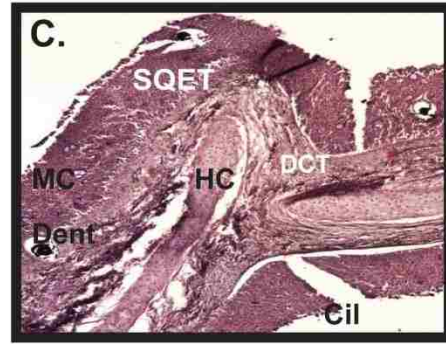
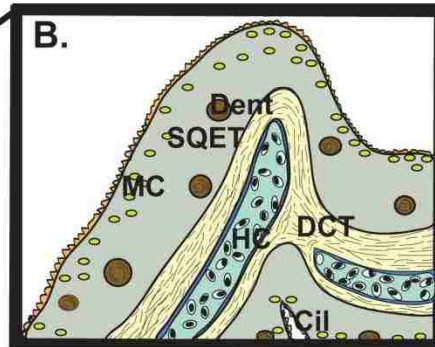
C.

Figure 4.3. Birefringence in *Mobula tarapacana*. A) Two adjacent ascending filter lobes connected by epithelial tissue under a polarized lens. The connective tissue surrounding the hyaline cartilage is visible. (Masson's Trichrome stain) B) The same tissue under partial cross polarization. The connective tissue begins to fluoresce. C) Tissue under cross polarization. The connective tissue fluoresces illustrating the highly organized structure.



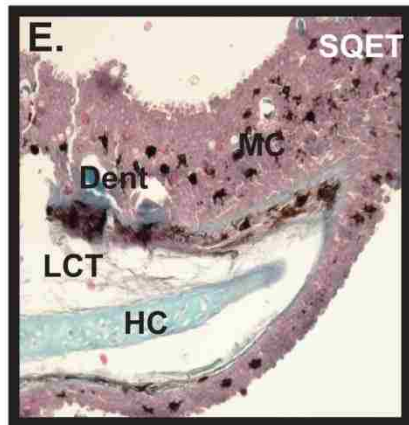
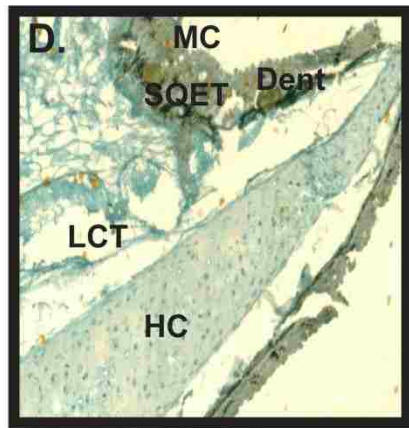
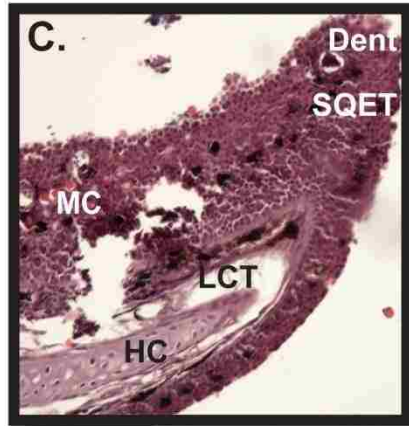
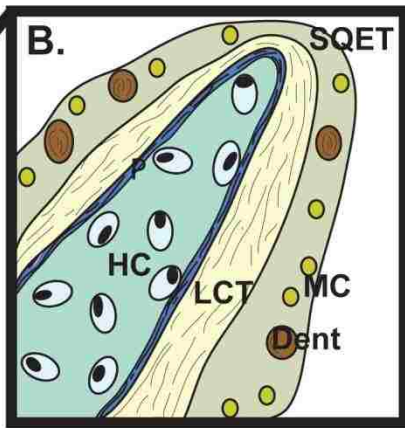
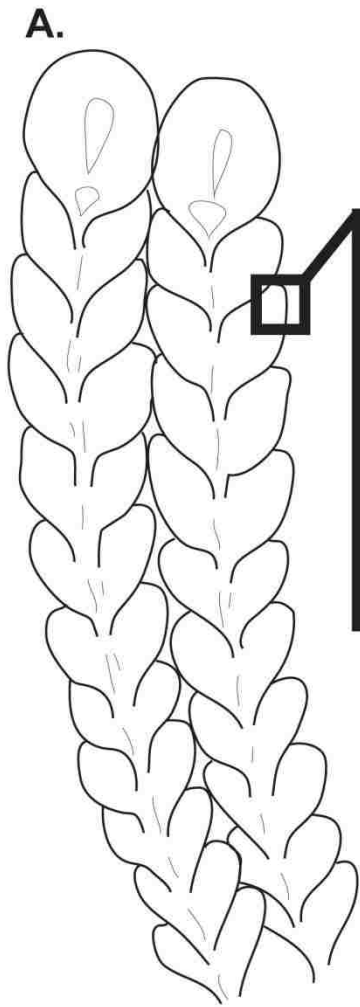
100 μ m

Figure 4.4. *Manta birostris* filter. *Manta birostris* lacks the paired lobe architecture. Instead the ascending lobes are continuous and there are finger-like, cartilaginous projections that extend down from the ventral lobe into the filter pore. The general composition of the lobe is the same as the Mobulas: cartilage core, loose connective tissue surrounding the cartilage, and a keratinized epithelium. *Manta birostris* lacks mucus producing cells, but does have denticles along the dorsal and ventral surface. The epithelium is much thicker on the dorsal side of the filter lobe than on the ventral side. Stains = C. Hematoxylin and Eosin, B. Dane's, C. Masson's Trichrome.



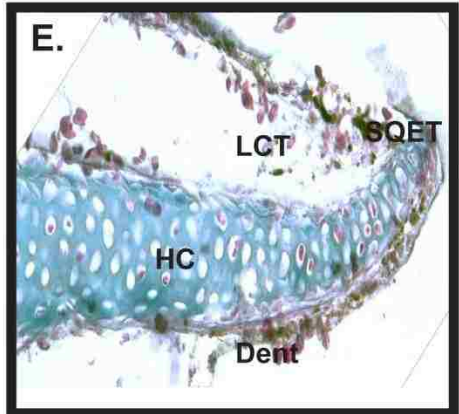
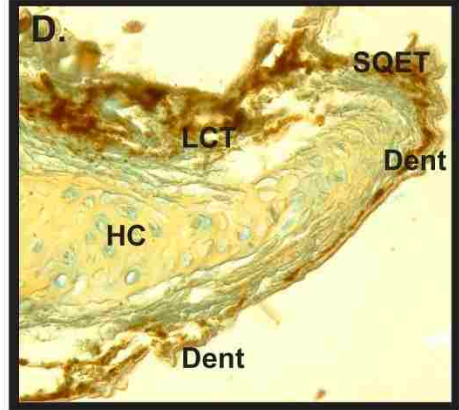
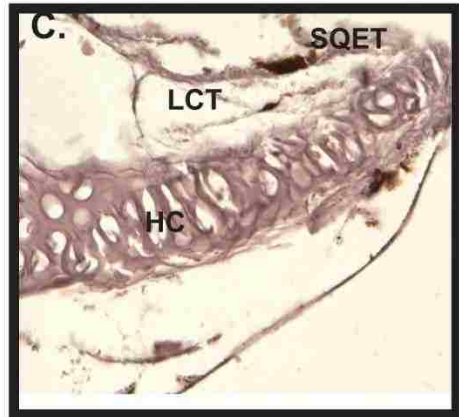
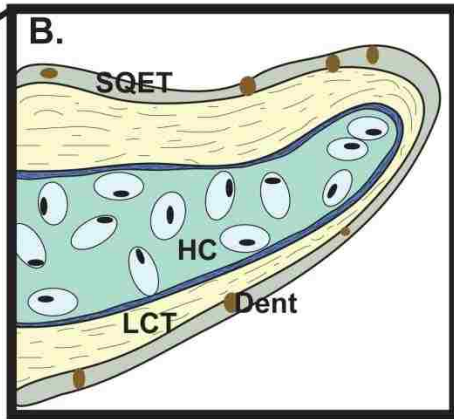
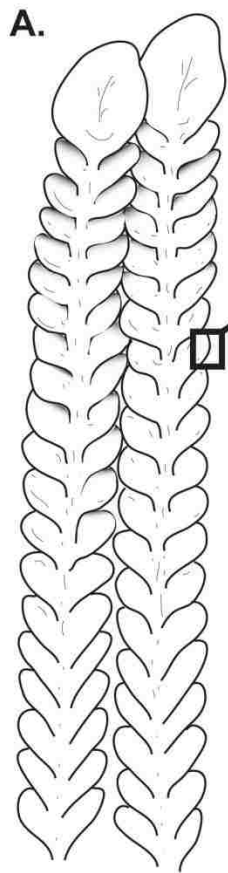
100 μ m

Figure 4.5. *Mobula tarapacana* filter lobes. *Mobula tarapacana* is the only *Mobula* with adjacent filter lobes fused by dense connective tissue and epithelial tissue. The keratinized epithelium is approximately the same thickness on the dorsal and ventral surface. Mucus cells and denticles are present within the epithelium. This is one of two *Mobula* species that has a well-defined cilia layer. Stains = C. Hematoxylin and Eosin, B. Dane's, C. Masson's Trichrome.



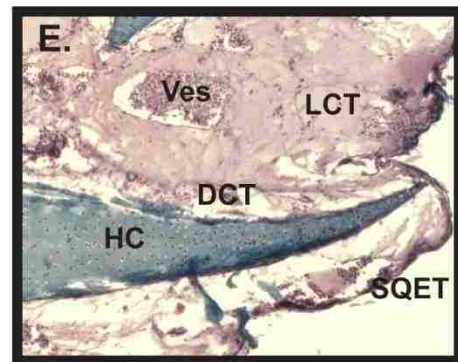
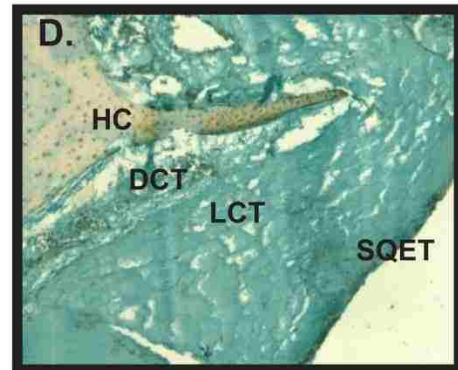
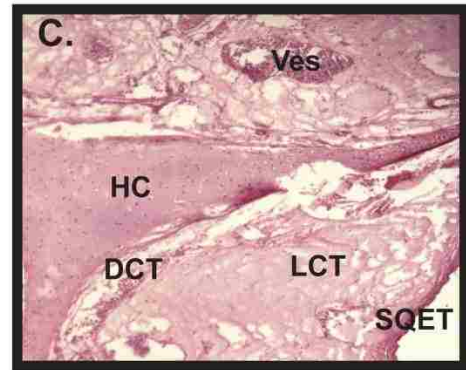
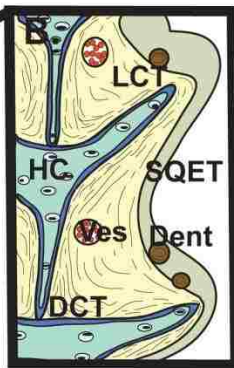
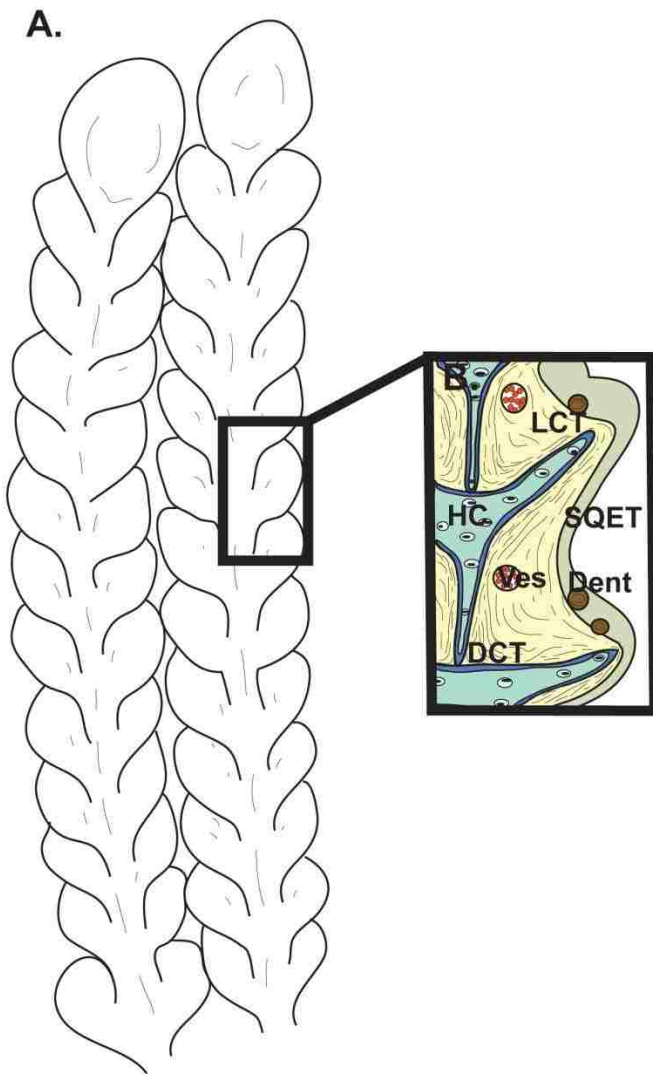
100 μ m

Figure 4.6. *Mobula munkiana* filter lobes. *Mobula munkiana* has a thicker dorsal lobe epithelium compared to the ventral lobe. However, the lobe does not appear to be as highly keratinous as other *Mobulas*. Both mucus cells and denticles are present along the dorsal and ventral surfaces. Stains = C. Hematoxylin and Eosin, B. Dane's, C. Masson's Trichrome.



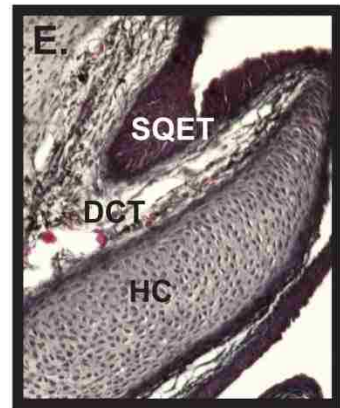
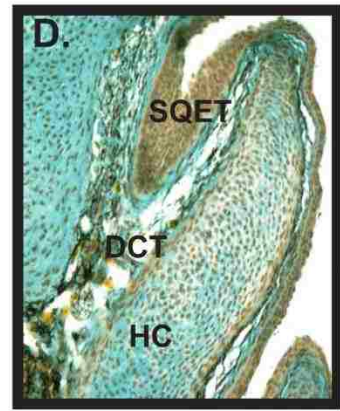
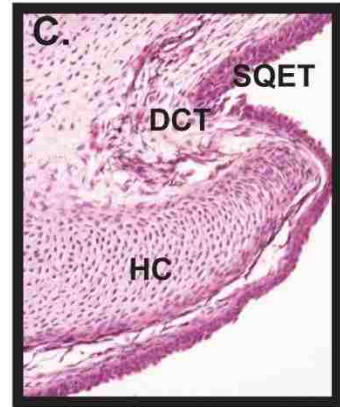
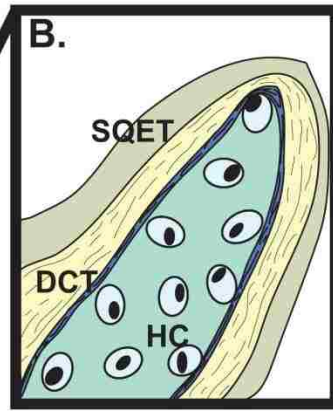
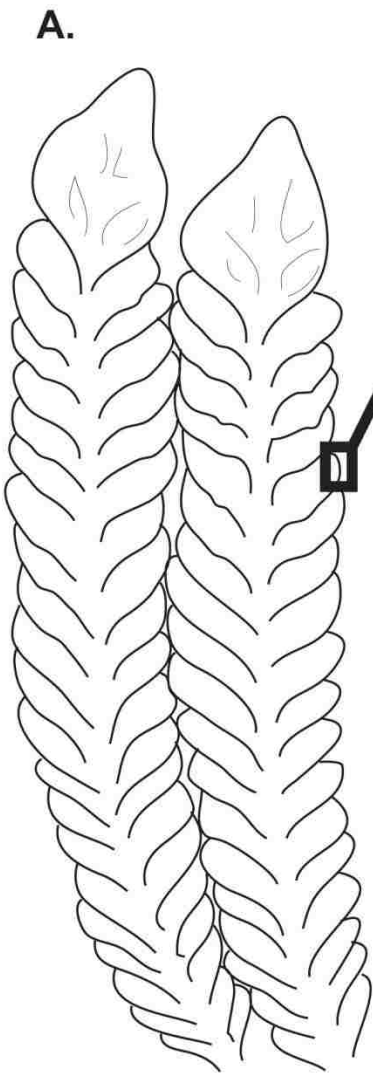
100 μ m

Figure 4.7. *Mobula thurstoni* filter lobes. *Mobula thurstoni* has a highly keratinous epithelium. Denticles are present; however, we did not detect the presence of mucus producing cells. The connective tissue surrounding the hyaline cartilage is very loose and thin. Stains = C. Hematoxylin and Eosin, B. Dane's, C. Masson's Trichrome.



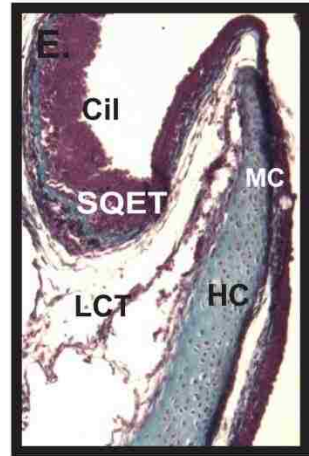
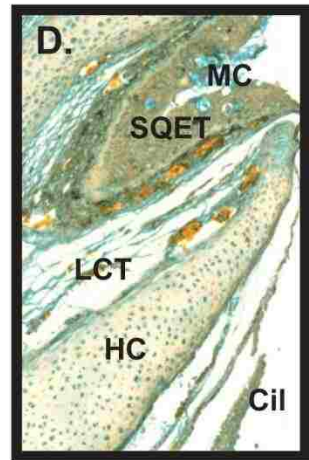
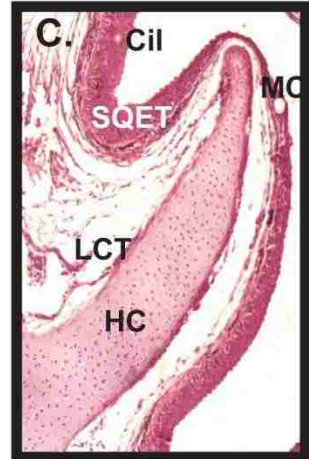
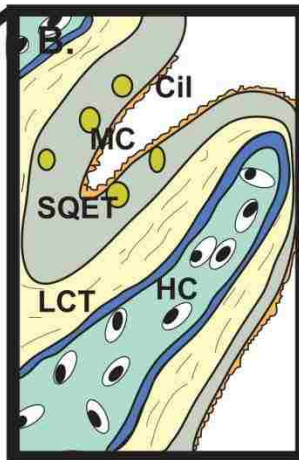
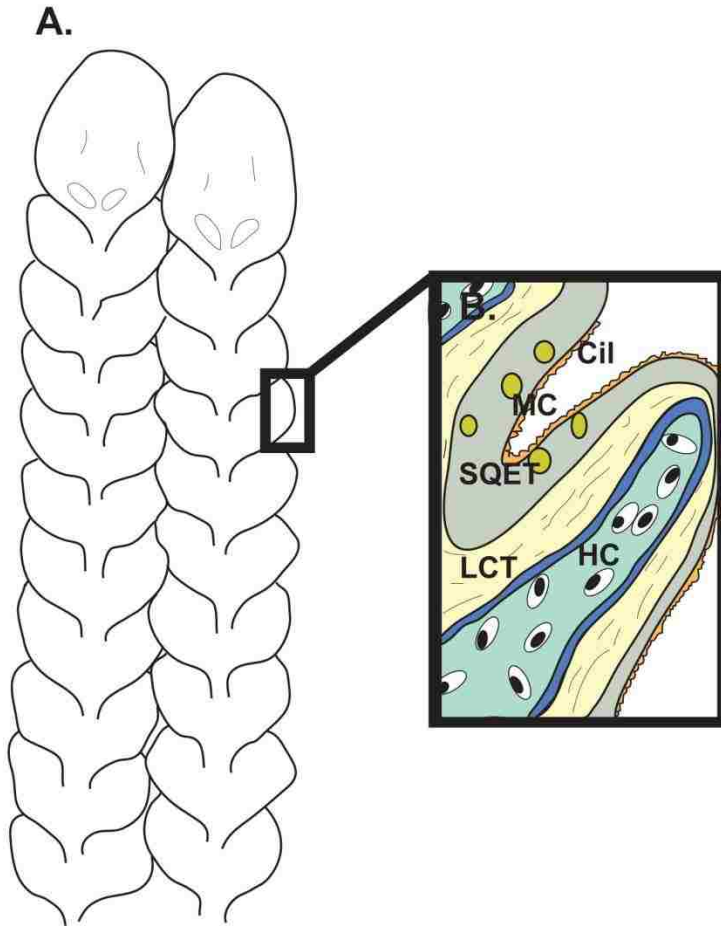
100 μ m

Figure 4.8. *Mobula hypostoma* filter lobes. *Mobula hypostoma* has both a dense layer of connective tissue surrounding the hyaline cartilage and also a loose layer of connective tissue surrounding the dense layer. The epithelium is thin. Denticles are abundant in *M. hypostoma* although they are not present on this particular slide. We did not detect the presence of mucus cells. Stains = C. Hematoxylin and Eosin, B. Dane's, C. Masson's Trichrome.



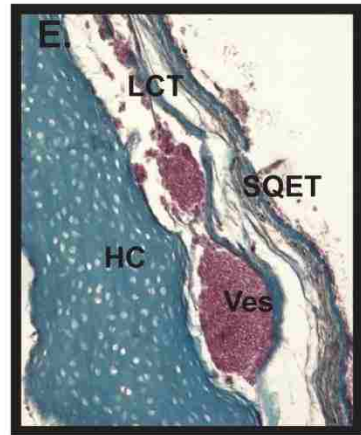
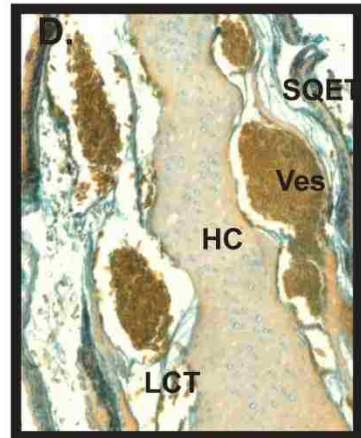
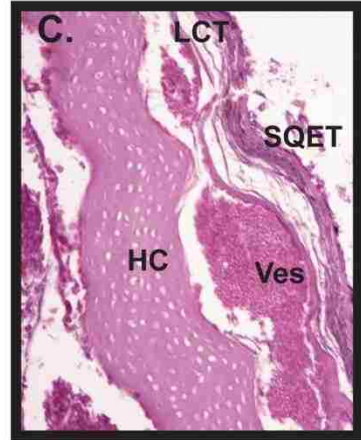
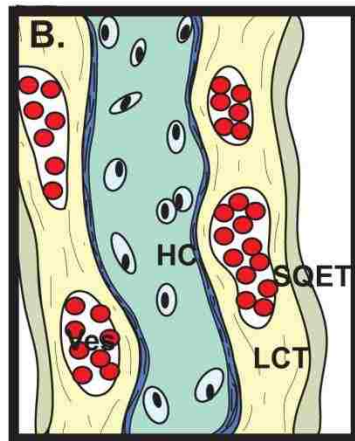
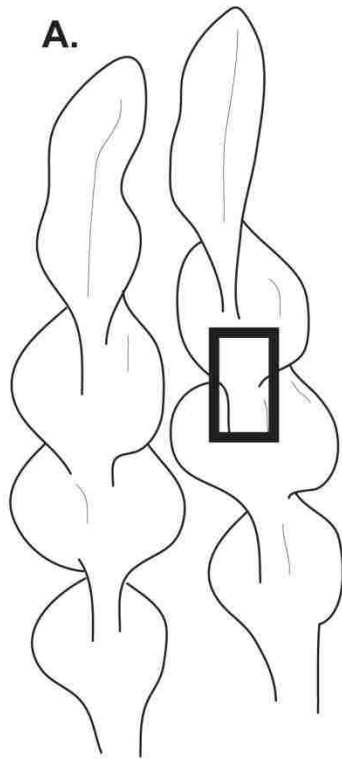
100 μ m

Figure 4.9. *Mobula mobular* (*Mobula japonica*) filter lobes. *Mobula mobular* has a highly keratinized epithelium that lacks denticles and mucus cells. The epithelium is thickest between two adjacent lobes (along the medial edge of the filter pore). Stains = C. Hematoxylin and Eosin, B. Dane's, C. Masson's Trichrome.



100 μ m

Figure 4.10. *Mobula kuhlii* filter lobes. *Mobula kuhlii* is the second *Mobula* containing cilia. The epithelium is thicker on the dorsal surface than on the ventral surface and mucus producing cells are found on both surfaces. Stains = C. Hematoxylin and Eosin, B. Dane's, C. Masson's Trichrome.



100 μ m

Figure 4.11. *Mobula eregoodootenke* filter lobes. *Mobula eregoodootenke* has distinctive filter lobes compared to other *Mobula*. The keratinous epithelium lacks denticles and mucus producing cells. Stains = C. Hematoxylin and Eosin, B. Dane's, C. Masson's Trichrome.

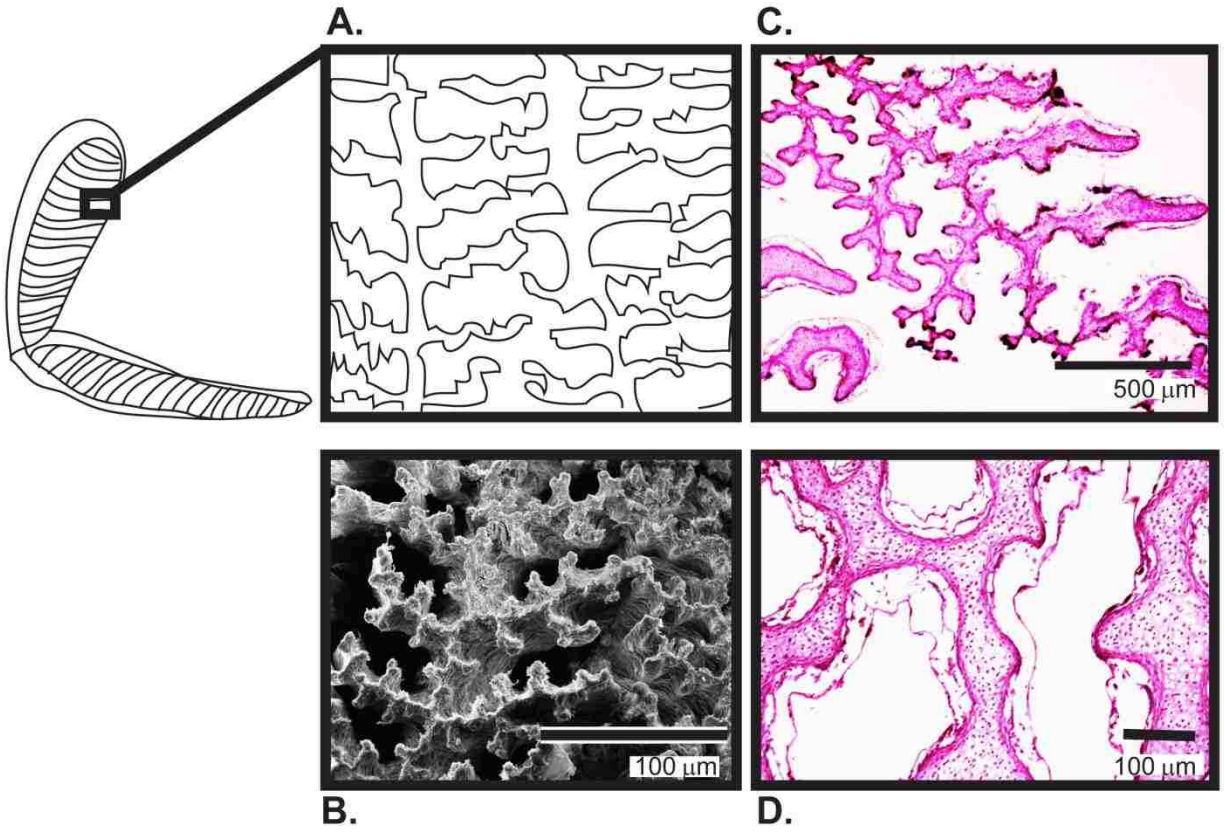


Figure 4.12. *Rhincodon typus* filter. *Rhincodon typus* is composed of a central cartilaginous skeleton with sets of paired filter lobes branching off the main skeletal support (A & B). The connective tissue surrounding the hyaline cartilage is loose and the epithelium is very thin compared to the mobulids (C & D). We did not detect the presence of mucus cells or denticles along the filter. Stain = Hematoxylin and Eosin.

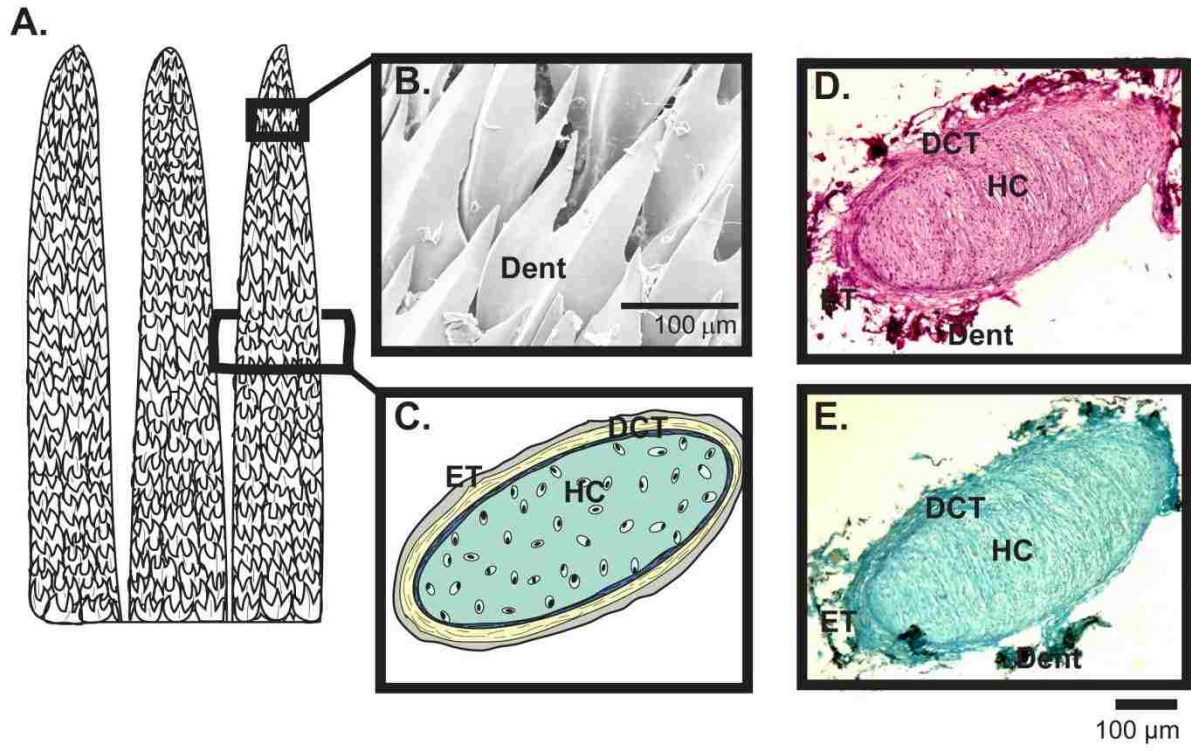
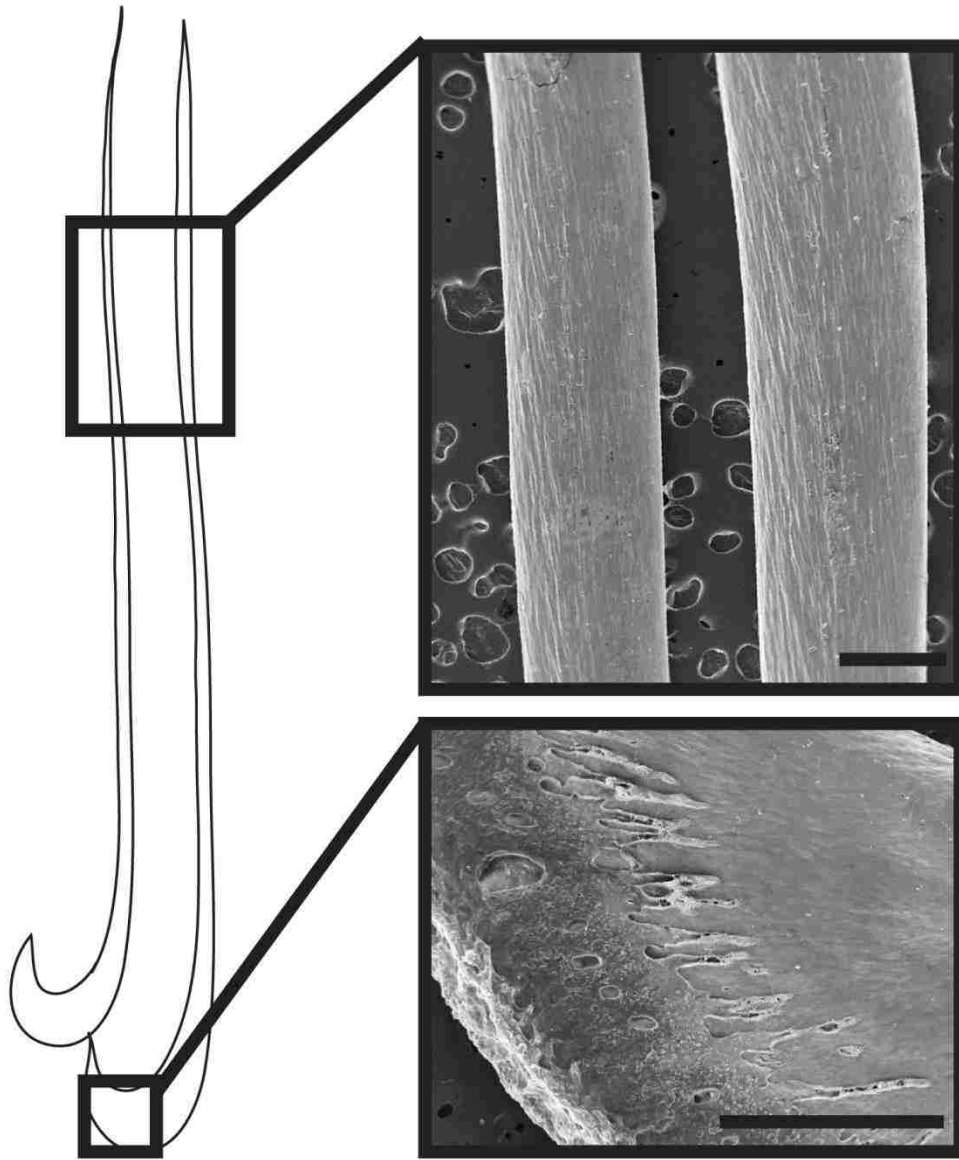


Figure 4.13. *Megachasma pelagios* rakers. *Megachasma pelagios* has rakers that more closely resemble gill rakers in bony fishes than the filter pads in the mobulids and whale shark. The rakers are completely covered by overlapping denticles (B). The raker core is hyaline cartilage surrounded by a dense connective tissue and a thin epithelium (C-E). Stains = D. Hematoxylin and Eosin and F. Masson's Trichrome.



500 microns

Figure 14. *Cetorhinus maximus* rakers. *Cetorhinus maximus* rakers are long and keratinous with no trace of a cartilage core. The medial edge of the raker is curved while the distal edge narrows into a point. The entire length of the ascending raker is smooth.

Chapter 5: Conclusion

We have used an integrative approach that includes live performance data, physical modeling, gross dissections, computed tomography, scanning electron microscopy, and histology to explore the links between filter morphology and filtration performance in the suspension feeding elasmobranch fishes. Our approach circumvents the major challenges of determining the modes of filtration in the mega-planktivores *in situ* because 1) we are not limited geographically, or by the feeding schedules of live animals, 2) we can explore the filtering elements up close with gross dissections and under microscopy, and 3) we can model the elements so that we can explore the mechanisms of particle capture at a smaller scale.

This study has yielded key findings toward the filtration modes and structure of the filter mechanism in the elasmobranchs. First, live performance data has shown that different species feeding in the same plankton blooms do so at differing speeds. Presumably they are targeting different sizes and types of plankton. By creating physical models of whale sharks, we have shown that the swimming speed and morphology of the buccopharyngeal cavity are intimately connected with the size of food particles being collected (Chapter 2). It is therefore possible, that the same shark could potentially feed in the exact same plankton bloom at different speeds and catch different sizes/types of plankton. Along those lines, two elasmobranchs with differing filter anatomy may feed in the same bloom and target different sizes/types of prey as well.

The structure of the filter is different in each lineage of elasmobranch (Chapters 3 and 4). The devil rays have a very different filter structure from any of the filtering sharks. The branchial arch is not only twisted so that the epibranchial and ceratobranchial arches are slightly offset, but the filter itself is structured so that it is composed of numerous repeating filter lobes along the anterior and posterior arch (Chapter 3). Filter lobes from each species are easily identified by the

shape of the ascending and, more importantly, the terminal lobes. Caution must be taken to correctly identify between species as the anterior and posterior lobes on a single arch may look very different and may even resemble different species. The ultrastructure of the filter may be smooth or covered with a layer of cilia. Denticles are present along the filter lobes in some species. In contrast to the off-set arch of the devil rays, the filtering sharks have the typical c-shaped arches seen in other fishes. The basking sharks have elongated, bristle-like keratinous rakers that resemble the baleen in whales (Chapter 4). The megamouth rakers are numerous and completely covered by denticles. Whale sharks filter is flattened and composed of many parallel rows referred to as reticulated mesh (Motta et al., 2010). The whale shark's filter is perhaps the most similar to the devil rays in that the filter mesh does not project into the buccopharyngeal cavity.

The branchial filter in devil rays is composed of a hyaline cartilage skeleton surrounded by a layer of loose or dense connective tissue and squamous epithelial layer. Three of the ten species of devil ray contain a large amount of mucus producing cells along the ascending filter lobes – evidence of sticky filtration. However, the other seven species do not appear to have mucus producing cells along the filter lobes and must therefore use another mode of particle capture and for transport to the esophagus. With the exception of basking sharks, the other sharks' filters are also composed of a hyaline cartilage core surrounded by a thin layer of connective tissue and a thin epithelium. Once again mucus producing cells are not present. The absence of mucus producing cells along the filter supports cross-flow filtration as the dominant mode of particle sequestration.

References

- Ari, C. and Correia, J.P. 2008. Role of sensory cues on food sensing behavior of a captive *Manta birostris* (Chondichthyes, Mobulidae). *Zoo Biol.* 27: 294-304.
- Ballintijn, C. M. (1972). Efficiency, mechanics and motor control of fish respiration. *Respir. Physiol.* 14, 125-141.
- Beckley, L.E., Cliff, G., Smale, M.J., Compagno, L.J.V., 1997. Recent strandings and sightings of whale sharks in South Africa. *Environ. Biol. Fish.* 50, 343–348.
- Bancroft, E.N. 1831. On several fishes of Jamaica. *Proceedings of the Zoological Society of London, 1831* 1: 134.
- Beebe, D.J., Mensing, G.A., Walker, G.M. 2002. Physics and applications of microfluidics in biology. *Annu. Rev. Biomed. Eng.* 4:261–86.
- Berra, T.M. & J.B. Hutchins. 1990. A specimen of megamouth shark, *Megachasma pelagios* (Megachasmidae) from Western Australia. *Rec. West. Aust. Mus.* 14: 651–656.
- Berra, T.M. & J.B. Hutchins. 1991. Natural history notes on the megamouth shark, *Megachasma pelagios*, from Western Australia. *West. Aust. Naturalist.* 18: 224–233.
- Bertmar, G. and Strömberg, C. (1969). The feeding mechanisms in plankton eaters. The epibranchial organs in whitefish. *Mar. Biol.* 3, 107-109.
- Bigelow, H. B. and Schroeder, W. C. (1953). Fishes of the Western North Atlantic. Sawfishes, Guitarfishes, Skates and Rays, Part 2, 514 pp. New Haven, CT: Sears Foundation for Marine Research.
- Bonnaterre, J.P. 1788. Tableau Encyclopédique et méthodique des trois règnes de la nature. Ichtyologie. Paris: Panckoucke.
- Booda, L. 1984. Manta rays wings, shark meat posing as scallops. *Sea Technology.* 25: 71.
- Bornbusch, A.H. 1988. Gill raker morphologies of anchovies (Teleostei: Engraulidae) from Rio Orinoco, Venezuela. *Copeia.* 1: 174-182.
- Bornbusch, A. H. and Lee, M. (1992). Gill raker structure and development in Indo-Pacific anchovies (Teleostei: Engrauloidea), with a discussion of the structural evolution of engrauloid gill rakers. *J. Morphol.* 214, 109-119.
- Bott, R., Langeloh, T. H. and Ehrfeld, E. (2000). Dynamic cross flow filtration. *Chem. Eng. J.* 80, 1-3, 245-249.

- Brainerd, E. L. (2001). Caught in the crossflow. *Nature* 412, 387-388.
- Butler, P. J. (1999). Respiratory system. In *Sharks, Skates, and Rays. The Biology of Elasmobranch Fishes* (ed. W. C. Hamlett), pp. 144-173. Baltimore, MD: Johns Hopkins University Press.
- Cadenat, J. 1959. Les diables de Mer (Raies pelagiques de la famille des Mobulidae). *Notes Africaines*. 80: 116-120.
- Callan, W. T. and Sanderson, S. L. (2003). Feeding mechanisms in carp: crossflow filtration, palatal protrusions and flow reversals. *J. Exp. Biol.* 206, 883-892.
- Campbell, R.A., and Munroe, T.A. 1974. Discovery of the lesser devil ray, *Mobula hypostoma*, in southern New England waters. *Chesapeake Science*, 15(2): 114-115.
- Canese, S., Cardinali, A., Romeo, T., Giusti, M., Salvati, E., Angiolillo, M., Greco, S. 2011. Diving behavior of the giant devil ray in the Mediterranean Sea. *Endang. Species Res.* 14: 171-176.
- Cheer, A. Y., Ogami, Y. and Sanderson, S. L. (2001). Computational fluid dynamics in the oral cavity of ram suspension-feeding fishes. *J. Theor. Biol.* 210, 463-474.
- Cione, A.L. and Reguero, M.A., 1998. A middle Eocene basking shark (Lamniformes: Cetorhinidae) from Antarctica. *Antarctic Science*. 10:1. 83-88.
- Collete, B.B. and Nauen, C.E. 1983. Scombrids of the world. FAO Fisheries Synopsis no. 125(2):1-137.
- Colman, J. G. (1997). A review of the biology and ecology of the whale shark. *J. Fish Biol.* 51, 1219-1234.
- Compagno, L.J.V. 1990. Alternative life-history styles of cartilaginous fishes in space and time. *Environ. Biol of Fishes*. 28. 33-75.
- Compagno, L.J.V. 1999. Systematics and body form. In: Hamlett, W.C. (Eds). *Sharks, Skates, and Rays: the Biology of Elasmobranch Fishes*. John Hopkins University Press. Baltimore. Pp. 1-42.
- Compagno, L.J.V. and Last, P.R. 1999. Mobulidae. In: Carpenter, K.E. and Niem, V.H. (Eds). *The Living Marine Resources of the Western Central Pacific*, 3(1). 1524-1529. Rome: FAO.
- Couturier, L.I.E., Marshall, A.D., Jaine, F.R.A., Kashiwagi, T., Pierce, S.J., Townsend, K.A., Weeks, J.J., Bennett, M.B., and Richardson, A.J. 2012. Biology, ecology, and conservation of the Mobulidae. *J. Fish. Biol.* 80: 1075-1119.

- Cuvier, G. 1829. Le règne animal distributè d'après son organization, pour servir de base à l'histoire naturelle des animaux et d'introduction à l'anatomie comparè. *Poissons*, 2. 2nd edition. Paris: Déterville.
- Dane, E.T., and Herman, D. L. 1963. AFIP Manual of Histological Staining Methods, 3rd ed., Ed. L. Luna: NY, McGraw-Hill Publ., c. 1968, p.83.
- Dean, MN, JJ Bizzarro & AP Summers. 2007. *The evolution of cranial design, diet and feeding mechanisms in batoid fishes. Integrative & Comparative Biology*. 47: 70-81
- Dewar, H. (2002). Preliminary Report: Manta Harvest in Lamakera, pp. 1-3. Pfleger Institute of Environmental Research.
- Dewar, H., Mous, P. and Domeier, M. (2008). Movements and site fidelity of the giant manta ray, *Manta birostris*, in the Komodo Marine Park, Indonesia. *Mar. Biol.* 155, 121-133.
- Dietrich, G., Kalle, K., Krauss, W., Siedler, G., 1980. General Oceanography. John Wiley & Sons, Inc., New York.
- Doyle, J. I., Solandt, J.-L., Fanshawe, S., Richardson, P., and Duncan, C. 2005. "Marine Conservation Society Basking Shark Watch Report 1987–2004." Marine Conservation Society, Ross-on-Wye, UK.
- Drenner, R. W. and Mummert, J. R. (1984). Selective particle ingestion by a filter feeding fish and its impact on phytoplankton community structure. *Limnol. Oceanogr.* 29, 941-948.
- Duffy, C.A.J., and Abbott, D. 2003. Sightings of mobulid rays from northern New Zealand, with confirmation of the occurrence of *Manta birostris* in New Zealand waters. *New Zealand J. of Mar. and Freshwater Research*. 37: 715-721.
- Eckert, S.A., Stewart, B.S., 2001. Telemetry and satellite tracking of whale sharks, *Rhincodon typus*, in the Sea of Cortez, Mexico, and the North Pacific Ocean. *Environ. Biol. Fish.* 60, 299–308.
- Friedland, K. D., Ahrenholz, D. W., Smith, J. W., Manning, M. and Ryan, J. (2006). Sieving functional morphology of the gill raker feeding apparatus of Atlantic menhaden. *J. Exp. Zool.* 305A, 974-985.
- Friedman, M., Shimada, K., Martin, L.D., Everhart, M.J., Liston, J., Maltese, A., and Triebold, M. 2010. 100-million year dynasty of giant planktivorous bony fishes in the Mesozoic seas. *Science*. 327: 990-993.
- Fowler, H.W. 1930. List of New Jersey Fishes of 1929. *Fish Culturist (Philidelphia)*. 9(8): 115-117.

- Garman, S. 1913. The plagiostomia (sharks, skates, and rays). *Memoirs of the Museum of Comparative Zoology at Harvard University*, 36.
- Garrido, S., Marcalo, A., Zwolinski, J. and van der Lingen, C. D. (2007). Laboratory investigations on the effect of prey size and concentration on the feeding behavior of *Sardina pilchardus*. *Mar. Ecol. Prog. Ser.* 330, 189-199.
- Gibson, R. N. (1988). Development, morphometry and particle retention capability of the gill rakers in the herring, *Clupea harengus* L. *J. Fish Biol.* 32, 949-962.
- Gillis, J.A., Dahn, R.D., and Shubin, N.H. 2009. Shared developmental mechanisms pattern the vertebrate gill arch and paired fin skeletons. *PNAS*, 106:14, 5720-5724.
- Gohar, H.A.F., and Bayoumi, A.R. 1959. On the anatomy of *Manta ehereburgi* with notes on *Mobula kuhlii*. *Publications of the Marine Biological Station, Al Ghardaga*, 10:91-238.
- Goodrich, J., Sanderson, S. A., Batjakas, I. E. and Kaufman, L. S. (2000). Branchial arches of suspension feeding. *Oreochromis esculentus*: sieve or sticky filter? *J. Fish Biol.* 56, 858-875.
- Gurr, G.T. 1953. *Biological Staining Methods*. London: G.T. Gurr
- Harder, W. (1975). The digestive tract. *In Anatomy of Fishes*, 135-162. Stuttgart: Eschweizerbartsche Verlagshuchhandlung.
- Heyman, W.D., Graham, R.T., Kjerfve, B., Johannes, R.E., 2001. Whale sharks *Rhincodon typus* aggregate to feed on fish spawn in Belize. *Mar. Ecol. Prog. Ser.* 215, 275–282.
- Homma, K., Maruyama, T., Itoh, T., Ishihara, H., and Uchida, S. 1999. Biology of the manta ray, *Manta birostris*, Walbaum, in the Indo-Pacific. *In: Seret, B. and Sire, J.Y. (eds). 5th Indo-Pacific Fish Conference*. 209-216. Noumea: Ichthyological Society of France.
- Hung, T.C., Piedrahita, R.H., and Cheer, A. 2012. Bio-inspired particle separator design based on the food retention mechanism by suspension-feeding fish. *Bioinspir. Biomim.* 7(4): Epub.
- Konstantinov, K. G., and Nizovtsev, G. P. 1980. The basking shark *Cetorhinus maximus*, in Kandalaksha Bay of the White Sea. *J. Ichthyol.* 19, 155–156.
- Knutsen, T., Melle, W. and Calise, L. (2001). Determining the mass density of marine copepods and their eggs with a critical focus on some of the previously used methods. *J. Plankton Res.* 23, 859-873.
- Kreffft, G. 1868. *Deratoptera alfredi* (Prince Alfred's ray). *Illustrated Sydney News* (11 July), 5(50), 1-16.

Kumari, U., Yashpal, M., Mittal, S. and Mitta, A. K. (2005). Morphology of the pharyngeal cavity, especially the surface ultrastructure of gill arches and gill rakers in relation to the feeding ecology of the catfish *Rita rita* (Siluriformes, Bagridae). *J. Morphol.* 265, 197-208.

LaBarbera, M. (1984). Feeding currents and particle capture mechanisms in suspension feeding animals. *Am. Zool.* 24, 71-84.

Langeland, A. and Nøst, T. (1995). Gill raker structure and selective predation on zooplankton by particulate feeding fish. *J. Fish Biol.* 47, 719-732.

Lloyd, R.E. 1908. On two species of eagle-rays with notes on the skull of the genus *Ceratoptera*. *Records Indian Museum (Calcutta)*. 2(2): 175-180.

Mallory, F.B. 1944. *Pathological technique*. Philadelphia: W.B. Saunders.

Marshall, A.D., Compagno, L.J.V., and Bennett, M.B. 2009. Redescription of the genus *Manta* with resurrection of *Manta alfredi* (Kreffft, 1868) (Chondrichthyes; Myliobatoidei; Mobulidae). *Zootaxa* 2301: 1-28.

Matthews, L.H. and Parker, H.W. 1950. Notes on the anatomy and biology of the basking shark (*Cetorhinus maximus* [Gunner]). *Proceedings of the Zoological Society*, London 120: 535-576.

McEachran, J.D., and Canapé, C. 1984. Mobulidae. In: Quero, J.C., Hureau, J.C., Karrer, C., Post, A., Saldanha, L. (Eds). *Checklist of the fishes of the eastern tropical Atlantic* (CLOFETA). Vol 1. JNICT, Lisbon, SEI, Pair, and UNESCO, Paris, p 73-76.

Mohanraj, G., Rajapackiam, S., Mohan, S., Batcha, H. and Gomathy, S. 2009. Status of elasmobranchs fishery in Chennai, India. *Asian Fisheries Science* 22: 607-615.

Moloney, C. L. and Field, J. G. (1991). The size-based dynamics of plankton food webs. I. A simulation-model of carbon and nitrogen flows. *J. Plankton Res.* 13, 1003-1038.

Montes Domínguez, H.M., and González-Isáias, M. 2007. Contribution to the knowledge of species of genus *Mobula* Rafinesque 1810 (Chondrichthes: Mobulidae). *The Anatomical Record* 290: 920-931.

Motta, P. J., Maslanka, M., Hueter, R. E., Davis, R. L., de la Parra, R., Mulvany, S. L., Habegger, M. L., Strother, J. A., Mara, K. R., Gardiner, J. M. et al. (2010). Feeding anatomy, filter-feeding rate, and diet of whale sharks *Rhincodon typus* during surface ram filter-feeding off the Yucatan Peninsula, Mexico. *Zoology* 113, 199-212.

Müller, J., and Henle, J. 1841. *Systematische Beschreibung der Plagiostoma*. Berlin: Verlag von Veit & Co.

Myers, R.F. 1999. *Micronesian reef fishes: a comprehensive guide to the coral reef fishes of Micronesia*, 3rd revised and expanded edition. Barrigada, Guam: Coral Graphics. 330.

- Nakaya, K., Matsumoto, R. and Suda, K. (2008). Feeding strategy of the megamouth shark *Megachasma pelagios* (Lamniformes: Megachasmidae). *J. Fish Biol.* 73, 17-34.
- Nelson, G. J. (1967). Epibranchial organs in lower teleostean fishes. *J. Zool.* 153, 71-89.
- Nelson, S.J. 1994. Fisheries of the world. 3rd Ed. New York. John Wiley and Sons.
- Nelson, J.D., 2004. Distribution and foraging ecology by whale sharks (*Rhincodon typus*) within Bahia de los Angeles, Baja California Norte, Mexico. MSc Thesis, University of San Diego, 118.
- Northcott, M.E. and Beveridge, M.C.M. 1988. The development and structure of pharyngeal apparatus associated with filter feeding in tilapias (*Oreochromis niloticus*). *J. Zool.* 215: 13-149.
- Notarbartolo-di-Sciara, G. 1987b. A revisionary study of the genus *Mobula* Rafinesque 1810 (Chondrichthyes, Mobulidae) with a description of a new species. *Zoological Journal of the Linnean Society* 91: 1-91.
- Oikawa, S. and Kanda, T. 1997. Some features of the gills of a megamouth shark and a shortfin mako, with reference to metabolic activity. In: Yano, K., Morrissey, J. F., Yabumoto, Y., and Nakaya, K., (eds.). Biology of the Megamouth Shark. Japan: Tokai University Press, 93-104.
- Paig-Tran, E.W.M., Bizzarro, J.J., Strother, J.A., and Summers, A.P. 2011. Bottles as models: predicting the effects of varying swimming speed and morphology on size selectivity and filtering efficiency in fishes. *J. Exp. Biol.* 214: 1643-1654.
- Parker, H. W., and Boeseman, M. (1954). The basking shark (*Cetorhinus maximus*) in winter. *Proc. Zool. Soc. Lond.* 124: 185–194.
- Philippi, R.A. 1892. Algunos peces de Chile. Anales del Museo Nacional de Chile, Seccion 1, *Zoologia* 3: 1-17.
- Putt, F.A. 1948. Modified eosin counterstain for formaldehyde-fixed tissues. *Archives of Pathology.* 45: 72.
- Piiper, J. and Schumann, D. (1967). Efficiency of O₂ exchange in the gills of the dogfish, *Scyliorhinus stellaris*. *Respir. Physiol.* 2, 135-148.
- Putt, F.A. 1948. Modified eosin counterstain for formaldehyde-fixed tissues. *Archives of Pathology.* 45: 72.
- Rajapackiam, S. Mohan, S., and Rudramurthy, N. 2007a. Utilization of gill rakers of lesser devil ray, *Mobula diabolus* – a new fish byproduct. *Marine Fisheries Information Service, Technical and Extension Series* 191: 22-23.
- Ross, L.G., Martinez-Palacios, C.A., Aguilar Valdez, M.d.C., Beveridges, M.C.M., and Chavez Sanchez, M.C. 2006. Determination of feeding mode in fishes: the importance of using structural

and functional feeding studies in conjunction with gut analysis in a selective zooplanktivore *Chhirostoma estor estor* Jordan 1880. *J. Fish Biol.* 68, 1782-1794.

Rubenstein, D. I. and Koehl, M. A. R. (1977). The mechanisms of filter-feeding: some theoretical considerations. *Am. Nat.* 111, 981-994.

Rubin, R. 2002. Manta rays: not all black and white. *Shark focus* 15: 4-5.

Sanderson, S. L., M. C. Stebar, K. L. Ackermann, S. H. Jones, I. E. Batjakas & L. Kaufman, 1996. Mucus entrapment of particles by a suspension-feeding tilapia (Pisces: Cichlidae). *J. Exp. Biol.* 199: 1743–1756.

Sanderson, S.L. and Wassersug, R. 1993. Convergent and alternative designs for vertebrate suspension feeding. In *The Skull* Vol. 3. Hanken, J. and Hall, B., Ed. (University of Chicago Press, IL, 1993). 37-112.

Sanderson, S. L., Cech, J. J., and Cheer, A. Y. (1994). Padlefish buccal flow velocity during ram suspension feeding and ram ventilation. *J. Exp. Biol.* 186, 145-156. *J Exp Biol.* 1654

Sanderson, S. L., Cheer, A. Y., Goodrich, J. S., Graziano, J. D. and Callan, W. T. (2001). Crossflow filtration in suspension-feeding fishes. *Nature* 412, 440-441.

Shimeta, J. and Jumars, P. A. (1991). Physical mechanisms and rates of particle capture by suspension-feeders. *Oceanogr. Mar. Biol. Annu. Rev.* 29, 191-257.

Sibanda, V., Greenwood, R. W. and Seville, J. P. K. (2001). Particle separation from using cross-flow filtration. *Powder Technol.* 118, 193-202.

Sibbing, F. A., J.W. M. Osse & A. Terlouw, 1986. Food handling in the carp (*Cyprinus carpio*): its movement patterns, mechanisms and limitations. *J. Zool., Lond.* (A) 210: 161–203.

Sims, D. W. (1999). Threshold foraging behaviour of basking sharks on zooplankton: life on an energetic knife-edge? *Proc. R. Soc. Lond. B.* 266, 1437-1443.

Sims, D. W. (2000). Filter-feeding and cruising swimming speeds of basking sharks compared with optimal models: they filter-feed slower than predicted for their size. *J. Exp. Mar. Biol. Ecol.* 49, 65-76.

Sims, D.W. 2008. Sieving a living: A review of the biology, ecology, and conservation status of the plankton-feeding basking shark (*Cetorhinus maximus*). In *Advances in Marine Biology*, Volume 54. Elsevier Ltd.

Sims, D. W. and Quayle, V. A. (1998). Selective foraging behaviour of basking sharks on zooplankton in a small-scale front. *Nature.* 393, 460-464.

- Skalski, J. R. (1996). Regression of abundance estimates from mark-recapture surveys against environmental covariates. *Can. J. Aquat. Fish. Sci.* 53, 196-204.
- Smith, A., 1829. Contributions to the natural history of South Africa. *Zool. J.* 16. 443–444.
- Smith, J. C. and Sanderson, S. L. (2007). Mucus function and crossflow filtration in a fish with gill rakers removed versus intact. *J. Exp. Biol.* 210, 2706-2713.
- Stephens, D. W. and Krebs, L. R. (1986). Foraging Theory, 247 pp. Princeton, NJ: Princeton University Press.
- Stevens, J. D. (2007). Whale shark (*Rhincodon typus*) biology and ecology: a review of the primary literature. *Fish. Res.* 84, 4-9.
- Summers, A. P. and Ferry-Graham, L. A. (2001). Ventilatory modes and mechanics of the hedgehog skate (*Leucoraja erinacea*): testing the continuous flow model. *J. Exp. Biol.* 204, 1577-1587.
- Tanaka, H., Aoki, I. and Ohshimo, S. (2006). Feeding habits and gill raker morphology of three planktivorous pelagic fish species off the coast of northern and western Kyushu in summer. *J. Fish Biol.* 68, 1041-1061.
- Taylor, L.R., Compagno, L.J.V., Struhsaker, P.J., 1983. Megamouth—a new species, genus, and family of lamnoid shark (*Megachasma pelagios*, family Megachasmidae) from the Hawaiian Islands. *Proc. Calif. Acad. Sci.* 43, 87–110.
- Taylor, J.G., 1989. Whale sharks of Ningaloo Reef, Western Australia: a preliminary study. *West. Aust. Nat.* 18, 7–12.
- Taylor, J.G., 1994. Whale Sharks, the giants of Ningaloo Reef. Angus & Robertson, Sydney, 176 pp.
- Taylor, J.G., 1996. Seasonal occurrence, distribution and movements of the whale shark, *Rhincodon typus*, at Ningaloo Reef, Western Australia. *Mar. Freshw. Res.* 47, 637–642.
- Taylor, J.G. 2007. Ram filter-feeding and nocturnal feeding of whale sharks (*Rhincodon typus*) at Ningaloo Reef, Western Australia. *Fisheries Research.* 84: 65–70
- Tomás, A. R. G., and Gomes, U. L. 1989. Observacoes sobre a presenca de *Cetorhinus maximus* (Gunnerus, 1765) (Elasmobranchii, Cetorhinidae) no sudeste a sul do Brasil. *Bolletín Institución Pesca – Sao Paulo.* 16, 111–116.
- Trakumas, S., Willeke, K., Reponen, T., Grinshpun, S. A. and Friedman, W. (2001). Comparison of filter bag, cyclonic, and wet dust collection methods in vacuum cleaners. *AIHA J.* 62, 573-583.

Valenciennes, A. 1837-1844. Ichtyologie des îles Canaries, ou histoire naturelle des poissons rapports par MM. Webb et Berthelot. In: P.B. Webb and Berthelot, S. (Eds), *Histoire naturelle des Îles Canaries*. Paris.

Valliant, L.L. 1879. Note sur une nouvelle espèce d'élasmobranchie hypotrème, le *Cephaloptera rochebrunei*. *Bulletin de la Société Philomantique, Paris*. 7(3): 187-188.

van den Berg, C., van den Boogaart, J. G. M., Sibbing, F. A. and Osse, J. W. M. (1994). Zooplankton feeding in common bream (*Abramis brama*), white bream (*Blicca bjoerkna*) and roach (*Rutilus rutilus*): experiments, models and energy intake. *Neth. J. Zool.* 44, 15-42.

van Guelpen, L., Markle, D. F. and Duggen, D. J. (1982). An evaluation of accuracy, precision, and speed of several zooplankton sampling techniques. *J. Cons. Int. Explor. Mer.* 40, 226-236.

Vigliano, F. A., Aleman, N., Quiroga, M. I. and Nieto, J. M. (2006). Ultrastructural characterization of gills in juveniles of the Argentinean silverside, *Odontesthes bonariensis* (Valenciennes, 1835) (Teleostei: Atheriniformes). *Anat. Histol. Embryol.* 35, 76-83.

Vivekanandan, E., Zala, M.S., 1994. Whale shark fishery off Veraval. *Indian J. Fish.* 41, 37-40.

Walbaum, J.J. 1792. *Petri artedi sueci genera piscium. Grypeswaldiae: A.F> Rose.*

Ware, D. M. (1978). Bioenergetics of pelagic fish: theoretical change in swimming and ration with body size. *J. Fish. Res. Board Can.* 35, 220-228.

White, W.T., Clark, T.B., Smith, W.D. and Bizzarro, J.J. 2006b. *Mobula japonica*. In: IUCN Red List of Threatened Species. Version 2010. Available at: <http://www.iucnredlist.org/apps/redlist/details/41833/0>.

Wood, F. G. 1957. Southern extension of the known range of the basking shark, *Cetorhinus maximus* (Gunnerus). *Copeia.*, 153-154.